

AD-A072 676

NAVAL POSTGRADUATE SCHOOL MONTEREY CA

F/G 8/12

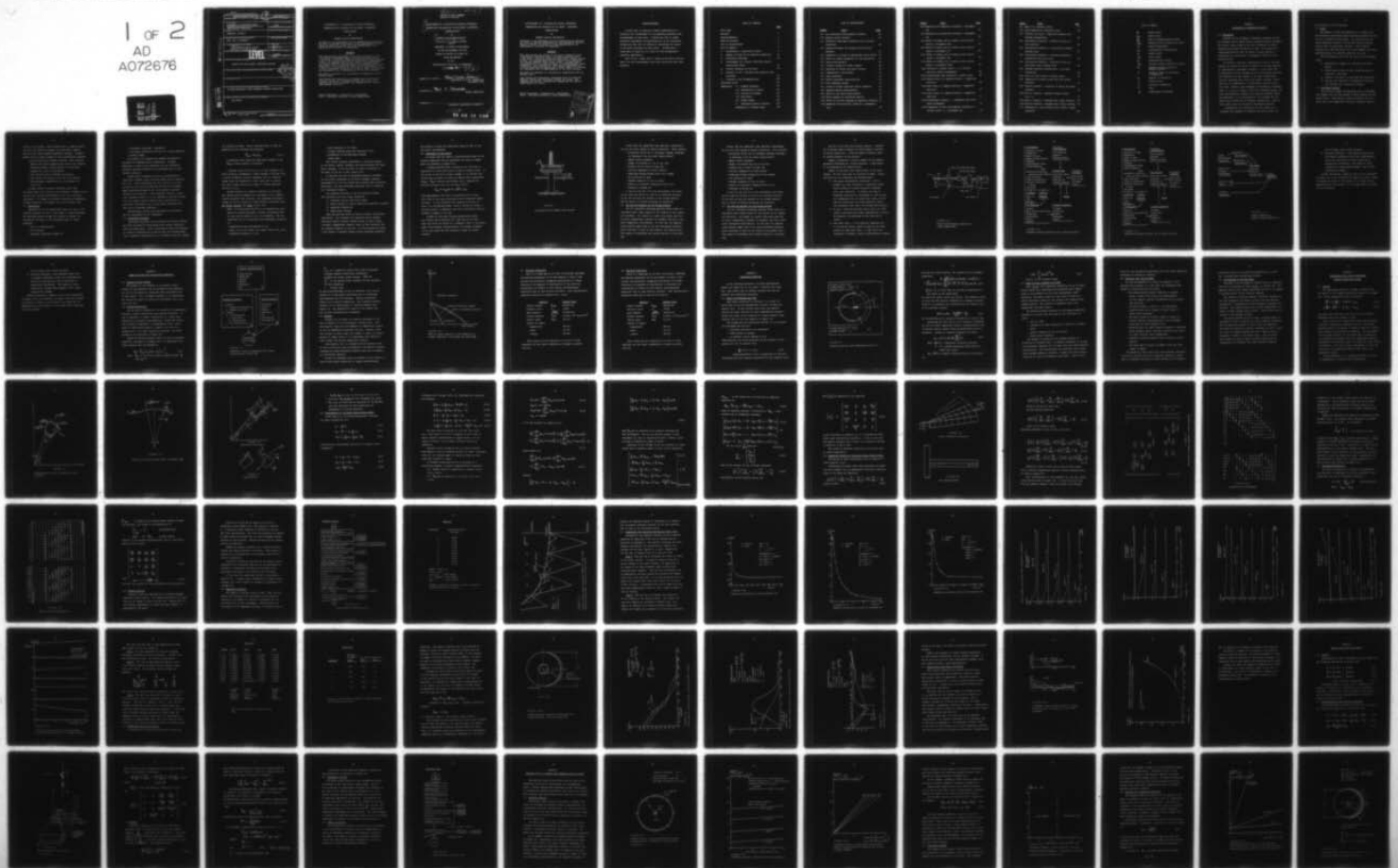
DEVELOPMENT OF A VISCOELASTIC FINITE DIFFERENCE FORMULATION FOR--ETC(U)

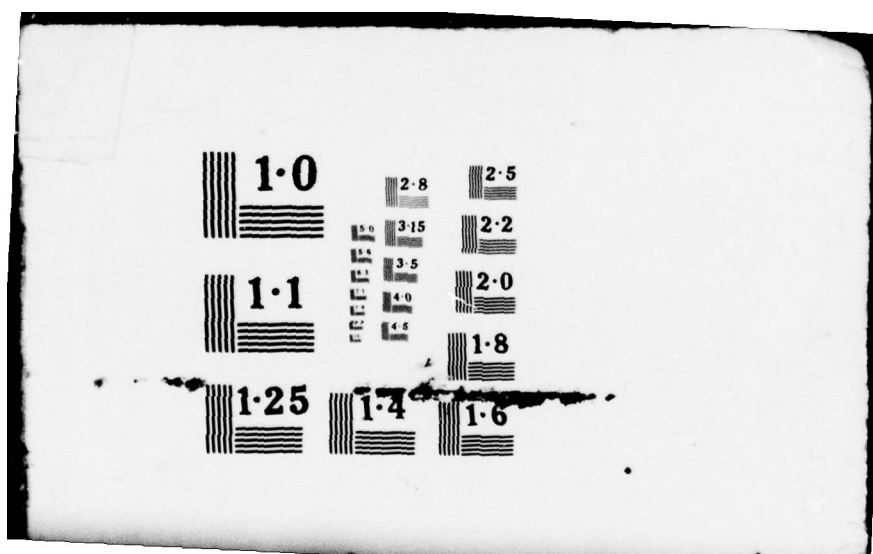
JAN 79 M W PRASKIEVICZ

UNCLASSIFIED

NL

1 OF 2
AD
A072676





UNCLASS

SECURITY CLASSIFICATION OF THIS PAGE (When Data Entered)

REPORT DOCUMENTATION PAGE

READ INSTRUCTIONS
BEFORE COMPLETING FORM

1. REPORT NUMBER

2. GOVT ACCESSION NO.

3. RECIPIENT'S CATALOG NUMBER

4. TITLE (and Subtitle)

DEVELOPMENT OF A VISCOELASTIC FINITE
DIFFERENCE FORMULATION FOR ANALYSIS OF ICE
SHEET-STRUCTURE INTERACTIONS

5. TYPE OF REPORT & PERIOD COVERED

THESIS

6. PERFORMING ORG. REPORT NUMBER

7. AUTHOR(s)

PRASKIEVICZ, MICHAEL W.

8. CONTRACT OR GRANT NUMBER(s)

9. PERFORMING ORGANIZATION NAME AND ADDRESS

MASS. INST. OF TECHNOLOGY

10. PROGRAM ELEMENT, PROJECT, TASK
AREA & WORK UNIT NUMBERS

11. CONTROLLING OFFICE NAME AND ADDRESS

CODE 031
NAVAL POSTGRADUATE SCHOOL
MONTEREY, CALIFORNIA, 93940

12. REPORT DATE

JAN 79

13. NUMBER OF PAGES

160

14. MONITORING AGENCY NAME & ADDRESS (if different from Controlling Office)

15. SECURITY CLASS. (of this report)

UNCLASS

15a. DECLASSIFICATION/DOWNGRADING
SCHEDULE

16. DISTRIBUTION STATEMENT (of this Report)

APPROVED FOR PUBLIC RELEASE; DISTRIBUTION UNLIMITED

17. DISTRIBUTION STATEMENT (of the abstract entered in Block 20, if different from Report)

18. SUPPLEMENTARY NOTES

19. KEY WORDS (Continue on reverse side if necessary and identify by block number)

ICE SHEET FORMULATION, FINITE DIFFERENCE, STRUCTURE INTERACTIONS

20. ABSTRACT (Continue on reverse side if necessary and identify by block number)

SEE REVERSE.

AD A072676

DDC FILE COPY

DD FORM 1473
1 JAN 73
(Page 1)EDITION OF 1 NOV 68 IS OBSOLETE
S/N 0102-014-6601

UNCLASS

SECURITY CLASSIFICATION OF THIS PAGE (When Data Entered)

DDC
AUG 14 1979
RECEIVED
UNCLASS

DEVELOPEMENT OF A VISCOELASTIC FINITE DIFFERENCE
FORMULATION FOR ANALYSIS OF ICE SHEET - STRUCTURE
INTERACTIONS

by

MICHAEL WALLACE PRASKIEVICZ

Submitted to the Department of Ocean Engineering on September 18, 1978, in partial fulfillment of the requirements for the degree of Master of Science in Ocean Engineering at the Massachusetts Institute of Technology.

ABSTRACT

This work reviews two models of ice sheet interaction with a particular structural shape, an isolated circular pile. A new model is developed using classical small element elastic theory. The ensuing equations are reduced by an adaptation of circular symmetry from a plane stress, two-dimensional representation to an infinite number of one-dimensional representations. The equations are then solved numerically by a finite difference technique and a finite number of solutions are recombined into an approximation of the true solution.

The model is extended to a viscoelastic formulation with the Maxwell model.

Some results and conclusions concerning areas of potential material failure and frictional effects are drawn. The computer code used is included and suggestions for further improvements are noted.

Thesis Supervisor: Professor P.C. Kircuchakis
Title: Assistant Professor of Ocean Engineering

9 Master's Thesis

Approved for public release;
distribution unlimited.

6 DEVELOPEMENT OF A VISCOELASTIC FINITE DIFFERENCE
FORMULATION FOR ANALYSIS OF ICE SHEET - STRUCTURE
INTERACTIONS.

by

10 MICHAEL WALLACE PRASKIEVICZ

B.S.E.E., U.S. Naval Academy
(1972)

SUBMITTED IN PARTIAL FULFILLMENT
OF THE REQUIREMENTS FOR THE
DEGREE OF MASTER OF SCIENCE IN
OCEAN ENGINEERING

at the

Massachusetts Institute of Technology

11 January 1979

12 162p.

Signature of Author . . .

Michael Wallace Praskiewicz

Department of Ocean Engineering
September, 1978

Certified by . . .

Paul C. Xirouchakis

Thesis Supervisor

Accepted by . . .

Chairman, Departmental Committee

251 450

79 08 13 098

DEVELOPEMENT OF A VISCOELASTIC FINITE DIFFERENCE
FORMULATION FOR ANALYSIS OF ICE SHEET - STRUCTURE
INTERACTIONS

by

MICHAEL WALLACE PRASKIEVICZ

Submitted to the Department of Ocean Engineering on September 18, 1978, in partial fulfillment of the requirements for the degree of Master of Science in Ocean Engineering at the Massachusetts Institute of Technology.

ABSTRACT

This work reviews two models of ice sheet interaction with a particular structural shape, an isolated circular pile. A new model is developed using classical small element elastic theory. The ensuing equations are reduced by an adaptation of circular symmetry from a plane stress, two-dimensional representation to an infinite number of one-dimensional representations. The equations are then solved numerically by a finite difference technique and a finite number of solutions are recombined into an approximation of the true solution.

The model is extended to a viscoelastic formulation with the Maxwell model.

Some results and conclusions concerning areas of potential material failure and frictional effects are drawn. The computer code used is included and suggestions for further improvements are noted.

Thesis Supervisor: Professor P.C. Xirouchakis
Title: Assistant Professor of Ocean Engineering

Accession For	
NTIS	General
DDC	TAB
Unannounced	
Justification	
By	
Distribution/	
Availability Codes	
Dist	Availand/or special
A	

ACKNOWLEDGEMENTS

I would like to express my sincere appreciation to Professor P.C. Xirouchakis for his guidance, patience, and encouragement in this work. I would also like to thank Professor Xirouchakis for providing part of the analytical formulation that was so critical in validating the honesty of the model developed in this thesis. Additionally, I would like to thank the U.S. Navy for this postgraduate education opportunity.

Most of all I would like to thank my wife Karan without whose love and encouragement this work would never have been possible.

TABLE OF CONTENTS

	<u>Page</u>
Title Page	
Abstract	2
Acknowledgements	3
Table of Contents	4
List of Illustrations	5
List of Symbols	8
1. Introduction - Qualitative Review	9
2. Summary of Some Sea Ice Material Properties	23
3. Analytical Modelling	28
4. Developement of a Finite Difference Elastic Constitutive Model	34
5. Viscous Extension of the Model	76
6. Analysis of Ice - Circular Pile Behavior with the model	82
7. Conclusions and Recommendations	100
References Cited	104
Appendices: A-1 Program Variables	107
A-2 Description of Arrays	109
A-3 Listing of Programs	111
A-4 User Notes	141
A-5 Sample Output	145
B Analytical Elastic Solution	152
Buckling of a Circular Ring	158

LIST OF ILLUSTRATIONS

<u>Number</u>	<u>Title</u>	<u>Page</u>
1-1	Ice interaction with monopod structure	16
1-2	Typical winter features	19
1-3	Parameters affecting structural load in marine conditions	20
1-4	Logical procedure for design criteria determination	21
2-1	Parameters to define an appropriate field theory	24
2-2	Effect on domain boundaries by load parameters	26
3-1	Indentation geometry	29
4-1	Stresses acting on a small element	35
4-2	Variation of direct and shear stresses	36
4-3	Compatibility relationship	37
4-4	Sign convention	37
4-5	Finite difference representation	44
4-6	Node numbering scheme	44
4-7	System of linear equations before expansion	46
4-8	Expanded matrix representation	47
4-9	Matrix in the band representation	49
4-10	Block diagram for subroutine Elastic	52
4-11	Effect of interval spacing on numerical stability	54
4-12	Numerical and analytical solutions - wavenumber zero	56

<u>Number</u>	<u>Title</u>	<u>Page</u>
4-13	Numerical and analytical solutions - wavenumber one	57
4-14	Numerical and analytical solutions - wavenumber two	58
4-15	Effect of radial size on radial stress distribution - wavenumber zero	59
4-16	Effect of radial size on radial stress distribution - wavenumber one	60
4-17	Effect of radial size on radial stress distribution - wavenumber two	61
4-18	Effect of radial size on radial stress distribution - wavenumber three	62
4-19	Variation of radial stress by Poisson ratio for several wavenumbers	63
4-20	Discontinuous edge loading of a finite plate	68
4-21	Radial stress vs. angular position - comparison with Ross	69
4-22	Hoop stress vs. angular position - comparison with Ross	70
4-23	Shear stress vs. angular position - comparison with Ross	71
4-24	Displacement loading comparison with first three wavenumbers	73
4-25	Comparison of exact and computed solutions at various ratios wavenumber one	74

<u>Number</u>	<u>Title</u>	<u>Page</u>
5-1	Model for a Maxwell liquid	77
5-2	Block diagram for subroutine Visco	81
6-1	Circular ice sheet - rigid pile geometry and loading configuration	83
6-2	Viscoelastic behavior - effective strain vs. load duration	84
6-3	Viscoelastic behavior - stress-strain diagram showing creep	85
6-4	Viscoelastic behavior - elastic-viscoelastic transition from load curves	87
6-5	Viscoelastic behavior - effective strain vs. time under three loading rates	89
6-6	Loading condition circular pile - ice sheet interaction	90
6-7	Ratio of shear stress to radial stress	91
6-8	Comparison of radial stress with and without friction	94
6-9	Elastic behavior - variation of radial and shear stresses	96
6-10	Elastic behavior - maximum vertical strain location	97
6-11	Elastic behavior - maximum hoop strain location	98
6-12	Elastic behavior - maximum shear strain location	99
C-1	Buckling of a thin circular plate around a rigid inclusion	159

LIST OF SYMBOLS

σ_r	radial stress
σ_{re}	shear stress
σ_θ	hoop or circumferential stress
σ_{EFF}	effective stress (defined by (6.1))
u_r	radial displacement
u_θ	circumferential displacement
ϵ_r	radial strain
ϵ_{re}	shear strain
ϵ_θ	circumferential strain
ϵ_{EFF}	effective strain (defined by (6.2))
θ	angular position around the circular geometry
η	"contact" angle or separation of boundaries
E	modulus of elasticity
ν	Poisson ratio
α	viscosity coefficient
T	time
μ_s	coefficient of friction

CHAPTER 1

Introduction - Qualitative Review1.1 Motivation

Interest in the strength of naturally occurring ice and the ultimate size to which marine structures must be designed has become a major topic as the last boundaries of easily accessible petroleum resources are used. The extension of engineering practice into the world's colder regions is subsequently an effort that is intimately related to this perceived need.

To satisfy a curiosity regarding this area of offshore design, the author set forth to discover a rational approach to establishing a meaningful standard. It was hoped that an appropriate theory, perhaps based on statistical patterns, was available that was similar to the many comprehensive theories regarding wind, wave, and seismic loading. Unfortunately, no comprehensive or universally accepted theory was found. However, many prominent investigators, including Assur [1][2][3], Bercha [4][5][6], Hirayama et al. [14][15], and Korzhavin [19][20], have proposed numerous models and approaches to the calculation of ice strength and the quantitative prediction of necessary design size. Some of these models will be reviewed in subsequent chapters.

Consequently, the motivation for this thesis is to recognize and segregate an accurate and useful theory for

the prediction of ice pressures.

1.2 Scope

The purpose of this investigation is to analyze the ice-structural interaction models presently proposed for the case of a vertical circular pile. The circular pile was chosen primarily because it is the most useful geometric form in areas of high tidal variance. Other authors, notably Tryde [30] and Bercha [5], have examined the other promising forms, the inclined wedge and the cone.

The investigation will take the form of the following steps:

- 1) Qualitatively compare the available analytical models.
- 2) Either improve upon the most promising model or construct a new model.
- 3) Analyze sensitivity to some important parameters.
- 4) Analyze some important ice properties affecting the circular pile interaction problem.

1.3 Structural Failure

The earliest designs contemplating an ice environment were highway and railroad bridges in North America and the Soviet Union. Some authors, notably Korzhavin [19] and Watts [32], have summarized structural collapses known to

be due to ice forces. These failures have a common thread; they were all caused by unusual ice jams which, coupled with an early thaw, produced unplanned loadings. Insights gained from a careful reading of these descriptions indicate:

- very few failures actually occurred. This evidence implies that early engineers had either very accurate analytical skills (hardly likely) or that early designs were overly conservative.
- some failures were by gradual ice-erosion.
- when failure did occur, it was due to an unusual meteorological complication or no allowance for ice at all.

No major marine structural failures, apart from ice-bound ships, were found in the literature. Perhaps this is because this hostile environment has yet to be seriously challenged. Ice damage on coastline facilities, breakwaters, docking facilities, and lights, have been recorded. [26]

1.4 Application

Applications of ice engineering extend not only to the offshore industry but over a wide range of related problems. The knowledge gained through the solution of marine ice uncertainty can apply to the following range of actual proposals:

- over ice transportation
- ice airfields
- submarine surfacing through ice

- icebreaker technology - navigation
- ice island construction for use as a mobile platform
- iceberg towing

The offshore oil industry has perhaps the greatest motivation in subduing arctic conditions. Although experience to date is not extensive, the few structures presently deployed emphasize the continuing need for more accurate analysis.

Present North American interest is concentrated in Cook Inlet, Alaska, [26], the North Slope, and the Beaufort Sea [9]. Arctic conditions are most severe, as it will be shown in the next few sections, and there are designs under construction which do not even consider a passive survival of a structure. These proposals include a vibratory icebreaker motion [7], ice melting by internal heating [17], air cushion mobile platform [22], construction of protective soil berms [9], or even mobile platforms that only drill in optimum conditions.

Scandinavian, Soviet, and Argentinian oil interests are not represented in the literature.

1.5 Historical Treatment

Analytical treatment of ice pressures and winter loading was first presented in fresh water civil works, especially dams and bridge piers. Early investigators faced the problems by correctly deducing that no matter what the loading condition or geometric possibilities, ice strength could not exceed

its crushing strength. Thus a limiting value of G_{CR} was imposed into the following relationship:

$$F_{MAX} = bh G_{CR} \quad (1.1)$$

b represents pier width and G_{CR} crush strength of ice
 F_{MAX} is force exerted on structure

A special study of the A.S.C.E. in 1931 (Committee on Power Division) recommended a crush strength of 400 psi [32]. A review of Russian, Polish, Canadian, and U.S. military design codes was conducted by Watts [32], and it reveals that most design criteria are simply a refined empirical version of (1.1).

Design criteria for offshore structures in the much more quantitatively unknown sea environment do not simplistically prescribe this relation. The paragraph relating to design for sea ice forces for fixed offshore structures from Det Norske Veritas 1974 Rules states [10]:

B401. For structures intended to be installed in areas where ice hazards may exist, relevant statistical data for the area in question are to be submitted. The ice conditions are to be described with particular attention to:

- concentration and distribution of ice
- types of ice (ice floes, ice ridges, rafted ice, etc.)
- mechanical properties of ice

- mean thickness of ice floes
- average drifting speed and direction of ice
- probability of encountering icebergs
- tidal range

This rather nebulous requirement is in stark contrast to the curves, tables, formulae, and data presented for other force loadings. It is here that the lack of analysis in the state of the art is most keenly felt.

To increase the body of knowledge presently available in the science regarding ice pressure loadings, numerous investigators in the last decade have proposed many alternate procedures. The more promising approaches will be analyzed in a subsequent chapter.

The proposed solutions to the ice pressure problem fall basically into four broad categories:

- 1) Classical elastic thin plate theory
- 2) Finite element or finite difference numerical solutions
- 3) Empirical formulation
- 4) Model basin testing

Each approach has merits as well as severe, restrictive limitations. For instance, the classical theory assumes thin plate elastic behavior (plane stress or plane strain, isotropic, homogeneous, elastic) which is most certainly not the complete behavior of sea ice. Yet the solution can yield a fair degree of accuracy within certain limiting conditions

and provide a closed form expression which is easy to use and easily reproducible.

1.6 Importance of Ice Forces

To insure that the reader is qualitatively aware of the enormous magnitude that ice pressures can exert, a simple model is presented in Figure 1-1.

A monopod platform with a radius at ice of 8 feet is subjected to an ice load driven by wind or current shear. If the extent of the floe is great enough, it is obvious that forces well in excess of local ice failure can be generated. Using a G_{CR} of 200 psi and formula (1.1), adjusted for projected frontal area, the ice force can be:

$$F_{MAX} \approx G_{CR} bh \approx 690 \text{ tons}$$

This approximately 700 tons is concentrated on a three foot slice of the leg, presenting severe structural considerations. If this structure were located in 80 feet of water, the overturning moment could be 20,700 foot-tons, a serious concern to foundation and soil resistance as well as flexural strength of the leg.

Perhaps an even more serious consideration which has recently been addressed [21] [25] [26] is the fact that this force can thrust at a frequency close to one hertz. Apart from resonant considerations, the fatigue strengths of the cold metal and cold weldments become of serious concern.

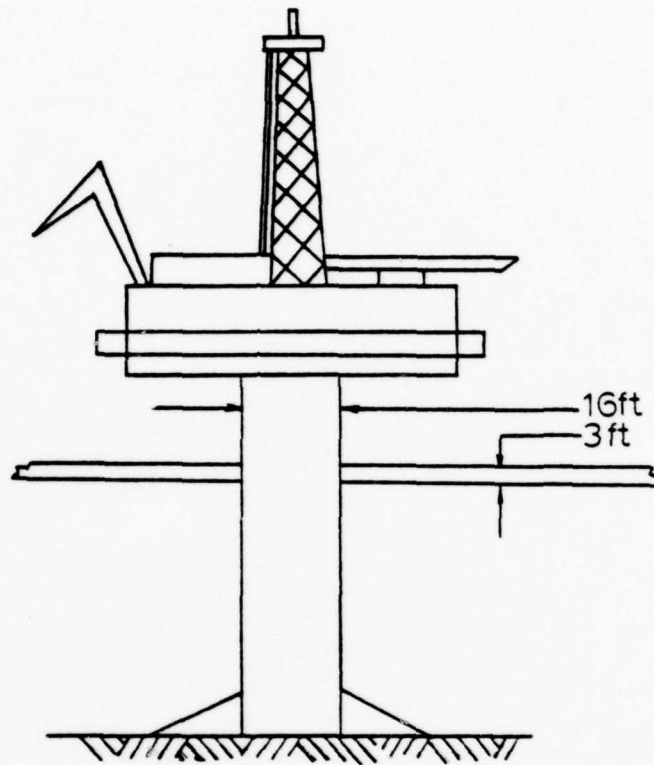


FIGURE 1-1

Ice interaction with monopod type structure

Peyton [26] has summarized some important requirements for the ice force design of marine structures. These include:

- Horizontal forces due to crushing, bending, buckling, or shearing of the ice sheet (quasi-static)
- Impact forces (dynamic)
- Weight of attached sea ice at low tide
- Buoyant lift of above at high tide
- Vertical components of sheet failure
- Diaphragm bending during water level change
- Ice accretion by spray
- Thermal expansion of ice in joints
- Rubble in structural framing carried by ice
- Abrasion by moving ice

It can be seen that in a cold environment, ice forces can be large and obvious as well as an insidious problem. In the next section the enormity of the design equation and the limits of present knowledge are presented.

1.7 Ice and the Enormity of the Design Problem

Ice is a naturally occurring material which forms in a convenient plate shape located at the surface of the liquid-air interface. Ice formed on a small fresh water pond can be clear, homogeneous, constant in thickness and have a sensible temperature distribution. In this case the engineer could possibly apply some of the more well-known classical plate solutions to find the ice behavior and predict with a fair degree of confidence any desired solution to his problem.

Peyton [26] has summarized some important requirements for the ice force design of marine structures. These include:

- Horizontal forces due to crushing, bending, buckling, or shearing of the ice sheet (quasi-static)
- Impact forces (dynamic)
- Weight of attached sea ice at low tide
- Buoyant lift of above at high tide
- Vertical components of sheet failure
- Diaphragm bending during water level change
- Ice accretion by spray
- Thermal expansion of ice in joints
- Rubble in structural framing carried by ice
- Abrasion by moving ice

It can be seen that in a cold environment, ice forces can be large and obvious as well as an insidious problem. In the next section the enormity of the design equation and the limits of present knowledge are presented.

1.7 Ice and the Enormity of the Design Problem

Ice is a naturally occurring material which forms in a convenient plate shape located at the surface of the liquid-air interface. Ice formed on a small fresh water pond can be clear, homogeneous, constant in thickness and have a sensible temperature distribution. In this case the engineer could possibly apply some of the more well-known classical plate solutions to find the ice behavior and predict with a fair degree of confidence any desired solution to his problem.

Sea ice is not that well behaved, however. Consider the situation shown in Figure 1-2 which depicts a profile of arctic coastal ice. A bottom founded structure could be located anywhere in the picture.

Figure 1-3 presents a careful summary of the unknown parameters affecting the design equation. A high degree of interdependence is characteristic.

Figure 1-4 presents four logical paths to the final design. All have been used in successful designs. Again, each path has its advantages and disadvantages.

- 1) From known environmental conditions - this is perhaps the ideal situation; a successful design could possibly be created anywhere at minimal cost, once perfected. Of course, the lack of knowledge regarding the environment at each locale, the rudimentary state of analytical tools, and the lack of correlation with known quantities makes this procedure years away, and perhaps unattainable.
- 2) In situ - This will provide better data, but still suffers from analytical model imperfection, as above. In addition, the gathering of this data can be costly.
- 3) Near full scale - a very practical approach, but it too can be costly, nearly as much as the final product in some cases [25]. It does offer the advantage of risking a small, inconsequential failure

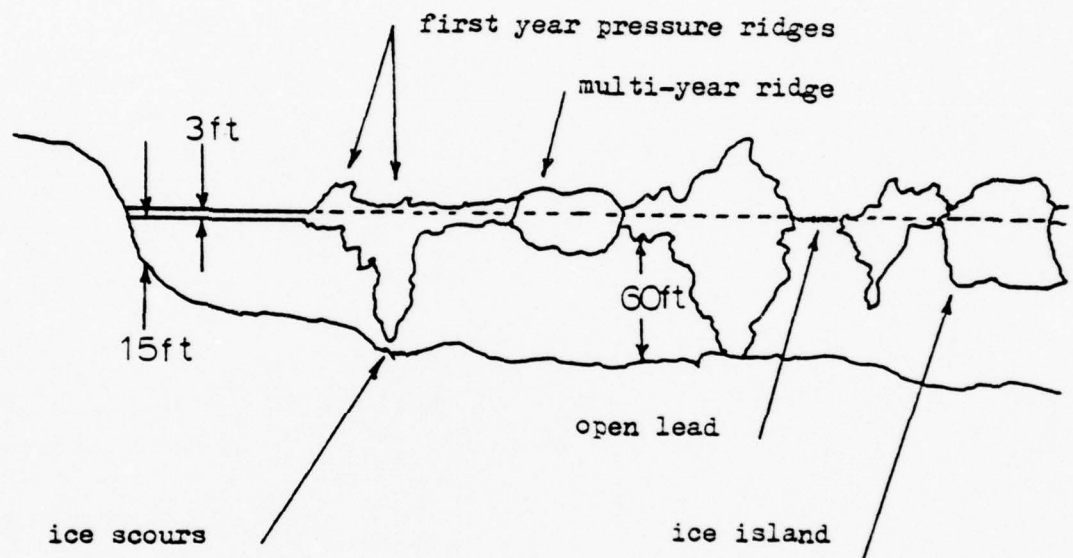


FIGURE 1-2

Typical winter features, Beaufort Sea
(after Croasdale [9])

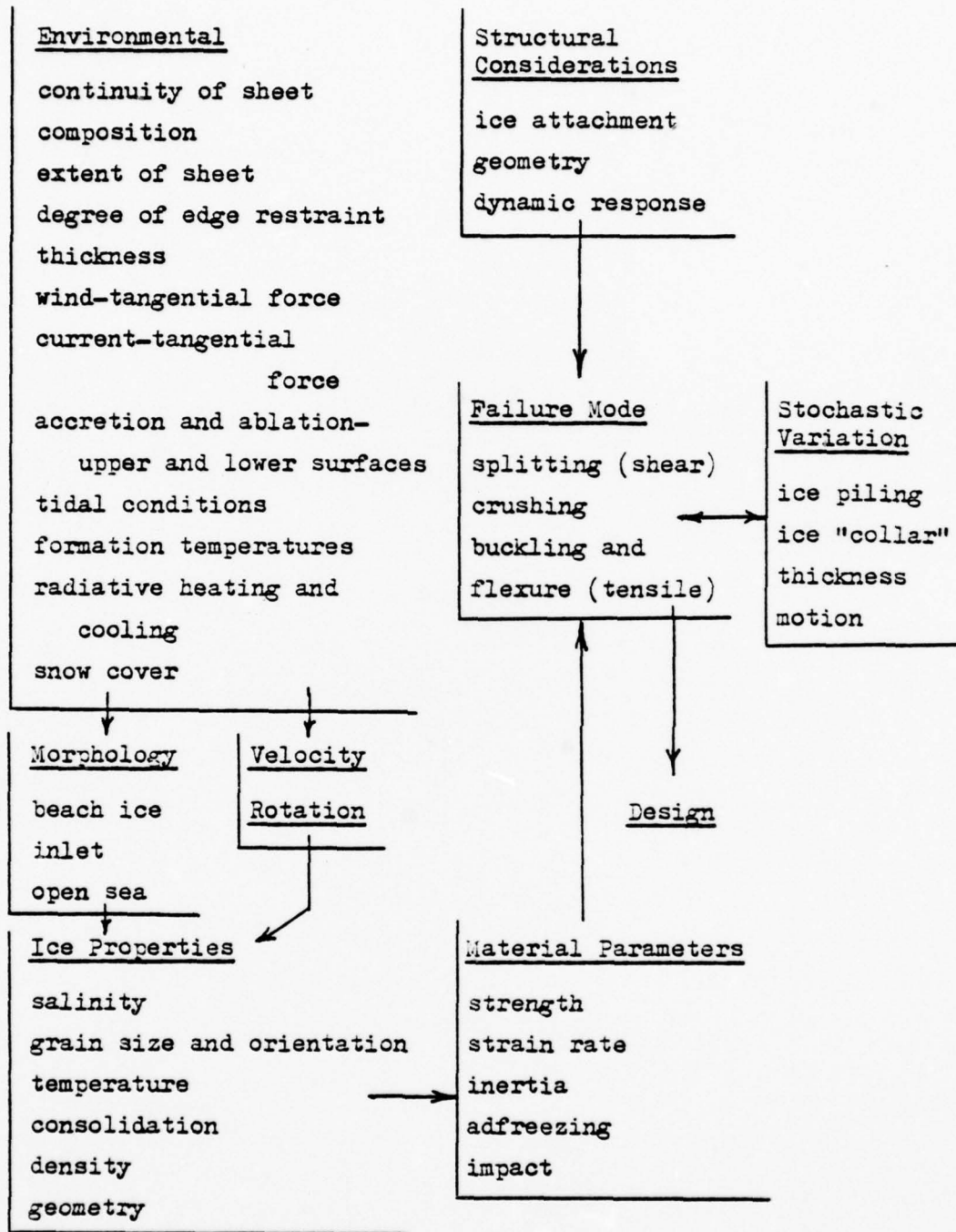


FIGURE 1-3

Parameters affecting structural load in marine conditions

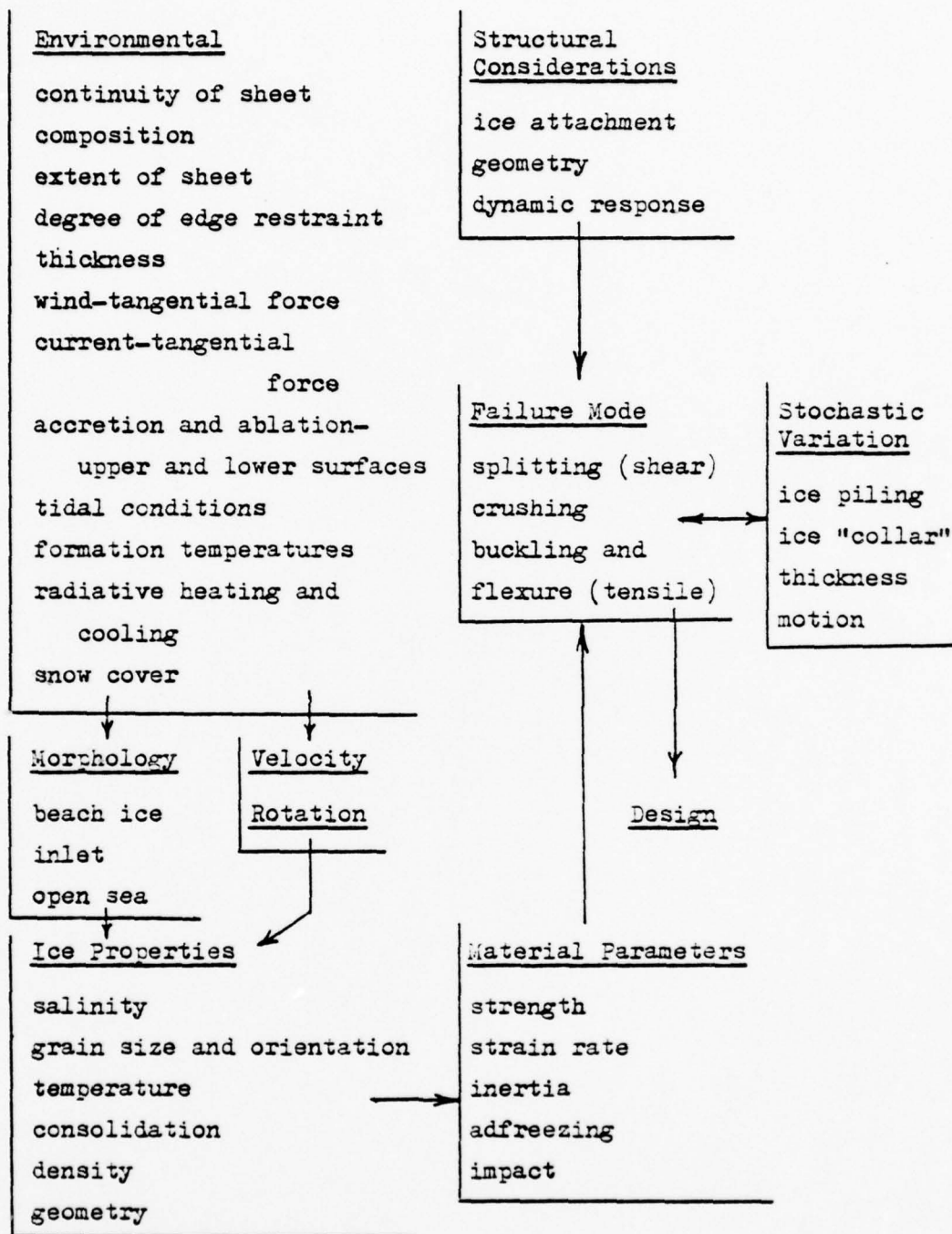


FIGURE 1-3

Parameters affecting structural load in marine conditions

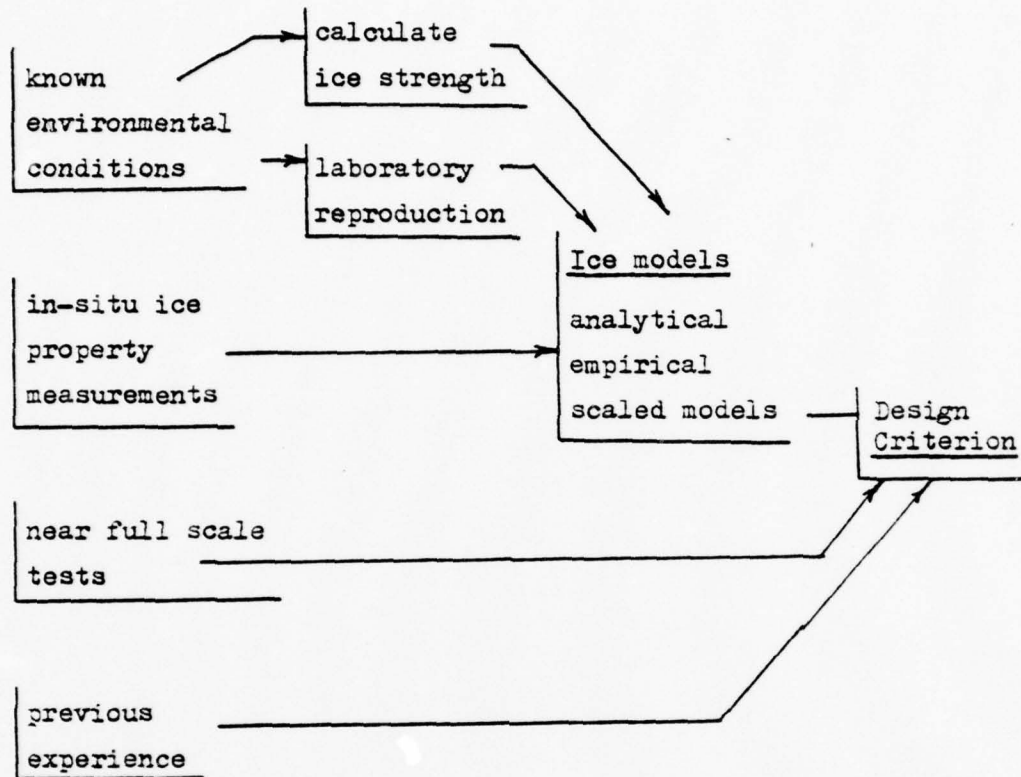


FIGURE 1-4

Logical procedure for
design criterion determination

over a larger, more serious accident.

- 4) Previous experience - This approach would yield the highest confidence level, but, unfortunately, little has been done and some of what has is proprietary information. Here again an overly conservative design would propagate other overly conservative designs.

Without presenting a complete review of the parameters in Figure 1-3 or the literature on Figure 1-4, both of which are beyond the scope of this thesis, it is hoped that an appreciation of the enormity of the design effort involving ice can be gained.

over a larger, more serious accident.

- 4) Previous experience - This approach would yield the highest confidence level, but, unfortunately, little has been done and some of what has is proprietary information. Here again an overly conservative design would propagate other overly conservative designs.

Without presenting a complete review of the parameters in Figure 1-3 or the literature on Figure 1-4, both of which are beyond the scope of this thesis, it is hoped that an appreciation of the enormity of the design effort involving ice can be gained.

CHAPTER 2

Summary of Some Sea Ice Material Properties2.1 Purpose of this Chapter

The purpose of this chapter is to present a brief outline of some important sea ice parameters and properties for use in developing the analytical model presented later in this thesis. For a thorough treatment of ice properties, the interested reader is referred to references [12], [13], [18], and [33].

2.2 Problem Formulation

Sea ice can be considered to be sensitive to temperature, salinity, crystal orientation, and seasonal variation. It can be considered to behave elastically for a short load duration and a moderate load magnitude. Katona and Vaudrey [18] describe an approach to an appropriate field theory which is sufficiently general to apply to the case of a circular pile - ice sheet interaction problem. The basic parameters are presented in Figure 2-1.

Katona and Vaudrey further reduce the list of material parameters (category I of Figure 2-1) to a functional form which contains only two parameters:

$$\sigma_{ij} = F_{ijkl} [\epsilon_{kl}(t'), \underline{x}], t' \Big|_0^t \quad (2.1)$$

where σ_{ij} is the stress tensor at spatial point \underline{x}
and time t

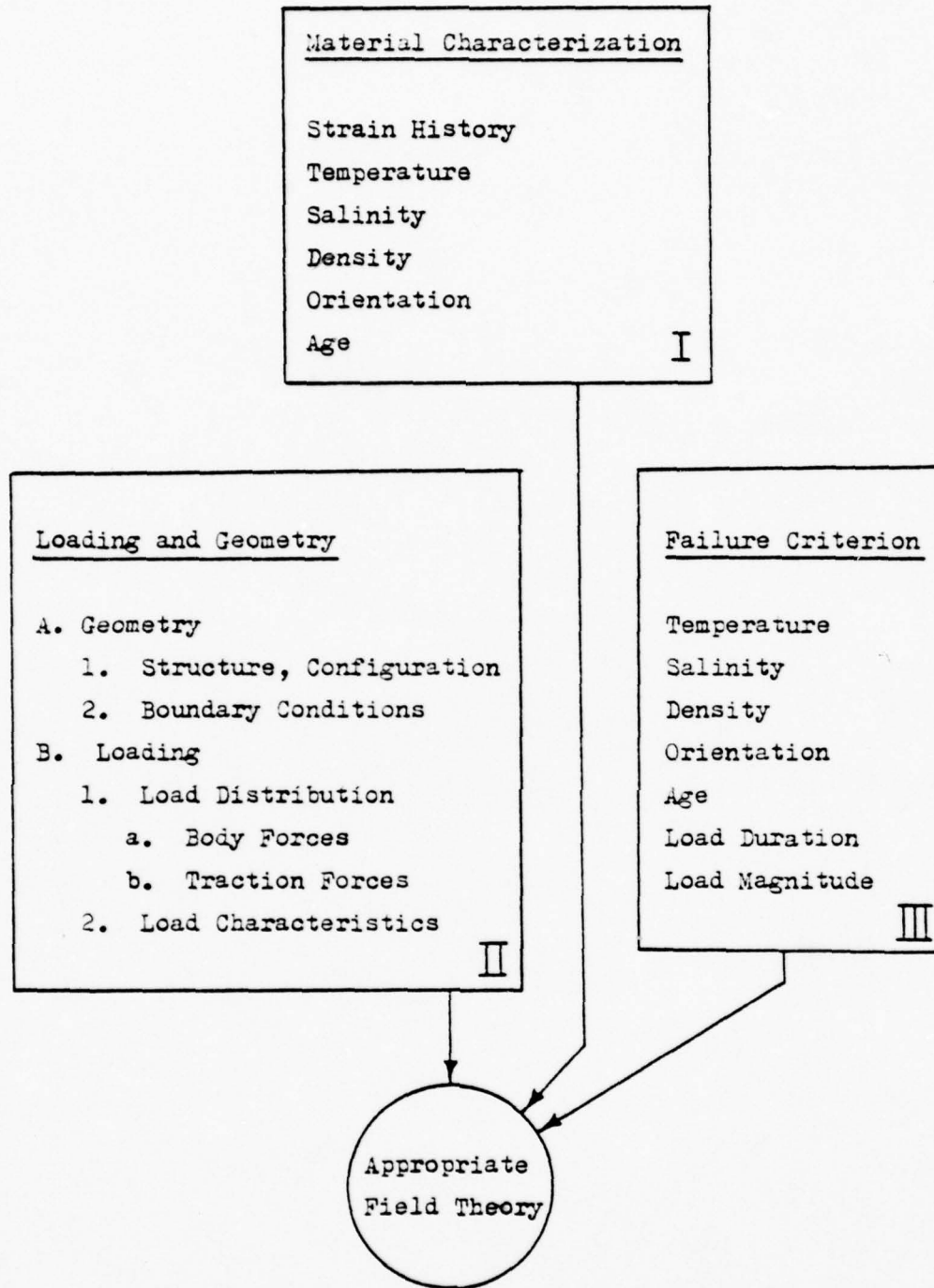


FIGURE 2-1

Parameters to define an appropriate field theory
(after Katona and Vaudrey [18])

F_{ijkl} is a symmetric fourth order tensor functional allowing complete anisotropic formulation

$\epsilon_{kl}(t')$ is the strain tensor history $0 < t' < t$

\underline{X} is the spatial point included for any variation of other parameters

t current time

By exploiting knowledge of sea ice behavior, (2.1) can be reduced to a viscoelastic representation by restricting load magnitude and load duration. Further restriction results in an elastic formulation. The resultant material behavior can be characterized as falling somewhere into Figure 2-2. The quantitative limits of the regions have not yet been experimentally determined.

2.3 Failure

Category III of figure 2-1 requires knowledge of the mode of failure of ice surrounding a circular pile. Most investigators work with an assumption of compression failure of the ice immediately preceding the pile. However, since this failure is quite large with respect to shear or tensile failure in simple tests, it is conceivable that tension or shear failure may precede compressive failure.

Additionally, if it is assumed that the greatest level of force on the pile will be produced at the point of rupture, cracking and large deformation behavior need only be applied for postfailure behavior.

Failure by limiting strain is possible also at levels of force below elastic limits and at larger time durations.

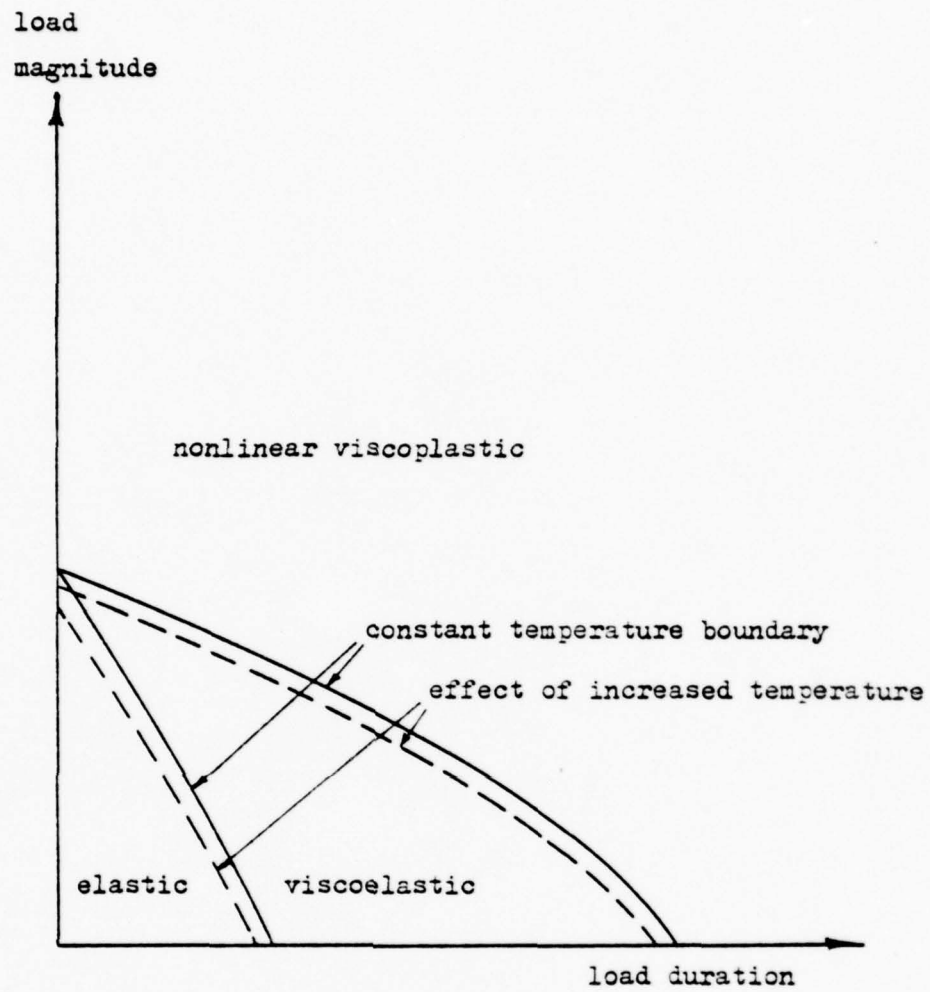


FIGURE 2-2

Effect on domain boundaries by load parameters at a constant temperature (after Katona and Vaudrey [18])

2.4 Material Properties

There is a large gap in the body of knowledge regarding the material properties of ice and nowhere is there a consistent and universally recognized presentation of values. Therefore, for purposes of construction of the model and presentation of results of this thesis, non-dimensional quantities will be used wherever possible. Some representative quantities which may be applied for clarity:

<u>Quantity</u>		<u>Typical Value</u>
Young's modulus	E_{REF}	300,000 psi
Poisson's ratio	ν	.33333
Shear modulus	$\frac{E_{REF}}{2(1+\nu)}$	112,500 psi
Viscous constant	α_{REF}	$1.2788 \times 10^9 \text{ (psi-sec)}^{-1}$
Elastic limit	σ_{yp}	150 psi
Failure by simple:		
• compression		400 psi
• shear		117 psi
• tension		200 psi

These values are not considered to be rate or time dependent for this model formulation, although in general they are.

2.4 Material Properties

There is a large gap in the body of knowledge regarding the material properties of ice and nowhere is there a consistent and universally recognized presentation of values. Therefore, for purposes of construction of the model and presentation of results of this thesis, non-dimensional quantities will be used wherever possible. Some representative quantities which may be applied for clarity:

<u>Quantity</u>		<u>Typical Value</u>
Young's modulus	E_{REF}	300,000 psi
Poisson's ratio	ν	.33333
Shear modulus	$\frac{E_{REF}}{2(1+\nu)}$	112,500 psi
Viscous constant	α_{REF}	$1.2788 \times 10^9 \text{ (psi-sec)}^{-1}$
Elastic limit	σ_{yp}	150 psi
Failure by simple:		
• compression		400 psi
• shear		117 psi
• tension		200 psi

These values are not considered to be rate or time dependent for this model formulation, although in general they are.

CHAPTER 3

Analytical Modelling

In the existing literature, two basic mathematical models were found for the ice sheet - circular pile problem. Both models will be quickly reviewed here and the features and limitations discussed.

3.1 Model of Frederking and Gold

This model, presented by reference [11], draws its basis from the earlier mathematical treatise of Noble and Hussein [24]. In this earlier work, Noble and Hussein derived the exact solution for dual trigonometric (Fourier) series that arise in the solution of a mixed boundary value problem, such as that one depicted in Figure 3-1.

The assumptions and limitations inherent in the analysis of Frederking and Gold are:

- Interface friction is not considered
- Plain strain is assumed
- An infinite elastic medium is used

Unfortunately, the series presented as the solution is reducible only for the special case:

$$\frac{G}{G'} (1-\nu') = (1-2\nu) \quad (3.1)$$

(primed quantities refer to properties of the pile)

Frederking and Gold, however, departed from this analysis early

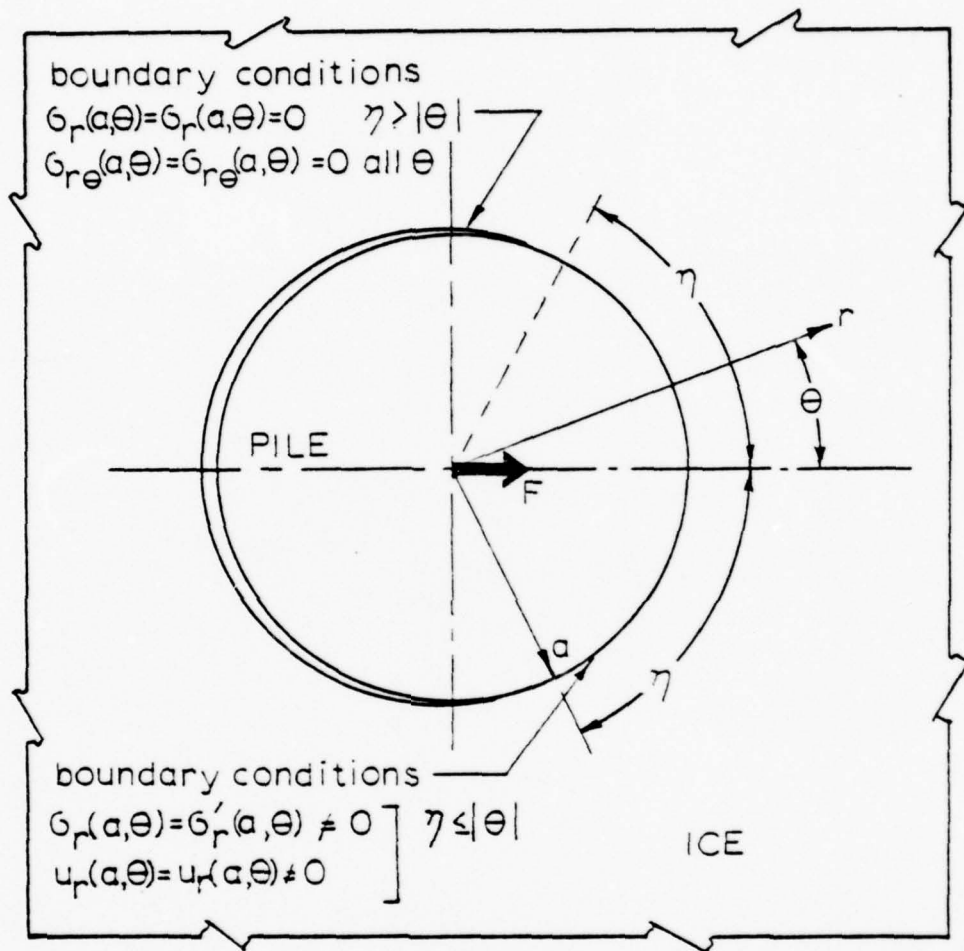


FIGURE 3-1

Indentation geometry (after Frederking and Gold [11])

and used the stress function ϕ suitable for the boundary conditions,

$$\phi = \frac{-F_x}{4\pi(1-\nu)} \left[2(1-\nu)r\theta \sin\theta - (1-2\nu) \left[r \ln r + \frac{a^2}{2r} \right] \cos\theta \right] + D_0 \ln r + \sum_{n=2}^{\infty} \left[\frac{1}{r^n} - \frac{n+1}{n-1} \frac{1}{a^2} \frac{1}{r^{n-2}} \right] D_n \cos n\theta \quad (3.2)$$

[where F_x is total force on the pile concentrated at the center of the rigid pile]

to derive the radial stress and strain. The infinite series of (3.2) was then greatly simplified by assuming a Poisson ratio of .5, whereupon the representation for radial strain at the interface becomes:

$$2G \epsilon_r(a, \theta) = \frac{F_x \cos\theta}{2\pi a} + \frac{D_0}{a^2} \quad (3.3)$$

The constant D_0 can be uniquely determined in terms of F_x .

Frederking and Gold then go on to develop a refinement of (3.3) in which temperature effects, viscoelasticity, and a relation between radial strain and penetration rate are discussed. Finally an equation relating total force:

$$F_x = K(T) L(\theta) \bar{\sigma}_0 \left[\frac{\dot{\epsilon}}{\dot{\epsilon}_0} \right]^{\zeta} a h \quad (3.4)$$

where $K(T)$ is a temperature correction function

ζ is a constant modifying yield stress by strain rate effect

and $L(\theta)$ is a geometry function based on (3.3) given

by:

$$L(\theta) = \int_{-\eta}^{\eta} (\cos \theta)^{1+\frac{1}{2}} d\theta \quad (3.5)$$

here η is the "contact" angle

3.2 Model of Ross, Hanagud, and Sidhu

Ross, et al., [27] considered adaptation of one of their earlier works [34] concerning elastic-plastic plate impact study to the problem of an ice floe surrounding a rigid inclusion. The model chosen for this study is based on a finite difference scheme for the solution of a plane-stress, dynamic problem. The problem is formulated with a two dimensional cartesian network.

The method presented contains the following assumptions, although it is clear that the model is not restricted to these:

- pile is rigid
- loading is by edge dislocation or stress on a finite plate
- perfect adhesion of ice to the pile
- plane stress situation

The method of solution of this dynamic problem is presented in reference [34]. It consists basically of solving the continuity equations for the body forces and hence particle accelerations. The accelerations are translated into strain rates through kinematic relations. Finally the stress-strain relations are used to determine stress rates. These stress

rates are then integrated numerically into new stress quantities whereupon the process is repeated.

3.3 Criteria for the new model

For the development of a model for analysis of the circular pile problem, it is felt that the following items should be incorporated into the ideal:

- The analysis should present variables to include stress, strain, their rates and displacements for the complete spatial distribution and at various time intervals.
- The model should at least be a two dimensional representation and be capable of plane stress or plane strain variation.
- The model should be flexible enough to accept the various material representations of ice including non-linear and time dependent ones.
- Geometrically, the model should be capable of handling mixed boundary values, interface friction, and finite or (semi) infinite sheet formulation.
- Fracture or material failure can be easily be incorporated.
- The model must of course be simple to use and economical to apply.

Unfortunately, these ideals are often mutually exclusive. In the next section and in the subsequent chapters, a model will be developed that meets at least several of the criteria

and will be shown to be useful for application to several ice - circular pile interaction problems.

3.4 Development of the New Model

The model to be developed in chapter four is a departure from the one described by Ross, et al., in section 3-2. The approach used by Ross seemed interesting in that it is capable of meeting several of the criteria required.

The method of solution remained critically dependent on the time integration procedure, however, and any numerical inaccuracies or instabilities would propagate throughout the solution. The dynamic problem also seemed inappropriate for study of slowly varying stress fields. Lastly, Ross gives no results for his dynamic problem.

The model proposed in this thesis, although similar in conception to Ross', exploits the radial symmetry associated with the physical problem to work in only one dimension. The method of solution is greatly dissimilar in that it does not treat the dynamic problem and uses a linear system of equations to arrive at the final result. The new model also treats the case of linear viscous behavior and has capabilities of extension into other material behavior.

CHAPTER 4

Development of a Finite DifferenceElastic Constitutive Model4.1 General

The equilibrium equations by Wang, reference [31], are applied to the element depicted in Figures 4-1 through 4-4. In two dimensional polar co-ordinates:

$$\frac{\partial G_r}{\partial r} + \frac{1}{r} \frac{\partial G_{r\theta}}{\partial \theta} + \frac{G_r - G_\theta}{r} = \rho \ddot{u}_r \quad (4.1)$$

$$\frac{1}{r} \frac{\partial G_\theta}{\partial \theta} + \frac{\partial G_{r\theta}}{\partial r} + \frac{2}{r} G_{r\theta} = \rho \ddot{u}_\theta \quad (4.2)$$

The right hand sides are body forces; the dots indicate differentiation with respect to time.

Since sea ice is a transversely orthotropic material, variation of mechanical properties in the Z Co-ordinate direction will be due mainly to salinity variation, temperature profile, and non-uniform thickness. For the purpose of this study, however, the ice sheet will be considered to be uniform in thickness with zero temperature gradient. (Extensions of the present model to account for these effects are possible.) For this reason, development of (4.1) and (4.2) into a two dimensional plane stress model is an appropriate choice.

Before proceeding, it is perhaps worthwhile to state the assumptions of a plane stress formulation:

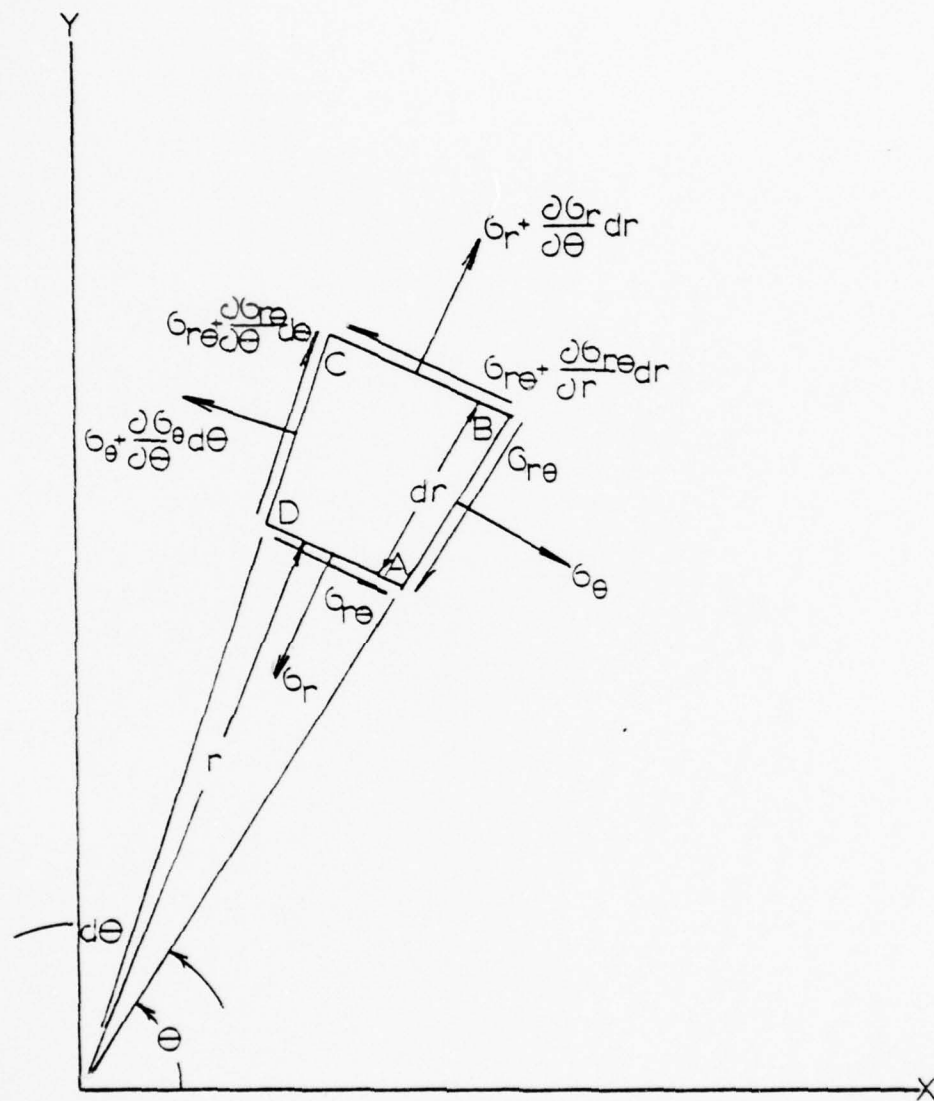


FIGURE 4-1

Stresses acting on a small element ABCD in polar coordinates

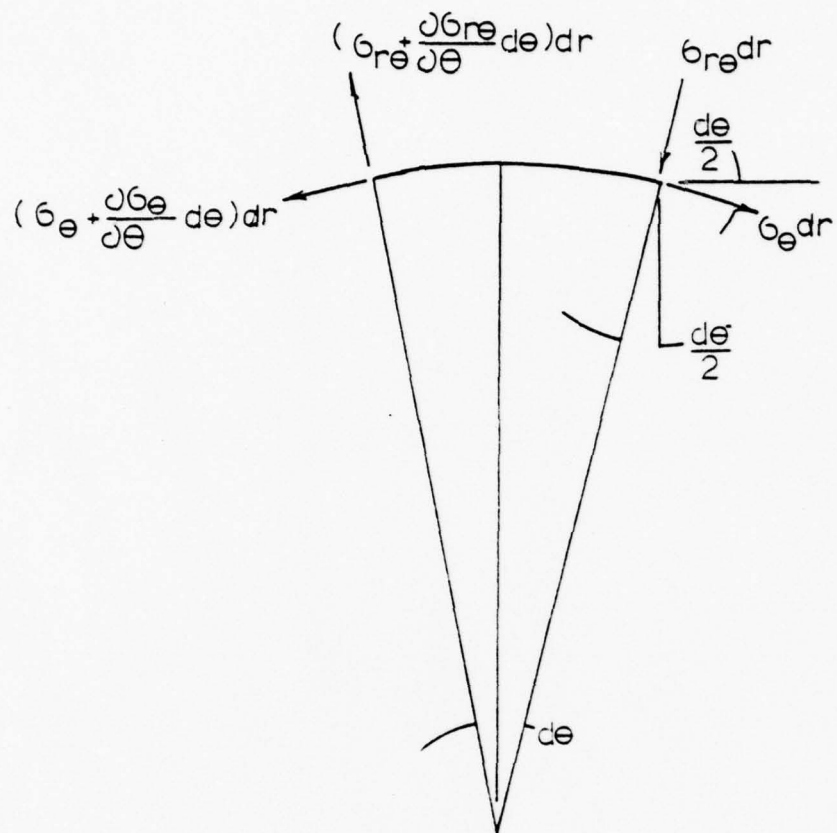


FIGURE 4-2

Variation of direct and shear stress with angular change

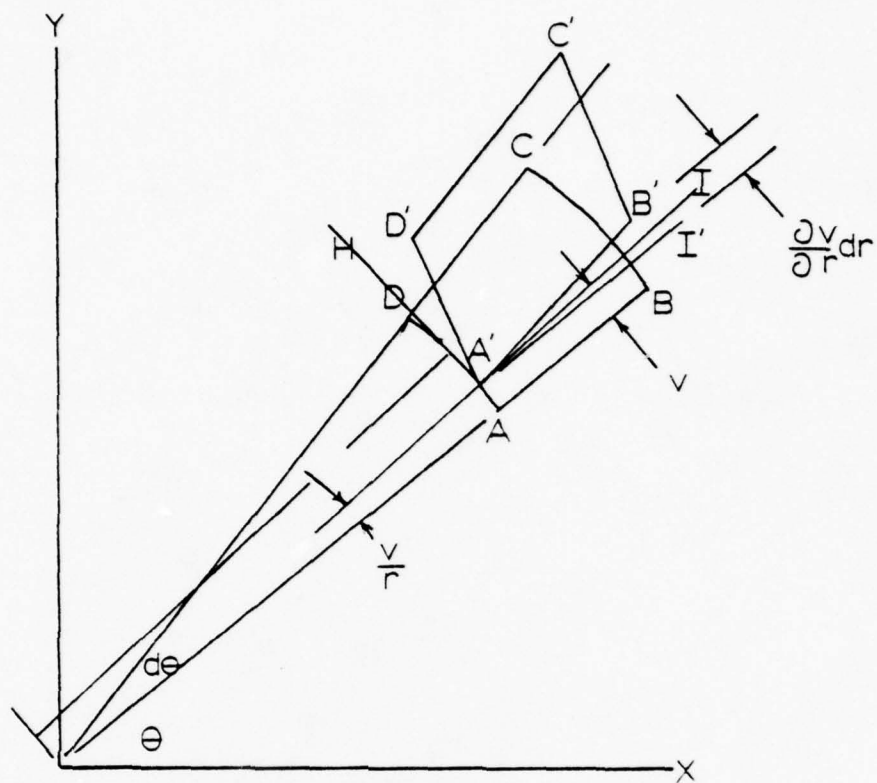


FIGURE 4-3
Compatibility relationship

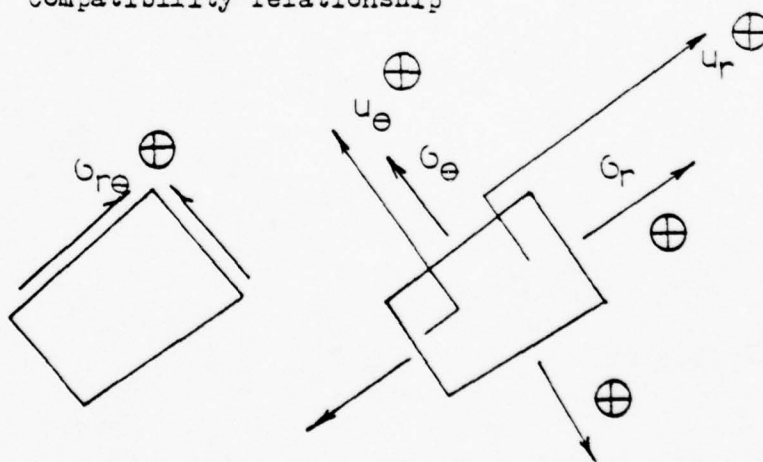


FIGURE 4-4
Sign convention

- $\sigma_z, \sigma_{rz}, \sigma_{\theta z}$ are zero on both faces of the sheet
- Therefore, $\sigma_z, \sigma_{rz}, \sigma_{\theta z}$ are zero throughout the sheet.
- The state of stress can be specified by $\sigma_r, \sigma_\theta, \sigma_{r\theta}$ only and variations of these quantities are independent of vertical position.

4.2 Development of the Plane Stress Elastic Model

After Wang [31], the strain-displacement relations for small deformations are:

$$\epsilon_r = \frac{\partial}{\partial r} u_r \quad (4.3)$$

$$\epsilon_\theta = \frac{u_r}{r} + \frac{1}{r} \frac{\partial}{\partial \theta} u_\theta \quad (4.4)$$

$$\epsilon_{r\theta} = \frac{1}{r} \frac{\partial}{\partial \theta} u_r + \frac{\partial}{\partial r} u_\theta - \frac{u_\theta}{r} \quad (4.5)$$

Stress-strain relationships dictated by the plane stress assumption:

$$\epsilon_r = \frac{1}{E} (\sigma_r - \nu \sigma_\theta) \quad (4.6)$$

$$\epsilon_\theta = \frac{1}{E} (\sigma_\theta - \nu \sigma_r) \quad (4.7)$$

$$\epsilon_{r\theta} = \frac{2(1+\nu)}{E} \sigma_{r\theta} \quad (4.8)$$

Combining (4.1) through (4.8), the following five equations are obtained.

$$\frac{\partial}{\partial r} \sigma_r + \frac{1}{r} \frac{\partial}{\partial \theta} \sigma_{re} + \frac{\sigma_r - \sigma_\theta}{r} = 0 \quad (4.9)$$

$$\frac{1}{r} \frac{\partial}{\partial \theta} \sigma_\theta + \frac{\partial}{\partial r} \sigma_{re} + \frac{2}{r} \sigma_{re} = 0 \quad (4.10)$$

$$\frac{\partial}{\partial r} u_r - \frac{1}{E} (\sigma_r - \nu \sigma_\theta) = 0 \quad (4.11)$$

$$\frac{1}{r} u_r + \frac{1}{r} \frac{\partial}{\partial \theta} u_\theta - \frac{1}{E} (\sigma_\theta - \nu \sigma_r) = 0 \quad (4.12)$$

$$\frac{1}{r} \frac{\partial}{\partial \theta} u_r + \frac{\partial}{\partial r} u_\theta - \frac{1}{r} u_\theta - \frac{2(1+\nu)}{E} \sigma_{re} = 0 \quad (4.13)$$

The body forces expressed in (4.1) and (4.2) were set to zero since it is not the purpose of this study to expose dynamic considerations or impact shock. For the range of validity of this model, inertial effects are negligible.

Equations (4.9) through (4.13) (or their cartesian counterparts) could be attacked directly in finite difference form, but the ensuing number of equations would be quite large and difficult to apply.

If boundary conditions are not to be mixed at a continuous boundary, a Fourier simplification is possible:

Let σ_r, σ_θ and u_r be expressed as a Fourier cosine (even) series,

Let σ_{re}, u_θ be expressed as a Fourier sine (odd) series,

$$\phi_r(r, \theta) = \sum_{m=0}^{\infty} \phi_{r_m}(r) \cos m\theta \quad (4.14)$$

ϕ_θ, u_r are similar

$$\phi_{re}(r, \theta) = \sum_{m=0}^{\infty} \phi_{re_m}(r) \sin m\theta \quad (4.15)$$

u_θ is similar

It is then possible to express (4.9):

$$\begin{aligned} & \frac{\partial}{\partial r} \left[\sum_{m=0}^{\infty} \phi_{r_m}(r) \cos m\theta \right] + \frac{1}{r} \frac{\partial}{\partial \theta} \left[\sum_{m=1}^{\infty} \phi_{re_m}(r) \sin m\theta \right] + \\ & + \frac{1}{r} \left[\sum_{m=0}^{\infty} \phi_{r_m}(r) \cos m\theta \right] - \frac{1}{r} \left[\sum_{m=0}^{\infty} \phi_{\theta_m}(r) \cos m\theta \right] = 0 \end{aligned} \quad (4.16)$$

which reduces to:

$$\begin{aligned} & \sum_{m=0}^{\infty} \frac{\partial}{\partial r} \phi_{r_m} \cos m\theta + \frac{m}{r} \sum_{m=1}^{\infty} \phi_{re_m} \cos m\theta + \\ & + \frac{1}{r} \sum_{m=0}^{\infty} (\phi_{r_m} - \phi_{\theta_m}) \cos m\theta \end{aligned} \quad (4.17)$$

Finally:

$$\left\{ \frac{\partial}{\partial r} \phi_{r_0} + 0 + \frac{1}{r} (\phi_{r_0} - \phi_{\theta_0}) \right\} = 0$$

$$\begin{aligned}
& \left\{ \frac{\partial}{\partial r} \phi_{r_1} + \frac{1}{r} \phi_{\theta_1} + \frac{1}{r} (\phi_{r_1} - \phi_{\theta_1}) \right\} \cos \theta \\
& \left\{ \frac{\partial}{\partial r} \phi_{r_2} + \frac{2}{r} \phi_{\theta_2} + \frac{1}{r} (\phi_{r_2} - \phi_{\theta_2}) \right\} \cos 2\theta \\
& \quad \cdot \quad \cdot \quad \cdot \\
& \quad \cdot \quad \cdot \quad \cdot
\end{aligned}
\tag{4.18}$$

Thus ϕ_{r_m} can be expressed as an equation relating only like wavenumbers. The set of solutions unique to each wavenumber can then be reconstituted into a Fourier series by using an appropriate number of waves.

Equations (4.10) through (4.13) can similarly be transformed into an infinite number of sets of five equations:

$$\left[\begin{aligned}
& \frac{\partial}{\partial r} \phi_{r_m} + \frac{m}{r} \phi_{\theta_m} + \frac{\phi_{r_m} - \phi_{\theta_m}}{r} \\
& - \frac{m}{r} \phi_{\theta_m} + \frac{\partial}{\partial r} \phi_{\theta_m} + \frac{2}{r} \phi_{\theta_m} \\
& \frac{\partial}{\partial r} u_{r_m} - \frac{1}{E} (\phi_{r_m} - \nu \phi_{\theta_m}) \\
& \frac{1}{r} u_{r_m} + \frac{m}{r} u_{\theta_m} - \frac{1}{E} (\phi_{\theta_m} - \nu \phi_{r_m}) \\
& - \frac{m}{r} u_{r_m} + \frac{\partial}{\partial r} u_{\theta_m} - \frac{1}{r} u_{\theta_m} - \frac{2(1+\nu)}{E} \phi_{\theta_m}
\end{aligned} \right] \tag{4.19}$$

= 0

($0 \leq m \leq \infty$)

$\sigma_{\theta m}$ in the fourth row of (4.19) can be explicitly expressed as:

$$\sigma_{\theta m} = \frac{E}{r} u_{r m} + \frac{E m}{r} u_{\theta m} + \nu \sigma_{r m} \quad (4.20)$$

Since no equation contains a derivative of $\sigma_{\theta m}$, this variable can be eliminated, yielding:

$$\begin{bmatrix} \frac{\partial}{\partial r} \sigma_r + \left(\frac{1-\nu}{r}\right) \sigma_r + \left(\frac{m}{r}\right) \sigma_{r\theta} + \left(\frac{-E}{r^2}\right) u_r + \left(\frac{-Em}{r^2}\right) u_\theta \\ \frac{\partial}{\partial r} \sigma_{r\theta} + \left(\frac{-m\nu}{r}\right) \sigma_r + \left(\frac{2}{r}\right) \sigma_{r\theta} + \left(\frac{-mE}{r^2}\right) u_r + \left(\frac{-Em^2}{r^2}\right) u_\theta \\ \frac{\partial}{\partial r} u_r + \left(\frac{\nu^2-1}{E}\right) \sigma_r + (0) \sigma_{r\theta} + \left(\frac{\nu}{r}\right) u_r + \left(\frac{\nu m}{r}\right) u_\theta \\ \frac{\partial}{\partial r} u_\theta + (0) \sigma_r + \left(\frac{-2(1+\nu)}{E}\right) \sigma_{r\theta} + \left(\frac{-m}{r}\right) u_r + \left(\frac{-1}{r}\right) u_\theta \end{bmatrix} \quad (4.21)$$

= 0

Let the vector \underline{Z}_m represent:

$0 \leq m \leq \infty$

$$\underline{Z}_m = \begin{Bmatrix} \sigma_{r m} \\ \sigma_{r\theta m} \\ u_{r m} \\ u_{\theta m} \end{Bmatrix} \quad (4.22)$$

Then (4.21) becomes the set of linear equations:

$$\frac{\partial}{\partial r} [I] \underline{Z}_m + [A] \underline{Z}_m = \underline{0} \quad (4.23)$$

where $[I]$ is the 4×4 identity matrix and

where $[\Delta]$ is expressed by the equation:

$$[A] = \begin{bmatrix} \frac{1-\nu}{r} & \frac{m}{r} & \frac{E}{r^2} & -\frac{Em}{r^2} \\ \frac{-m\nu}{r} & \frac{2}{r} & -\frac{mE}{r^2} & -\frac{Em^2}{r^2} \\ \frac{-(1-\nu^2)}{E} & 0 & \frac{\nu}{r} & \frac{\nu m}{r} \\ 0 & -\frac{2(1+\nu)}{E} & -\frac{m}{r} & -\frac{1}{r} \end{bmatrix} \quad (4.24)$$

(4.23) represents an infinite set of 4 simultaneous first order linear differential equations. It can be seen that two spatial variables would result in an equation relating a derivative in Θ as well.

The system of equations expressed by (4.23) can only be solved numerically.

4.3 Numerical Solution of the Plane Stress Elastic Model

The method of finite differences will be exploited to solve equation (4.23)

Considering the finite mesh scheme presented in Figure 4-5 and in Figure 4-6, the appropriate difference equations valid at the nodes are expressed:

$$\frac{1}{2h} [I] \left\{ -3 \underline{\underline{Z}}_m^1 + 4 \underline{\underline{Z}}_m^2 - \underline{\underline{Z}}_m^3 \right\} + [A] \underline{\underline{Z}}_m^1 = \underline{\underline{0}}$$

valid at node 1

(4.25)

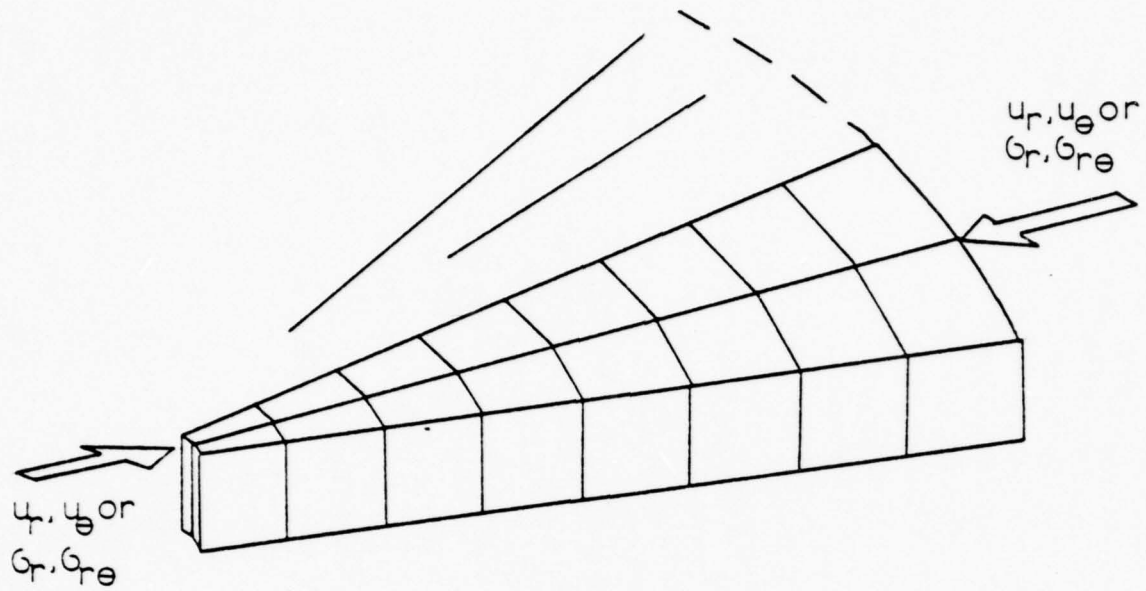


FIGURE 4-5

Finite difference representation

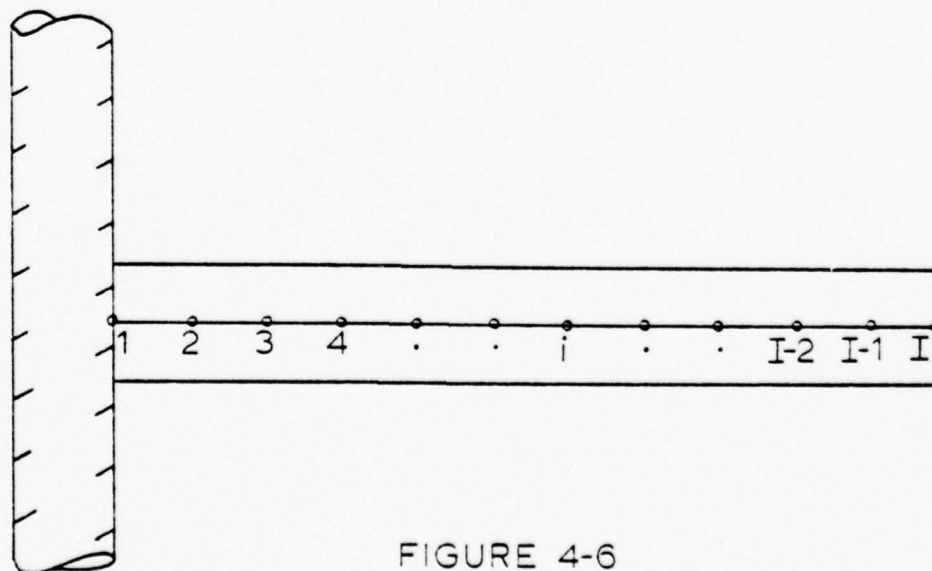


FIGURE 4-6

Node numbering scheme

$$\frac{1}{2h}[I] \left\{ 3 \underline{\underline{Z}}_m^I - 4 \underline{\underline{Z}}_m^{I-1} + \underline{\underline{Z}}_m^{I-2} \right\} + [A] \underline{\underline{Z}}_m^I = \underline{\underline{0}} \quad (4.26)$$

valid at the I-th or last node,
and the central difference

$$\frac{1}{2h}[I] \left\{ \underline{\underline{Z}}_m^{i+1} - \underline{\underline{Z}}_m^{i-1} \right\} + [A] \underline{\underline{Z}}_m^i = \underline{\underline{0}} \quad (4.27)$$

valid at all interior nodes.

Recasting equations (4.25), (4.27), and (4.26):

$$\left\{ [A] - \frac{3}{2h}[I] \right\} \underline{\underline{Z}}_m^1 + \frac{2}{h}[I] \underline{\underline{Z}}_m^2 - \frac{1}{2h}[I] \underline{\underline{Z}}_m^3 = \underline{\underline{0}} \quad (4.28)$$

$$-\frac{1}{2h}[I] \underline{\underline{Z}}_m^{i-1} + [A] \underline{\underline{Z}}_m^i + \frac{1}{2h}[I] \underline{\underline{Z}}_m^{i+1} = \underline{\underline{0}} \quad (4.29)$$

$$\frac{1}{2h}[I] \underline{\underline{Z}}_m^{I-2} - \frac{2}{h}[I] \underline{\underline{Z}}_m^{I-1} + \left\{ [A] + \frac{3}{2h}[I] \right\} \underline{\underline{Z}}_m^I = \underline{\underline{0}} \quad (4.30)$$

Equations (4.28), (4.29), and (4.30) are then loaded into a suitable simultaneous equation - matrix representation as shown in Figure 4-7.

This representation is then expanded into the full coefficient matrix shown in Figure 4-8. It should be noted that even the simplest scheme, a three node model, will require

$$\begin{bmatrix} [A] \left| -\frac{3}{2h}[I] \right|_{r_{\Theta i=1}} & \frac{2}{h}[I] & -\frac{1}{2h}[I] & . & . \\ -\frac{1}{2h}[I] & [A] \left| \right|_{r_{\Theta i=2}} & \frac{1}{2h}[I] & . & . \\ -\frac{1}{2h}[I] & \frac{-1}{2h}[I] & [A] \left| \right|_{r_{\Theta i=3}} & \frac{1}{2h}[I] & . \\ . & . & . & . & . \\ . & . & . & . & . \end{bmatrix}$$

FIGURE 4-7

The system of linear equations - before expansion

	1	2	3	4	5	6	7	8	9	10	11	12			
1	B_{11}	B_{12}	B_{13}	B_{14}	$\frac{2}{h}$	0	0	0	$-\frac{1}{2h}$	0	0	0	.	.	.
2	B_{21}	B_{22}	B_{23}	B_{24}	0	$\frac{2}{h}$	0	0	0	$-\frac{1}{2h}$	0	0	.	.	.
3	B_{31}	B_{32}	B_{33}	B_{34}	0	0	$\frac{2}{h}$	0	0	0	$-\frac{1}{2h}$	0	.	.	.
4	B_{41}	B_{42}	B_{43}	B_{44}	0	0	0	$\frac{2}{h}$	0	0	0	$-\frac{1}{2h}$.	.	.
5	$-\frac{1}{2h}$	0	0	0	A_{11}	A_{12}	A_{13}	A_{14}	$\frac{1}{2h}$	0	0	0	.	.	.
6	0	$-\frac{1}{2h}$	0	0	A_{21}	A_{22}	A_{23}	A_{24}	0	$\frac{1}{2h}$	0	0	.	.	.
7	0	0	$-\frac{1}{2h}$	0	A_{31}	A_{32}	A_{33}	A_{34}	0	0	$\frac{1}{2h}$	0	.	.	.
8	0	0	0	$-\frac{1}{2h}$	A_{41}	A_{42}	A_{43}	A_{44}	0	0	0	$\frac{1}{2h}$.	.	.
9	.	.	.	$-\frac{1}{2h}$	0	0	0	A_{11}	A_{12}	A_{13}	A_{14}	$\frac{1}{2h}$	0	0	0
10	.	.	.	0	$-\frac{1}{2h}$	0	0	A_{21}	A_{22}	A_{23}	A_{24}	0	$\frac{1}{2h}$	0	0
11	.	.	.	0	0	$-\frac{1}{2h}$	0	A_{31}	A_{32}	A_{33}	A_{34}	0	0	$\frac{1}{2h}$	0
12	.	.	.	0	0	0	$-\frac{1}{2h}$	A_{41}	A_{42}	A_{43}	A_{44}	0	0	0	$\frac{1}{2h}$
.	$-\frac{1}{2h}$	0	0	0	A_{11}	A_{12}	A_{13}	A_{14}
.
.
4(I-1)-3	.	$-\frac{1}{2h}$	0	0	0	A_{11}	A_{12}	A_{13}	A_{14}	$\frac{1}{2h}$	0	0	0	.	.
4(I-1)-2	.	0	$-\frac{1}{2h}$	0	0	A_{21}	A_{22}	A_{23}	A_{24}	0	$\frac{1}{2h}$	0	0	.	.
4(I-1)-1	.	0	0	$-\frac{1}{2h}$	0	A_{31}	A_{32}	A_{33}	A_{34}	0	0	$\frac{1}{2h}$	0	.	.
4(I-1)	.	0	0	0	$-\frac{1}{2h}$	A_{41}	A_{42}	A_{43}	A_{44}	0	0	0	$\frac{1}{2h}$.	.
4I-3	.	$\frac{1}{2h}$	0	0	0	$\frac{2}{h}$	0	0	0	C_{11}	C_{12}	C_{13}	C_{14}	.	.
4I-2	.	0	$\frac{1}{2h}$	0	0	0	$\frac{2}{h}$	0	0	C_{21}	C_{22}	C_{23}	C_{24}	.	.
4I-1	.	0	0	$\frac{1}{2h}$	0	0	0	$\frac{2}{h}$	0	C_{31}	C_{32}	C_{33}	C_{34}	.	.
4I	.	0	0	0	$\frac{1}{2h}$	0	0	0	$\frac{2}{h}$	C_{41}	C_{42}	C_{43}	C_{44}	.	.

FIGURE 4-8

Expanded matrix representation

reduction of a 144 element square matrix (12 equations in 12 unknowns). Even a numerical scheme such as the Gauss elimination or the Gauss-Jordan reduction scheme is too laborious for hand calculation, so a machine solution must be employed.

Figure 4-8 represents the expansion of equations (4.28) through (4.30). The elements noted represent the corresponding position in (4.24). As an example:

$$\overset{2}{\underset{33}{A}} = \frac{r}{r} \quad \left| \quad r \text{ is evaluated at node } 2 \right.$$

Elements labeled B_{ij} or C_{ij} represent modification to $[A]$ required by forward difference and backward difference equations (4.25) and (4.26). The matrix is a square matrix distinguished by a band twelve elements wide. Even for a small number of node equations the ensuing sparse matrix is wasteful in space and computation time. Consequently the representation in Figure 4-8 is further compressed to a band storage array depicted in Figure 4-9.

4.4 Non-dimensionalization

In order to produce array elements of approximately the same order of magnitude, (4.23) was converted to non-dimensional form by the following conversion:

$$\text{on stress} \quad \frac{\sigma}{\sigma_{REF}} = \bar{\sigma} \quad (\text{non-dimensional})$$

$$\text{where} \quad \sigma_{REF} = E_{REF}$$

	1	2	3	4	5	6	7	8	9	10	11	12	13	14	15	16	17
1	0	0	0	0	0	0	0	0	$\frac{1}{h_{11}}$	$\frac{1}{h_{12}}$	$\frac{1}{h_{13}}$	$\frac{1}{h_{14}}$	$\frac{2}{h}$	0	0	0	$-\frac{1}{2h}$
2	0	0	0	0	0	0	0	$\frac{1}{h_{21}}$	$\frac{1}{h_{22}}$	$\frac{1}{h_{23}}$	$\frac{1}{h_{24}}$	0	$\frac{2}{h}$	0	0	0	$-\frac{1}{2h}$
3	0	0	0	0	0	0	$\frac{1}{h_{31}}$	$\frac{1}{h_{32}}$	$\frac{1}{h_{33}}$	$\frac{1}{h_{34}}$	0	0	$\frac{2}{h}$	0	0	0	$-\frac{1}{2h}$
4	0	0	0	0	0	$\frac{1}{h_{41}}$	$\frac{1}{h_{42}}$	$\frac{1}{h_{43}}$	$\frac{1}{h_{44}}$	0	0	0	$\frac{2}{h}$	0	0	0	$-\frac{1}{2h}$
5	0	0	0	0	$-\frac{1}{2h}$	0	0	0	$\frac{2}{h_{11}}$	$\frac{2}{h_{12}}$	$\frac{2}{h_{13}}$	$\frac{2}{h_{14}}$	$\frac{1}{2h}$	0	0	0	0
6	0	0	0	0	$-\frac{1}{2h}$	0	0	$\frac{2}{h_{21}}$	$\frac{2}{h_{22}}$	$\frac{2}{h_{23}}$	$\frac{2}{h_{24}}$	0	$\frac{1}{2h}$	0	0	0	0
7	0	0	0	0	$-\frac{1}{2h}$	0	$\frac{2}{h_{31}}$	$\frac{2}{h_{32}}$	$\frac{2}{h_{33}}$	$\frac{2}{h_{34}}$	0	0	$\frac{1}{2h}$	0	0	0	0
8	0	0	0	0	$-\frac{1}{2h}$	$\frac{2}{h_{41}}$	$\frac{2}{h_{42}}$	$\frac{2}{h_{43}}$	$\frac{2}{h_{44}}$	0	0	0	$\frac{1}{2h}$	0	0	0	0
9	0	0	0	0	$-\frac{1}{2h}$	0	0	0	$\frac{3}{h_{11}}$	$\frac{3}{h_{12}}$	$\frac{3}{h_{13}}$	$\frac{3}{h_{14}}$	$\frac{1}{2h}$	0	0	0	0
10	0	0	0	0	$-\frac{1}{2h}$	0	0	$\frac{3}{h_{21}}$	$\frac{3}{h_{22}}$	$\frac{3}{h_{23}}$	$\frac{3}{h_{24}}$	0	$\frac{1}{2h}$	0	0	0	0
11	0	0	0	0	$-\frac{1}{2h}$	0	$\frac{3}{h_{31}}$	$\frac{3}{h_{32}}$	$\frac{3}{h_{33}}$	$\frac{3}{h_{34}}$	0	0	$\frac{1}{2h}$	0	0	0	0
12	0	0	0	0	$-\frac{1}{2h}$	$\frac{3}{h_{41}}$	$\frac{3}{h_{42}}$	$\frac{3}{h_{43}}$	$\frac{3}{h_{44}}$	0	0	0	$\frac{1}{2h}$	0	0	0	0
13	0	0	0	0	$-\frac{1}{2h}$	0	0	0	$\frac{4}{h_{11}}$	$\frac{4}{h_{12}}$	$\frac{4}{h_{13}}$	$\frac{4}{h_{14}}$	$\frac{1}{2h}$	0	0	0	0
.
4(I-2) -3	0	0	0	0	$-\frac{1}{2h}$	0	0	0	$\frac{I-2}{h_{11}}$	$\frac{I-2}{h_{12}}$	$\frac{I-2}{h_{13}}$	$\frac{I-2}{h_{14}}$	$\frac{1}{2h}$	0	0	0	0
4(I-2) -2	0	0	0	0	$-\frac{1}{2h}$	0	0	$\frac{I-2}{h_{21}}$	$\frac{I-2}{h_{22}}$	$\frac{I-2}{h_{23}}$	$\frac{I-2}{h_{24}}$	0	$\frac{1}{2h}$	0	0	0	0
4(I-2) -1	0	0	0	0	$-\frac{1}{2h}$	0	$\frac{I-2}{h_{31}}$	$\frac{I-2}{h_{32}}$	$\frac{I-2}{h_{33}}$	$\frac{I-2}{h_{34}}$	0	0	$\frac{1}{2h}$	0	0	0	0
4(I-2)	0	0	0	0	$-\frac{1}{2h}$	$\frac{I-2}{h_{41}}$	$\frac{I-2}{h_{42}}$	$\frac{I-2}{h_{43}}$	$\frac{I-2}{h_{44}}$	0	0	0	$\frac{1}{2h}$	0	0	0	0
4(I-1) -3	0	0	0	0	$-\frac{1}{2h}$	0	0	0	$\frac{I-1}{h_{11}}$	$\frac{I-1}{h_{12}}$	$\frac{I-1}{h_{13}}$	$\frac{I-1}{h_{14}}$	$\frac{1}{2h}$	0	0	0	0
4(I-1) -2	0	0	0	0	$-\frac{1}{2h}$	0	0	$\frac{I-1}{h_{21}}$	$\frac{I-1}{h_{22}}$	$\frac{I-1}{h_{23}}$	$\frac{I-1}{h_{24}}$	0	$\frac{1}{2h}$	0	0	0	0
4(I-1) -1	0	0	0	0	$-\frac{1}{2h}$	0	$\frac{I-1}{h_{31}}$	$\frac{I-1}{h_{32}}$	$\frac{I-1}{h_{33}}$	$\frac{I-1}{h_{34}}$	0	0	$\frac{1}{2h}$	0	0	0	0
4(I-1)	0	0	0	0	$-\frac{1}{2h}$	$\frac{I-1}{h_{41}}$	$\frac{I-1}{h_{42}}$	$\frac{I-1}{h_{43}}$	$\frac{I-1}{h_{44}}$	0	0	0	$\frac{1}{2h}$	0	0	0	0
4I-3	$\frac{1}{2h}$	0	0	0	$-\frac{2}{h}$	0	0	0	$\frac{I}{h_{11}}$	$\frac{I}{h_{12}}$	$\frac{I}{h_{13}}$	$\frac{I}{h_{14}}$	0	0	0	0	0
4I-2	$\frac{1}{2h}$	0	0	0	$-\frac{2}{h}$	0	0	$\frac{I}{h_{21}}$	$\frac{I}{h_{22}}$	$\frac{I}{h_{23}}$	$\frac{I}{h_{24}}$	0	0	0	0	0	0
4I-1	$\frac{1}{2h}$	0	0	0	$-\frac{2}{h}$	0	$\frac{I}{h_{31}}$	$\frac{I}{h_{32}}$	$\frac{I}{h_{33}}$	$\frac{I}{h_{34}}$	0	0	0	0	0	0	0
4I	$\frac{1}{2h}$	0	0	0	$-\frac{2}{h}$	$\frac{I}{h_{41}}$	$\frac{I}{h_{42}}$	$\frac{I}{h_{43}}$	$\frac{I}{h_{44}}$	0	0	0	0	0	0	0	0

FIGURE 4-9

Matrix in the band representation

E_{REF} is taken as the average Young's modulus through the thickness, and length is non-dimensional by

$$\frac{L}{L_{REF}} = \bar{L} \quad (\text{non-dimensional})$$

where $L = R_{IN}$ or inner radius

Equation (4.23) becomes non-dimensional and the coefficient matrix (4.24) becomes:

$$\begin{bmatrix} \frac{1-\nu}{RAD} & \frac{m}{RAD} & \frac{-1}{RAD^2} & \frac{-m}{RAD^2} \\ \frac{-m\nu}{RAD} & \frac{2}{RAD} & \frac{-m}{RAD^2} & \frac{-m^2}{RAD^2} \\ \nu^2-1 & 0 & \frac{\nu}{RAD} & \frac{\nu m}{RAD} \\ 0 & -2(1+\nu) & \frac{-m}{RAD} & \frac{-1}{RAD} \end{bmatrix} \quad (4.31)$$

Here

$$RAD = 1 + (i-1)\left(\frac{R_{out}}{R_{IN}} - 1\right) \frac{1}{h} \quad (4.32)$$

and will vary within the array according to node position i .

4.5 Machine Solution

Equation (4.23) was implemented in a Fortran language subroutine called elastic. For reasons discussed in the next section, the number of nodes used was 400. Consequently the core storage requirements in double precision amounts to approximately 60K words.

Solution of (4.23) was by means of an I.M.S.L. subroutine called LEQTLB [16]. This method of solution of a system of linear equation is described by [23] as the Crout factorization. The Crout factorization is similar to Gauss reduction methods but the lower triangular decomposition is used instead. Partial pivoting and row normalization are employed.

LEQTLB was slightly modified into a double precision routine and labeled dpband by the author. This routine is included as an integral part of subroutine elastic and is listed in Appendix A.

Subroutine elastic was written for the multics system implemented on a Honeywell 6180 used by the Massachusetts Institute of Technology Information Processing Center. Approximate CPU time for one solution was 16 seconds.

A flow chart for subroutine elastic is presented in Figure 4-10. A symbol table, description of common blocks, listing, and a user's guide are included in Appendices A-1 through A-4.

4-6 Numerical Stability

The number of stations chosen is 400. Table 4-I and Figure 4-11 illustrate the convergence of the numerical solution as the number of stations is increased for the particular case of zero wavenumber. Having checked the convergence of the numerical solution, the question now is

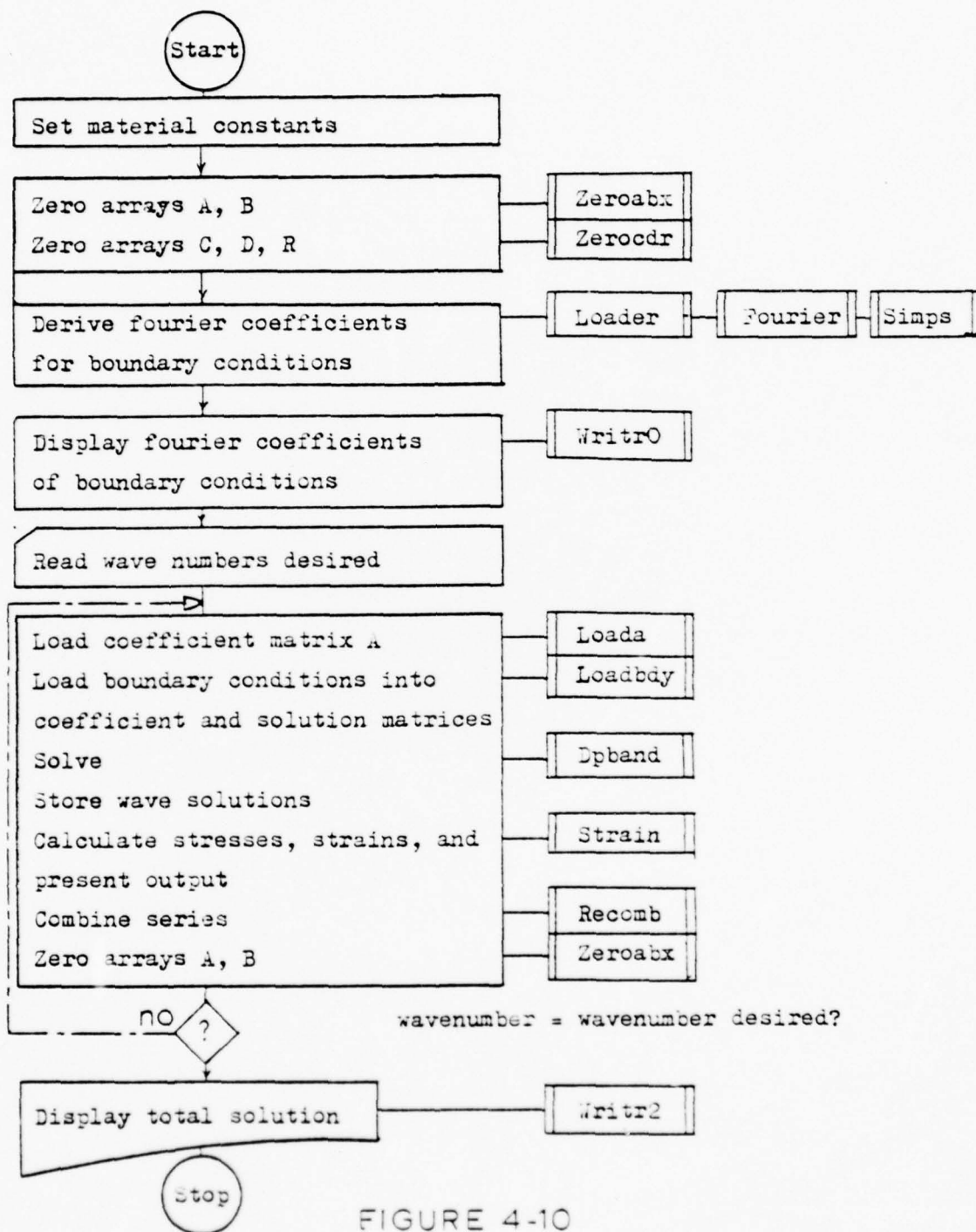
Subroutine Elastic

FIGURE 4-10

Block diagram for subroutine Elastic

Table 4-I

Wavenumber	Maximum Oscillation (per cent)
------------	-----------------------------------

0	0.0075
1	1.7500
2	0.0000
3	0.0000
4	0.0000
5	0.0000
6	0.0000
7	0.0000
8	0.0000
9	0.0000
10	0.0000

Radius - outer = 20.

Radius - inner = 1.

$u_r = u_\theta = 0.$ inner boundary

$G_r = -.66666667$ outer boundary

$G_\theta = 0.$ outer boundary

Maximum oscillation in numerical solution by wavenumber
(solution carried to five digits)

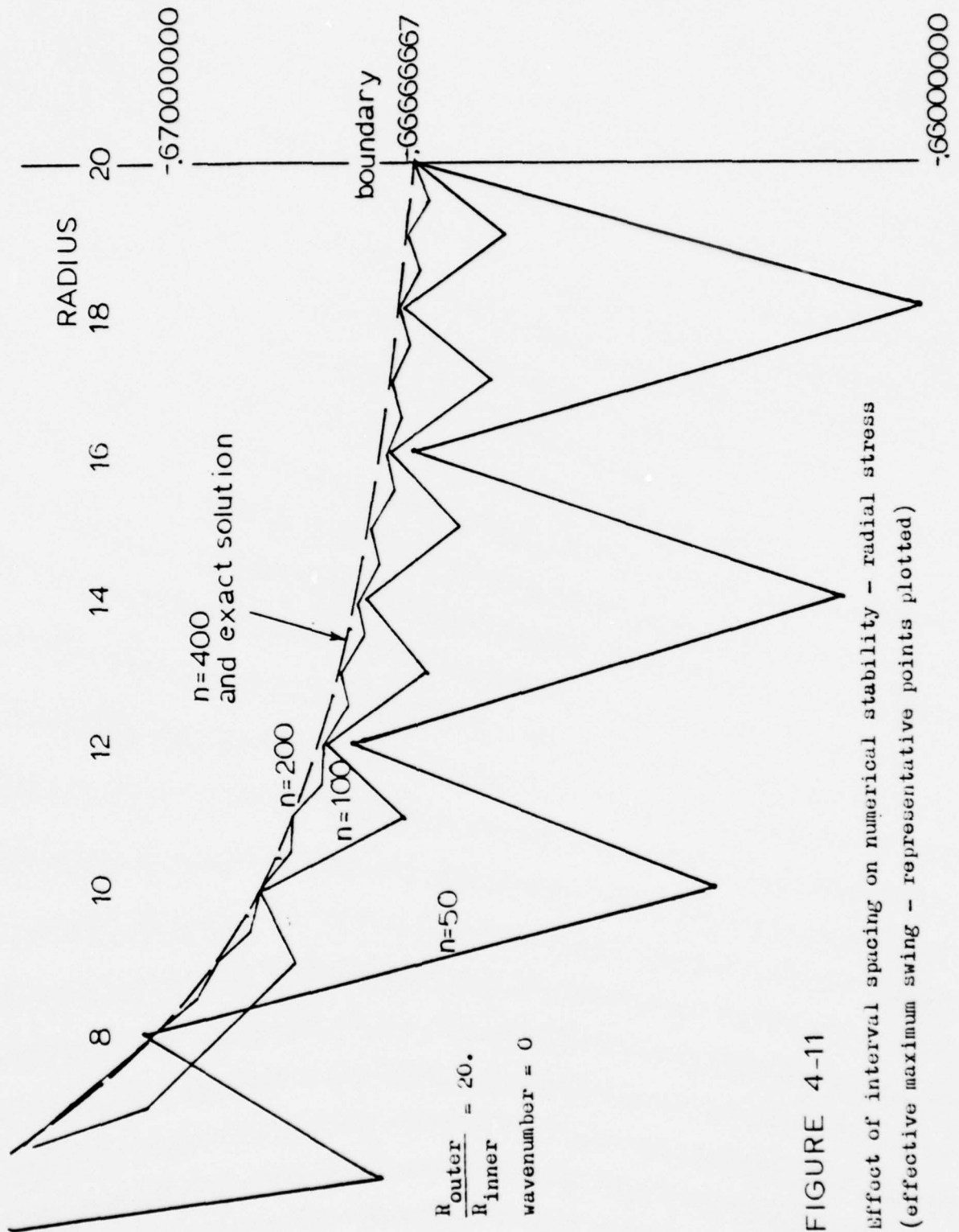


FIGURE 4-11
 Effect of interval spacing on numerical stability - radial stress
 (effective maximum swing - representative points plotted)

whether the numerical scheme is consistent, i.e. whether this convergent numerical solution is the true solution. This is done in the following section.

4.7 Comparison with Analytic Solution and other Tests

Fortunately, the analytic solutions to the relations expressed in equations (4.21) can be obtained and are presented in Appendix B. The analytic solutions and their computed counterparts are illustrated in Figures 4-12 through 4-14 for wave numbers 0, 1, and 2 respectively for the case of radial stress at $R_{out}/R_{in} = 20$.

Test A This was run to determine the effect of radius on the inner stresses. It would be expected that for a stress loading of the outer boundary, the importance of the radius on the inner boundary would decrease with increased plate diameter. This has been determined to be so numerically, and some results are presented in Figures 4-15, 4-16, 4-17, and 4-18. It is also noteworthy that the higher wave numbers have very little effect on the inner stress solution. A conclusion here can be drawn that will save much computational effort if only a limited amount of data is desired.

Test B This was run to determine the sensitivity of the solution to the Poisson effect. The results for four wave numbers are presented as Figure 4-19. Wave number one appeared to be almost entirely insensitive, whereas wave number zero appeared to be the most sensitive.

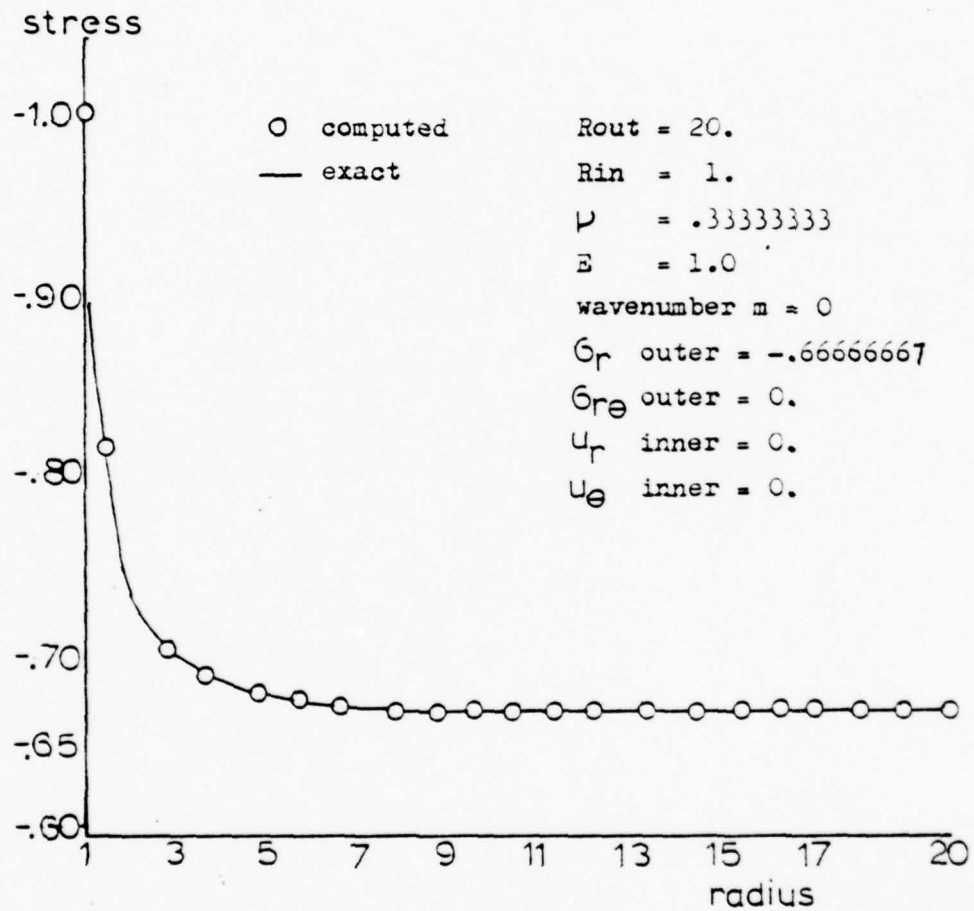


FIGURE 4-12

Numerical and analytical solutions wavenumber zero

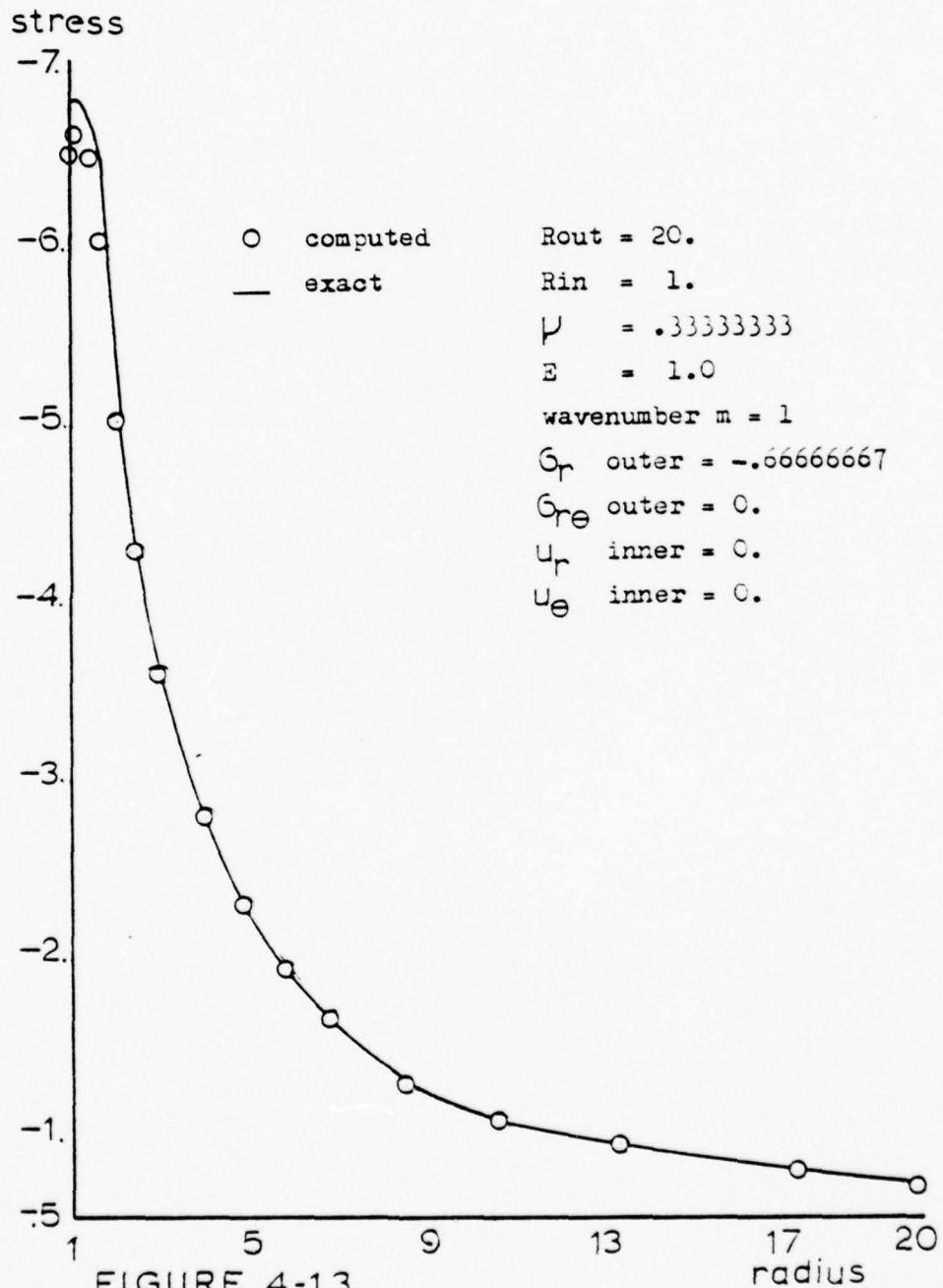


FIGURE 4-13

Numerical and analytical solutions for wavenumber one

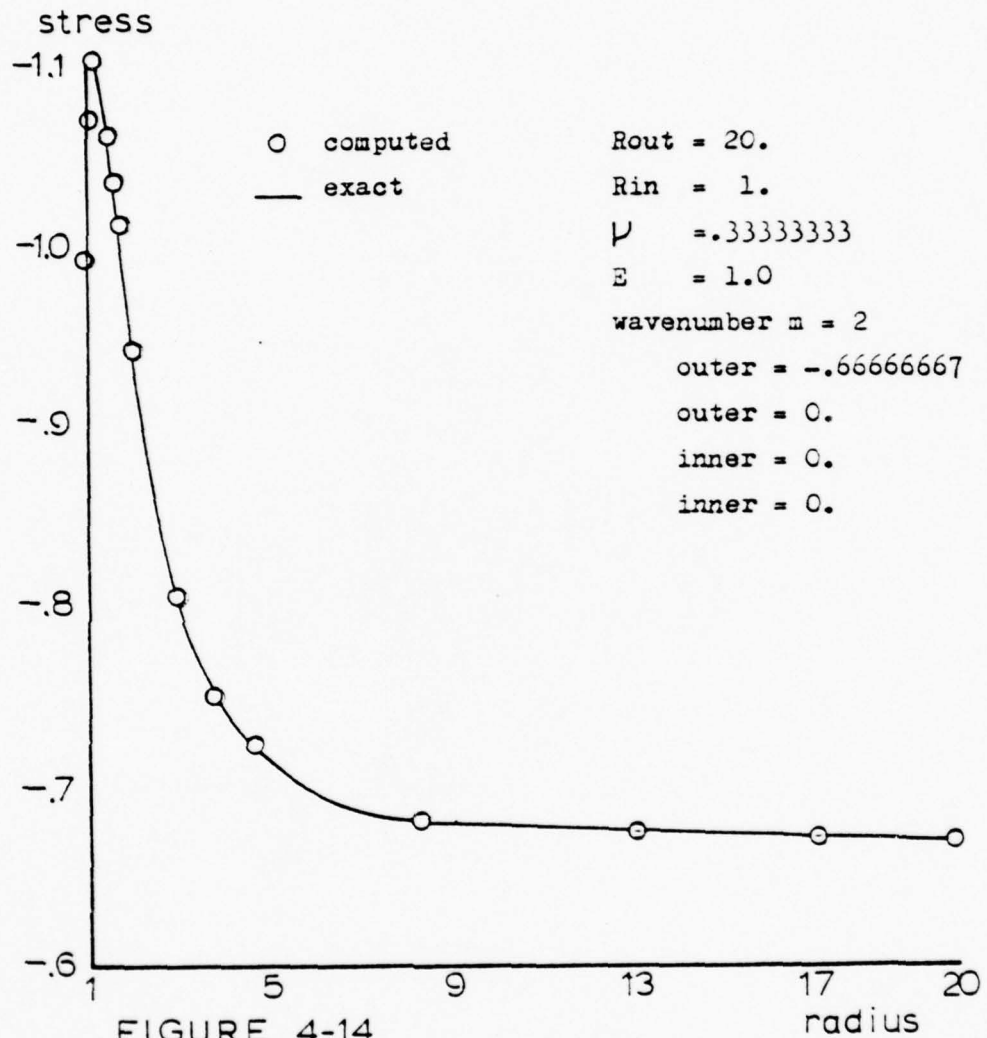


FIGURE 4-14

Numerical and analytical solutions for wavenumber two

Effect of radial size on radial stress distribution - wavenumber 0

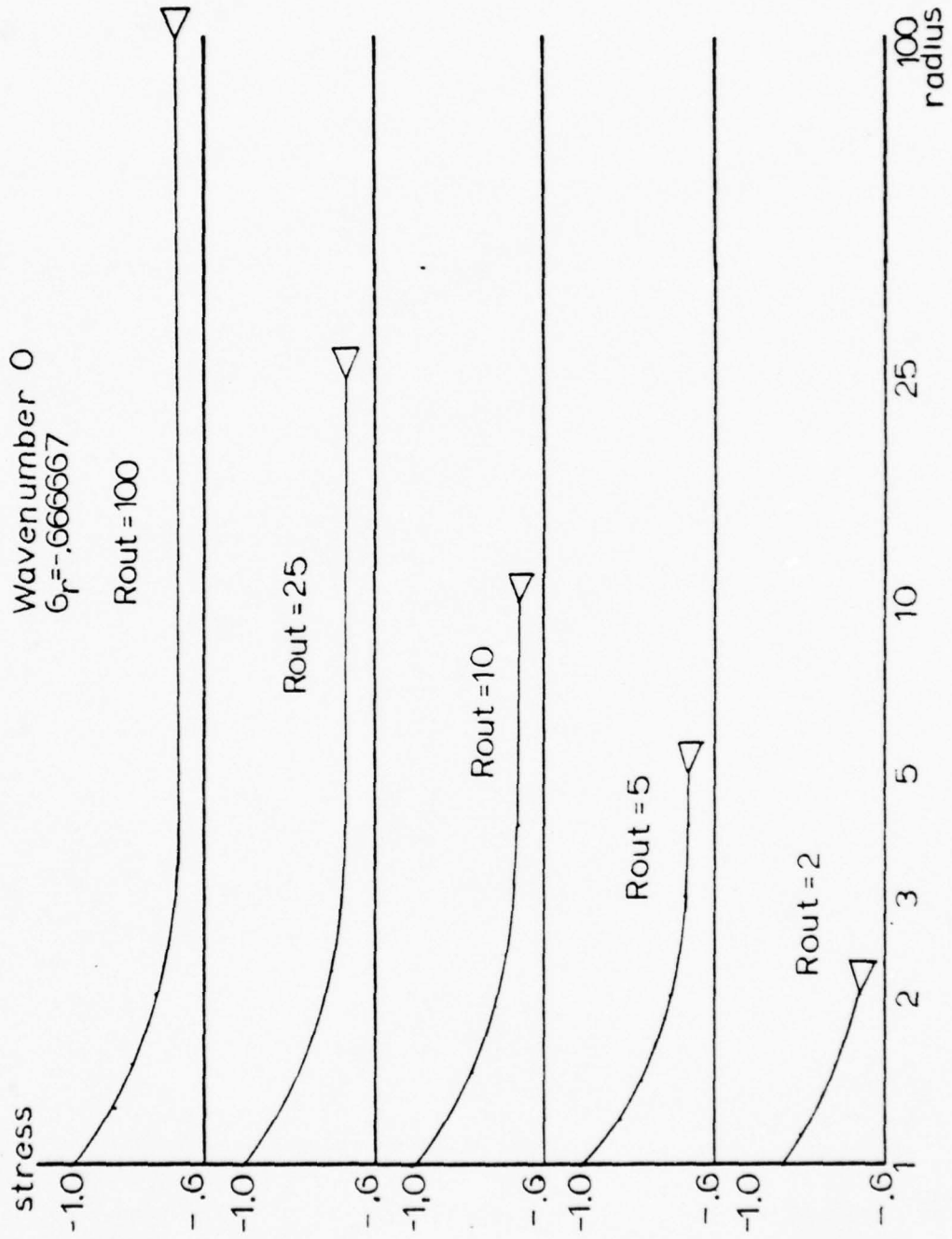


FIGURE 4-15

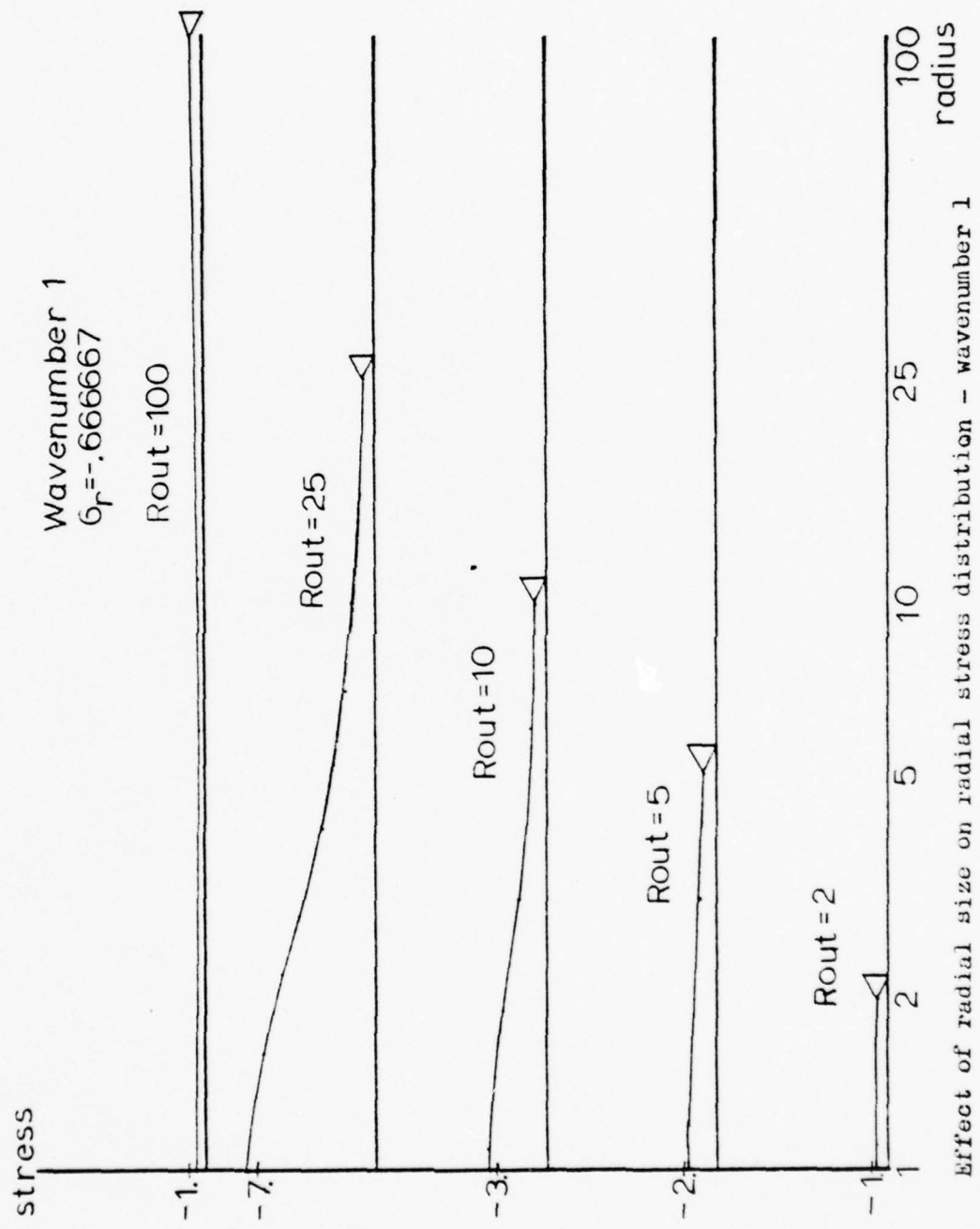


FIGURE 4-16

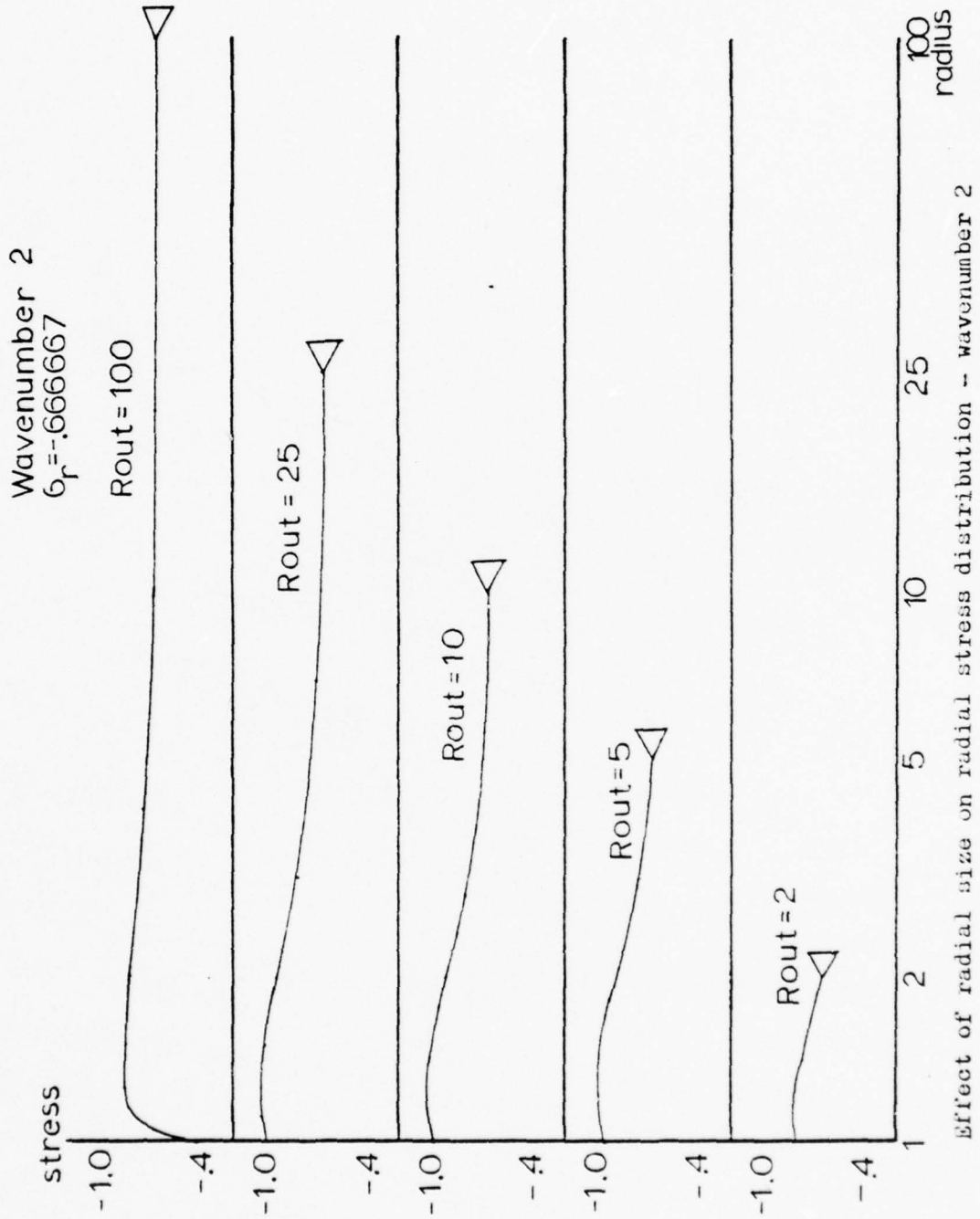


FIGURE 4-17

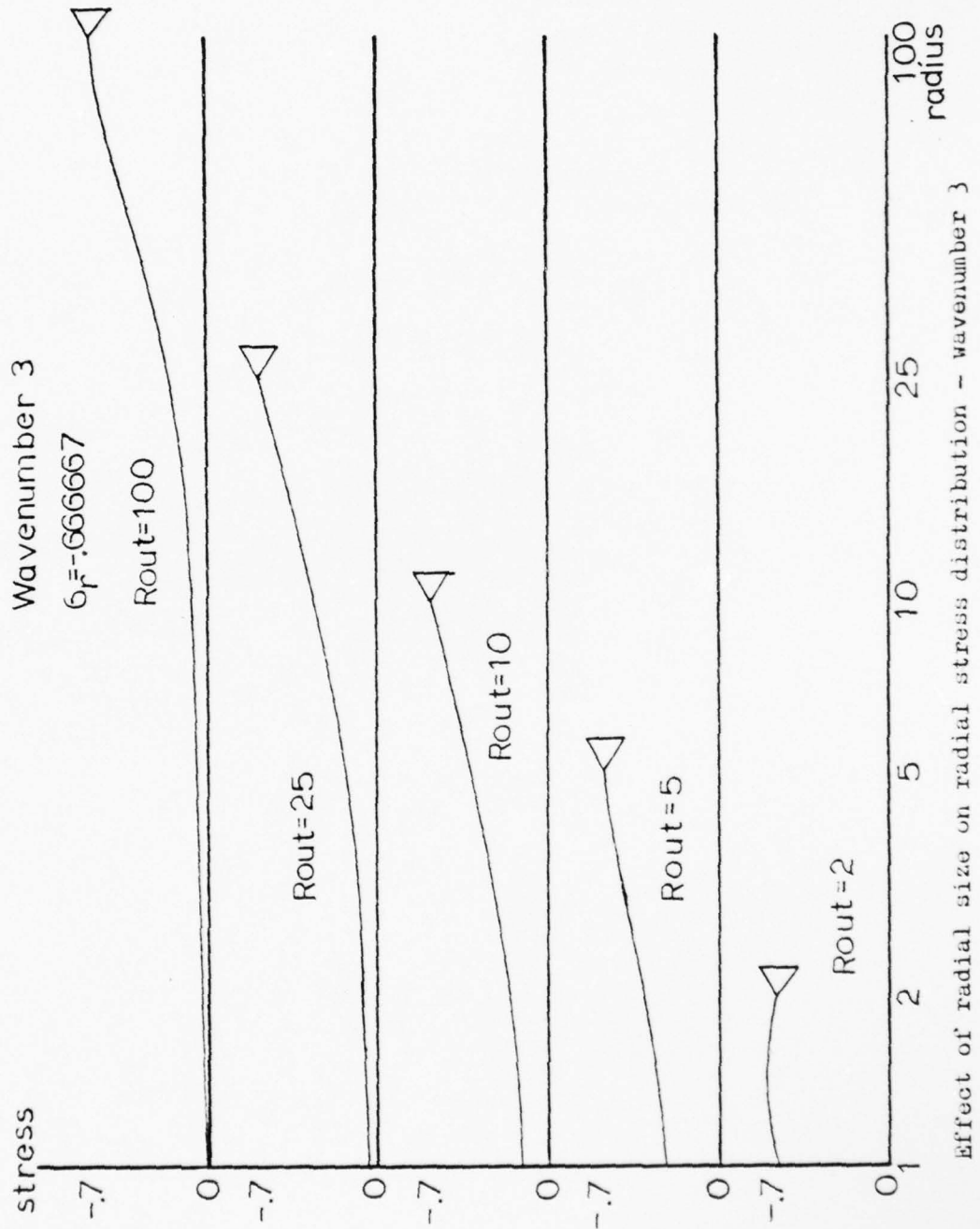


FIGURE 4-18

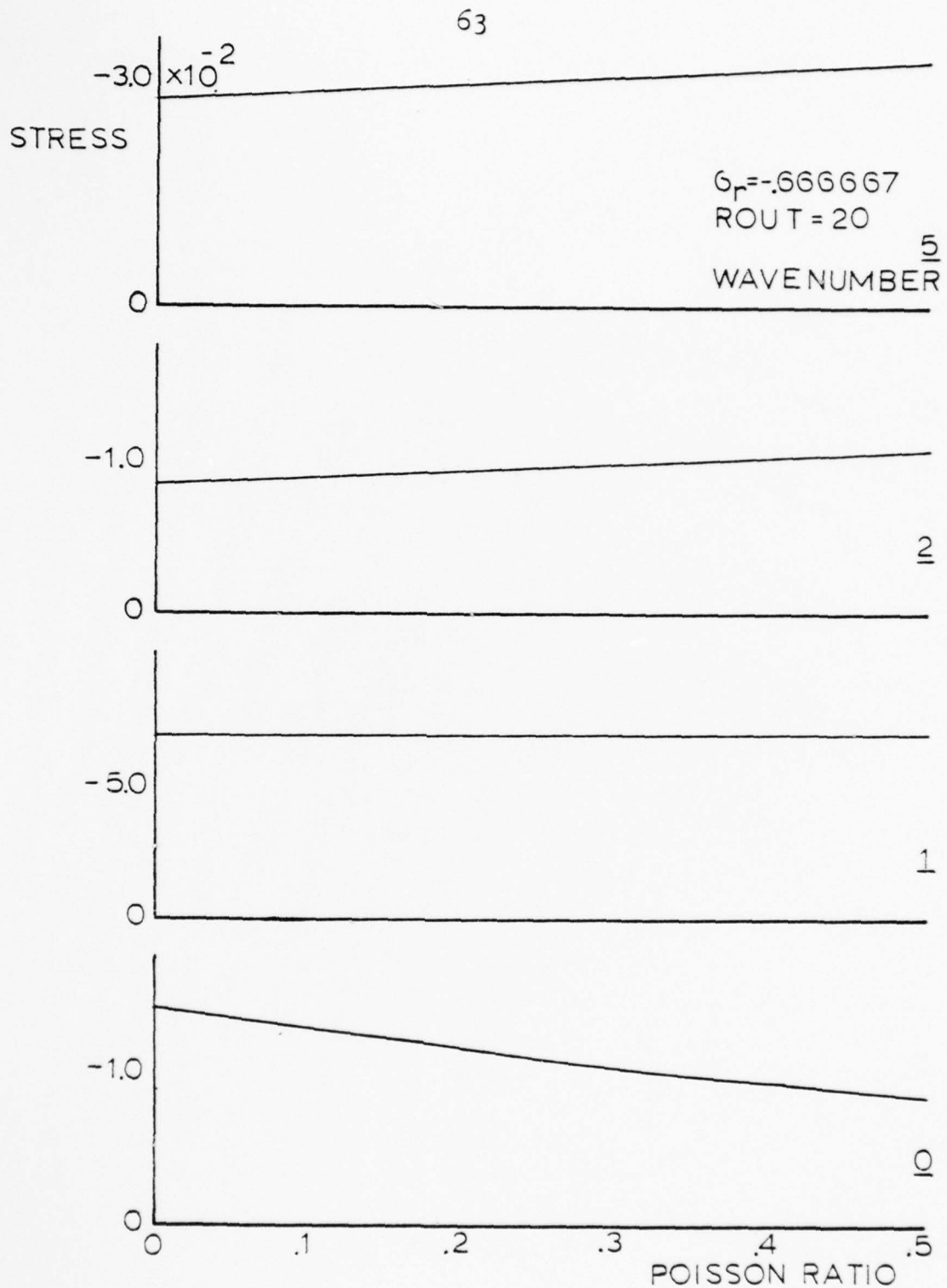


FIGURE 4-19

Variation of radial stress at the inner boundary
as a function of poisson ratio for several wavenumbers

The next two tests were of load magnitude and shape and designed to test for linearity.

Test C The load magnitude was varied by integral multiples, retaining the same distribution. Results were exact multiples as well. No results are presented.

Test D The test of load shape was more of a test of the Fourier subroutine which converts boundary conditions into series. The following radial loading was supplied:

<u>#1</u>	<u>#2</u>	<u>#3</u>
$\sigma_r = 1. \cos \Theta$	$= 1. - 1. \cos \Theta$	$= 1.$
$\sigma_{\theta} = 0.$	$= 0.$	$= 0.$
$u_r \text{ INNER} = 0.$	$= 0.$	$= 0.$
$u_{\theta} \text{ INNER} = 0.$	$= 0.$	$= 0.$

The results were excellent and are presented in Table 4-II.

Test E The last test concerned the radius at which the finite plate could be considered infinite for practical purposes. This test is similar to Test A. This test was somewhat inconclusive since above a certain radius some solutions became unstable again and innacurate. A practical limit of radial spacing was chosen at $n=400$, since the marginal accuracy of finer differences was outweighed by increases in computational time, cost, and round off error. Results of this test are presented as Test E in Table 4-III.

4.8 Comparison with Ross' Solution

In Section 3.2 a review of the analysis of Ross was

Table 4-II

<u>Radius</u>	<u>Run 1</u>	<u>Run 2</u>	<u>Sum</u>	<u>Run 3</u>
1.00	9.72992	-8.2323	1.49762	1.49759
2.90	5.34873	-4.2905	1.05823	1.05824
4.80	3.36513	-2.3445	1.02063	1.02047
6.70	2.46372	-1.4538	1.00992	1.00989
8.60	1.95948	-0.95387	1.00561	1.00551
10.50	1.64134	-0.63805	1.00329	1.00328
12.40	1.42509	-0.42309	1.00200	1.00200
14.30	1.27047	-0.26917	1.00130	1.00119
16.20	1.15562	-0.15491	1.00065	1.00065
18.10	1.06816	-0.067790	1.00037	1.00027
20.00	1.00002	-0.11921e-04	1.00000	1.00000
	$U_r, U_\theta = 0$ inner outer $G_r = \cos \theta$ $G_\theta = 0$ $R_{out} = 20$	$U_r, U_\theta = 0$ inner outer $G_r = 1 - \cos \theta$ $G_\theta = 0$ $R_{out} = 20$		$U_r, U_\theta = 0$ inner outer $G_r = 1$ $G_\theta = 0$ $R_{out} = 20$

Test of elastic routine by variation of load
shape

Table 4-III

<u>Wavenumber</u>	$\frac{G_{r \text{ outer}}}{G_{r \text{ inner}}} = 10$	5% deviation Instability	
	<u>@Rout</u>	<u>@Rout</u>	<u>@Rout</u>
0	>100	>100	15
1	>100	50	10
2	>100	>100	75
3	25	>100	>100
>4	<25	>100	>100

Practical extent of finite condition at certain wavenumbers
by variation of outer radius

presented. This paper, reference [27], also included an example in which the loading depicted in Figure 4-20 was analyzed. Below the stated elastic limit, it was possible to compare the model developed in this chapter. An effort was made to correlate this result with a similar loading applied to the method developed in this chapter. The comparison is presented as Figures 4-21, 4-22, 4-23.

Although the basic shape and critical values of cross-over are similar, discrepancies were noted with respect to the hoop stress and also with respect to the order of magnitude. By changing the displacement loading magnitude to .01 inches vice .01 feet, the numbers were much alike. No explanation was found for the difference in hoop stress, but from equation (4.20):

$$\sigma_{\theta m} = \frac{E}{r} u_{rm} + \frac{E_m}{r} u_{\theta m} + \nu \sigma_{rm}$$

Evaluated at R_m ; $u_{\theta}, u_r = 0$ (boundary conditions)

produces

$$\sigma_{\theta m} = \nu \sigma_{rm}$$

or a non-zero value for any non-zero radial stress.

This loading was also run with 3, 5, and 11 wave numbers and no effect was found on the value of inner face stress, although significant variations existed toward the edge. This is as expected, since the influence of the trigonometric components m do not substantially contribute to the center

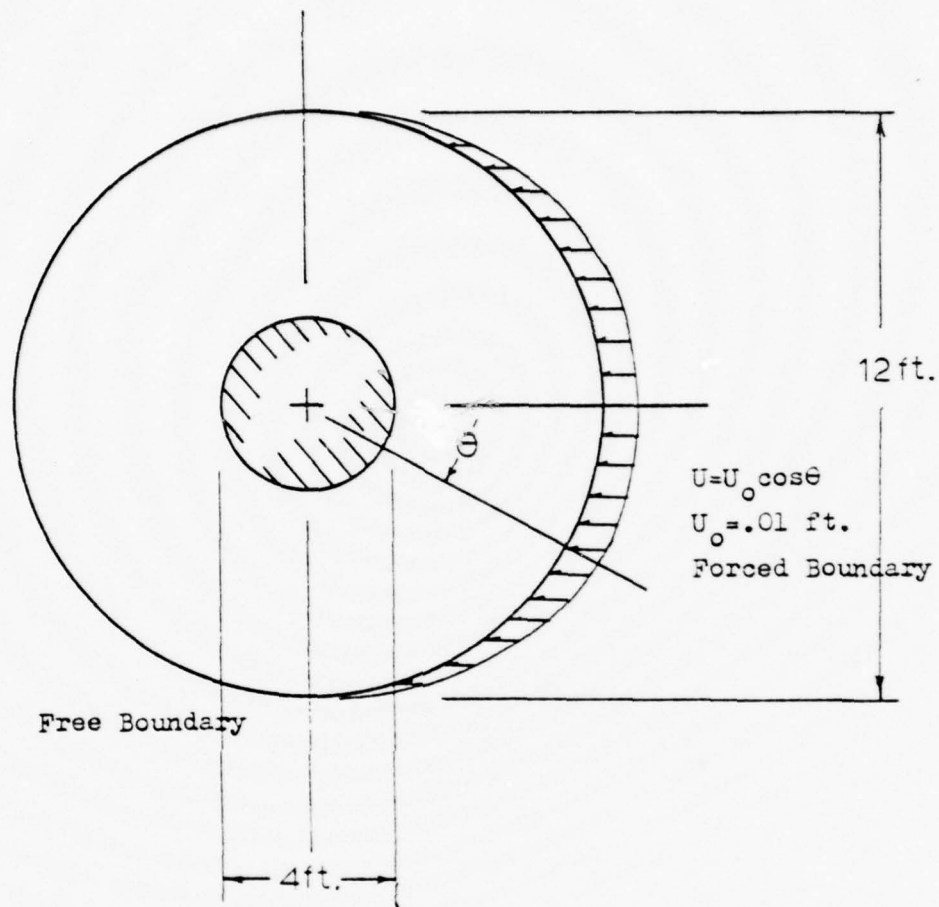


FIGURE 4-20

Discontinuous edge loading of a finite plate about
a rigid inclusion (after Ross, et al, [27])

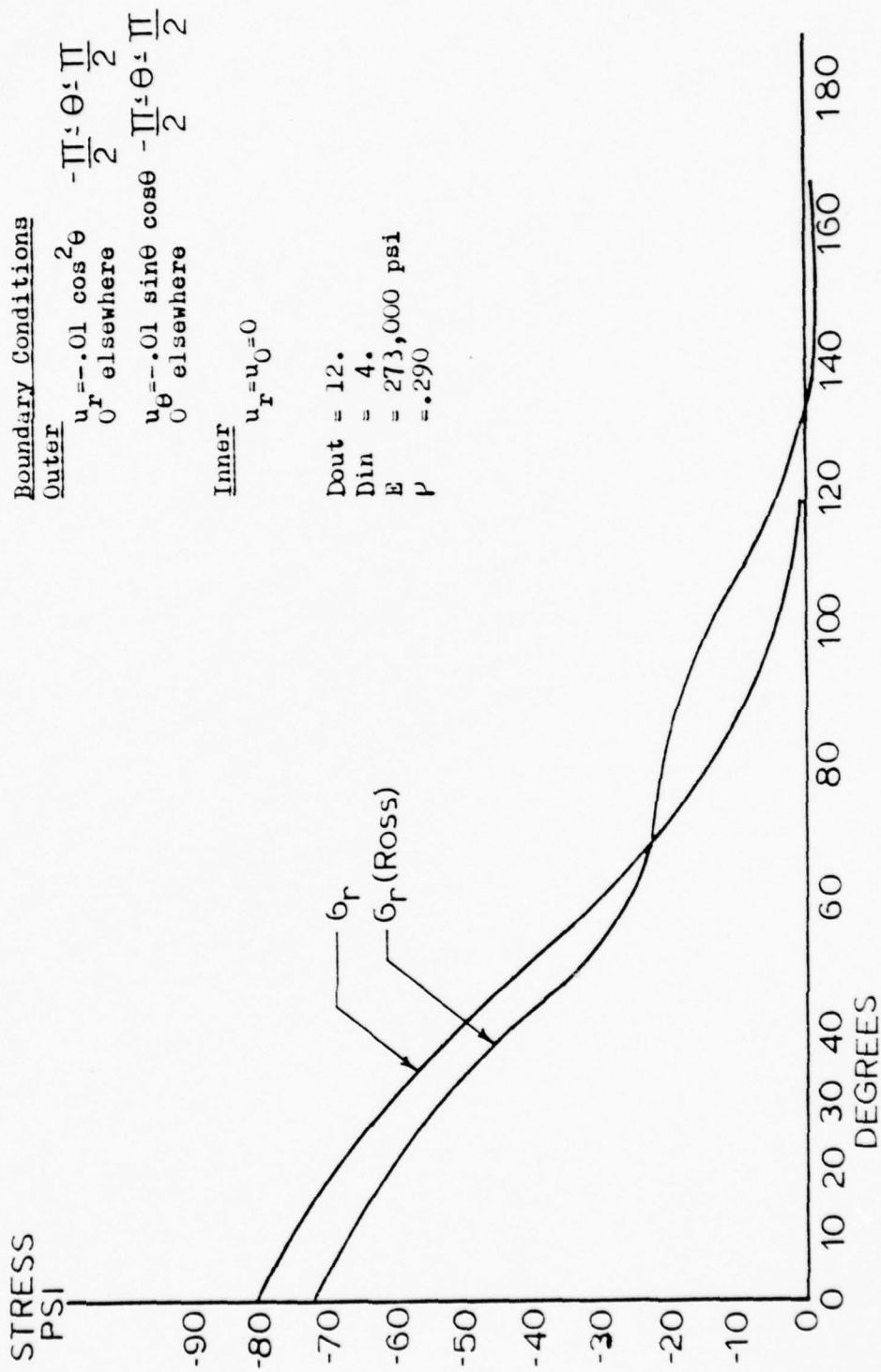
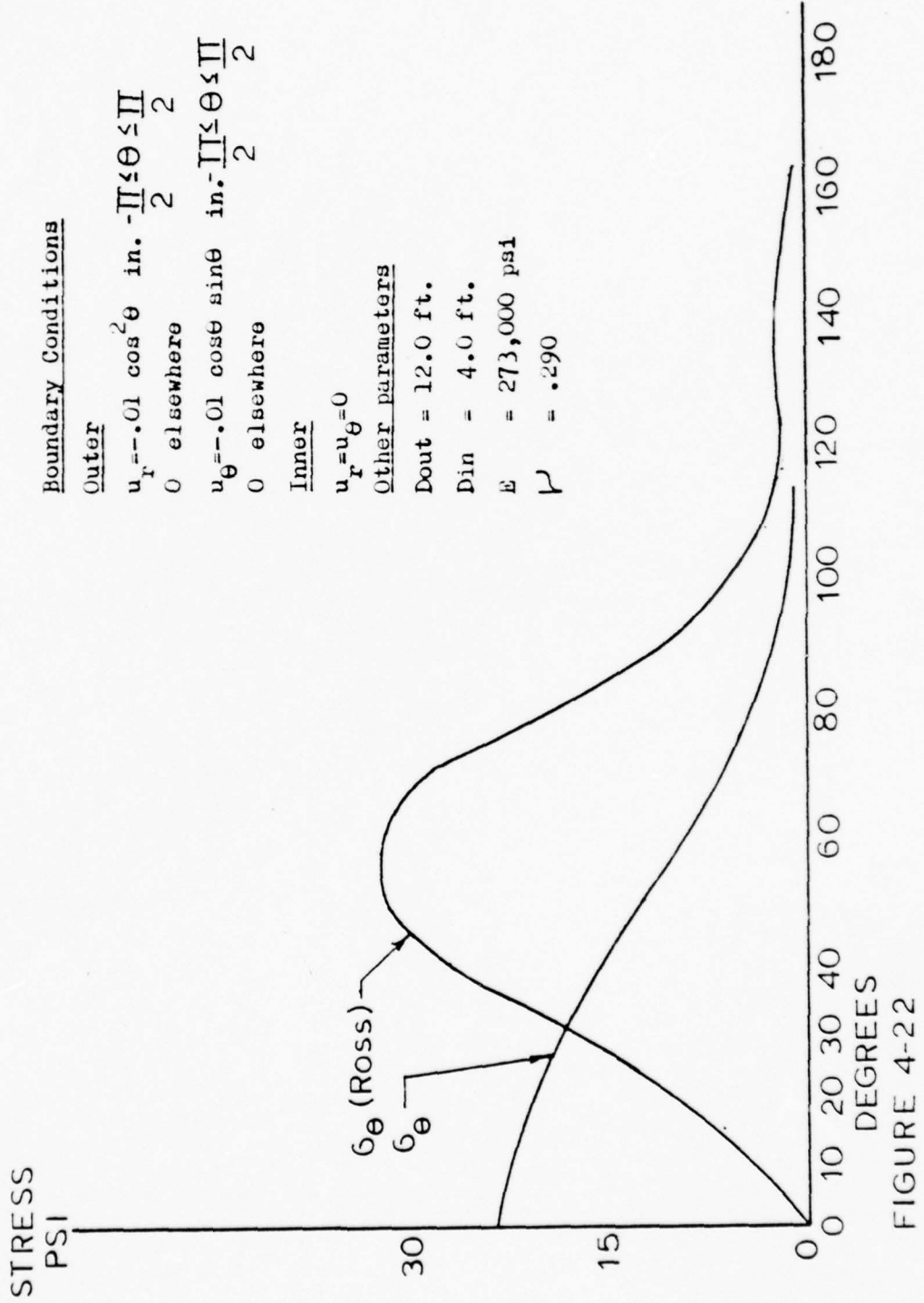


FIGURE 4-21

Radial stress vs. angular position - comparison with Ross' solution



Hoop stress vs. angular position - comparison with Ross' solution

Boundary ConditionsOuter

$$u_r = -.01 \cos^2 \theta \quad \text{in.} \quad -\frac{\pi}{2} \leq \theta \leq \frac{\pi}{2}$$

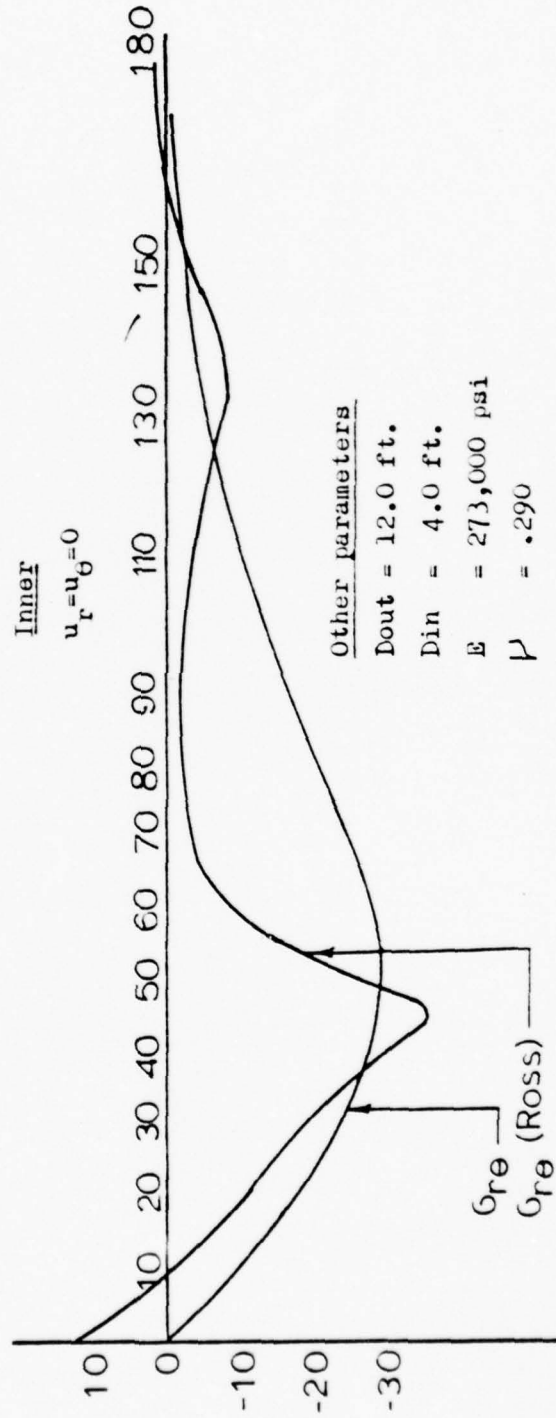
$$0 \quad \text{elsewhere}$$

$$u_\theta = -.01 \cos \theta \sin \theta \quad \text{in.} \quad -\frac{\pi}{2} \leq \theta \leq \frac{\pi}{2}$$

$$0 \quad \text{elsewhere}$$

Inner

$$u_r = u_\theta = 0$$

Other parameters

$$D_{out} = 12.0 \text{ ft.}$$

$$D_{in} = 4.0 \text{ ft.}$$

$$E = 273,000 \text{ psi}$$

$$\nu = .290$$

FIGURE 4-23

Shear stress vs. angular position - comparison with Ross' solution

stress as the edge of the plate is extended toward (perceived) infinity.

Figure 4-24 displays the radial loading represented by three Fourier coefficients and the original loading. It can be seen that even for this discontinuous loading, three wave numbers presents a good approximation.

4.9 Peculiarities and Range of Validity

This elastic formulation is derived from the basic plane stress equations and consequently should be useful where plane stress is appropriate. The model achieves significant accuracy up to a ratio of outer radius to inner radius of 25:1 . Beyond this, the solution diverges from the analytical derivation.

The worst case is at wave number one (Figure 4-25). It is doubtful that the infinite case can be modeled by a finite difference technique in this problem, since a boundary loading for the first wave number at all radii will produce a significant solution at the pile. Consequently, this elastic model is useful for radial limits of outer radius/inner radius ratios less than 25.

The buckling limit of a thin plate is an important consideration. The analytic derivation of one buckling load is presented as Appendix C. The equations of plane stress do not allow for deflections in the third dimension, therefore they will not predict the failure by this mode. External means

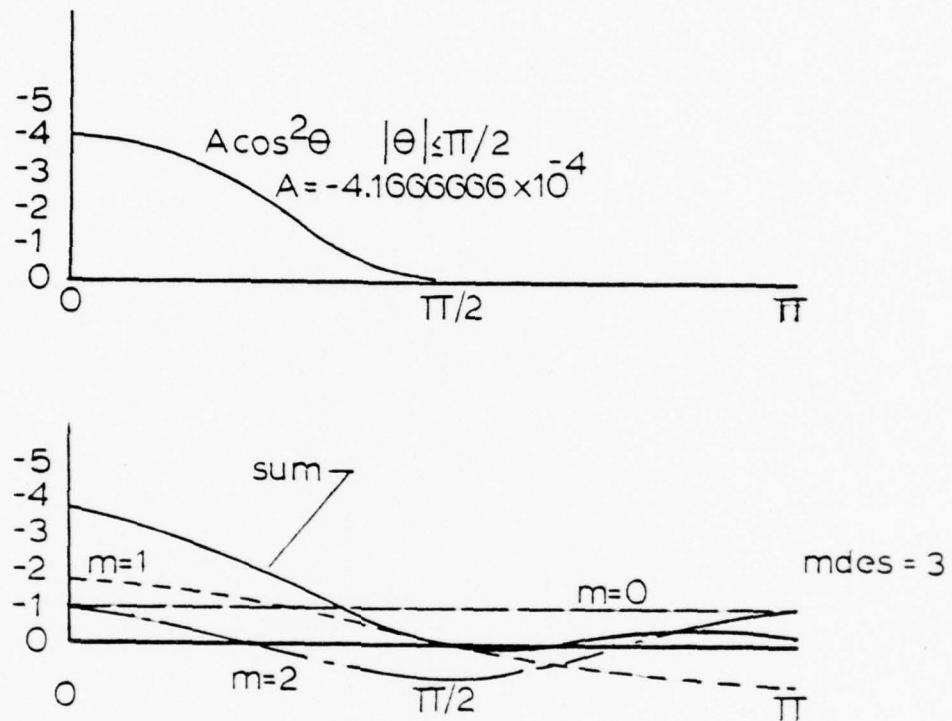


FIGURE 4-24

Displacement loading (radial) applied to boundary
of Ross' solution - comparison with first three
wavenumbers

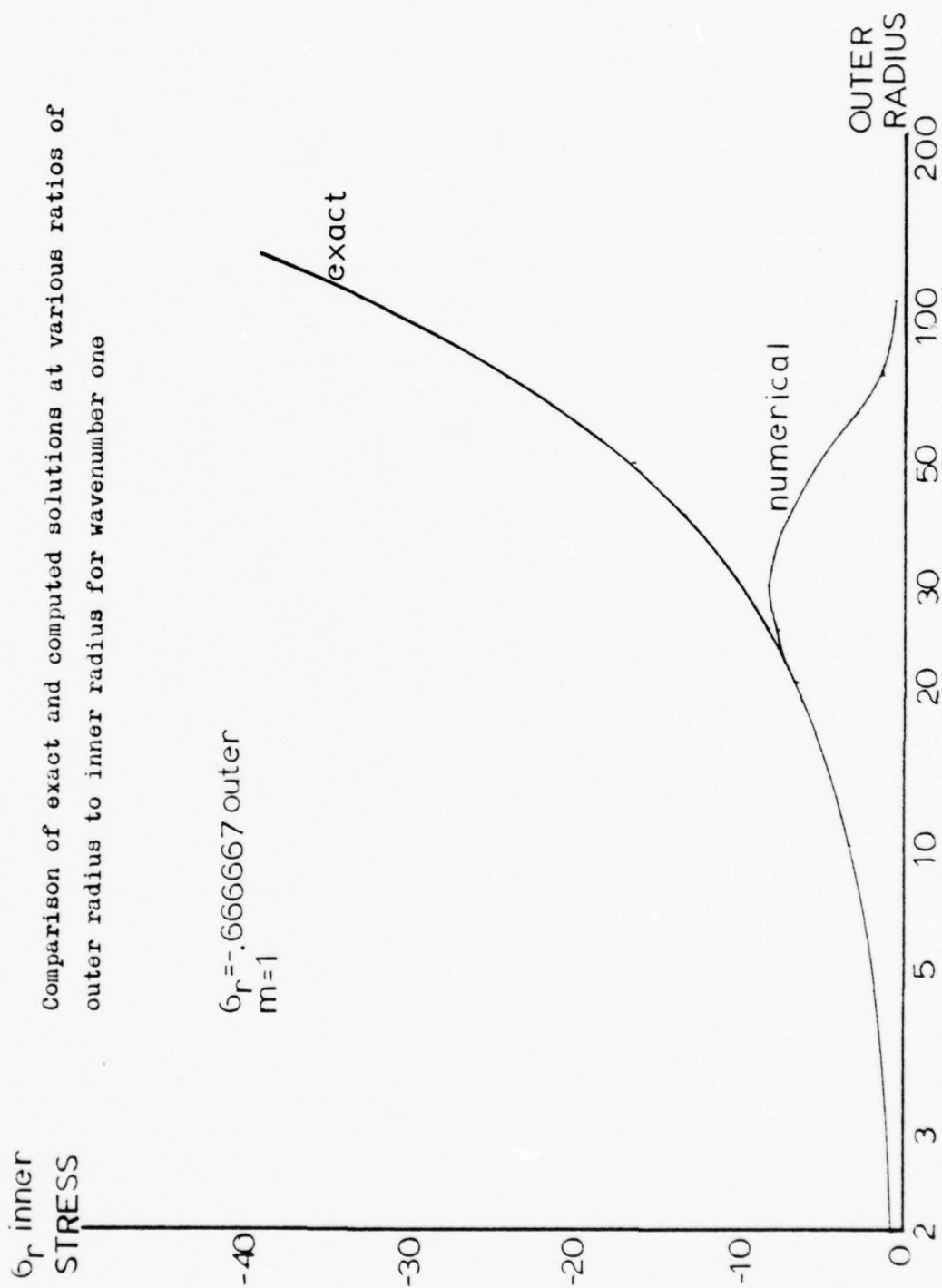


FIGURE 4-25

must be applied to the program to preclude this occurrence.

The plate is assumed to be attached to the rigid inclusion (frozen-in problem). The partial movement of either boundary cannot be supported by this method, although it is conceivable that a more general two-dimensional model could.

Finally, the model can support an application of forces or displacement at either boundary, which can in turn be discontinuous. The degree of refinement is limited by the wavenumbers considered. The accuracy is limited by the circumferential spacing chosen.

CHAPTER 5

Viscous Extension of the Model5.1 General

Considering the simple rheological model in Figure 5-1, the following differential relations hold:

$$\dot{\epsilon}_r = \dot{\epsilon}_{r \text{ VISCOUS}} + \dot{\epsilon}_{r \text{ ELASTIC}} \quad (5.1)$$

$$\dot{\epsilon}_\theta = \dot{\epsilon}_{\theta \text{ VISCOUS}} + \dot{\epsilon}_{\theta \text{ ELASTIC}} \quad (5.2)$$

$$\dot{\epsilon}_{r\theta} = \dot{\epsilon}_{r\theta \text{ VISCOUS}} + \dot{\epsilon}_{r\theta \text{ ELASTIC}} \quad (5.3)$$

$$\text{where } \dot{\epsilon}_{\text{VISCOUS}} = f_{\text{FUNCTION}}(\sigma) \quad (5.4)$$

The Maxwell model is chosen for its simplicity and because it is possible to generalize into a non-linear creep law. Additionally, some investigators have modeled sea ice behavior this way experimentally, and physical values are available [33].

5.2 Incorporation of the Viscosity Relations

The stress-strain relations of (4.6), (4.7), and (4.8) can be expressed using (5.1), (5.2), and (5.3):

$$\dot{\epsilon}_r = \alpha (\sigma_r - \nu \sigma_\theta) + \frac{1}{E} (\dot{\sigma}_r - \nu \dot{\sigma}_\theta) \quad (5.5)$$

$$\dot{\epsilon}_\theta = \alpha (\sigma_\theta - \nu \sigma_r) + \frac{1}{E} (\dot{\sigma}_\theta - \nu \dot{\sigma}_r) \quad (5.6)$$

$$\dot{\epsilon}_{r\theta} = \frac{2\alpha(1+\nu)}{E} \sigma_{r\theta} \quad (5.7)$$

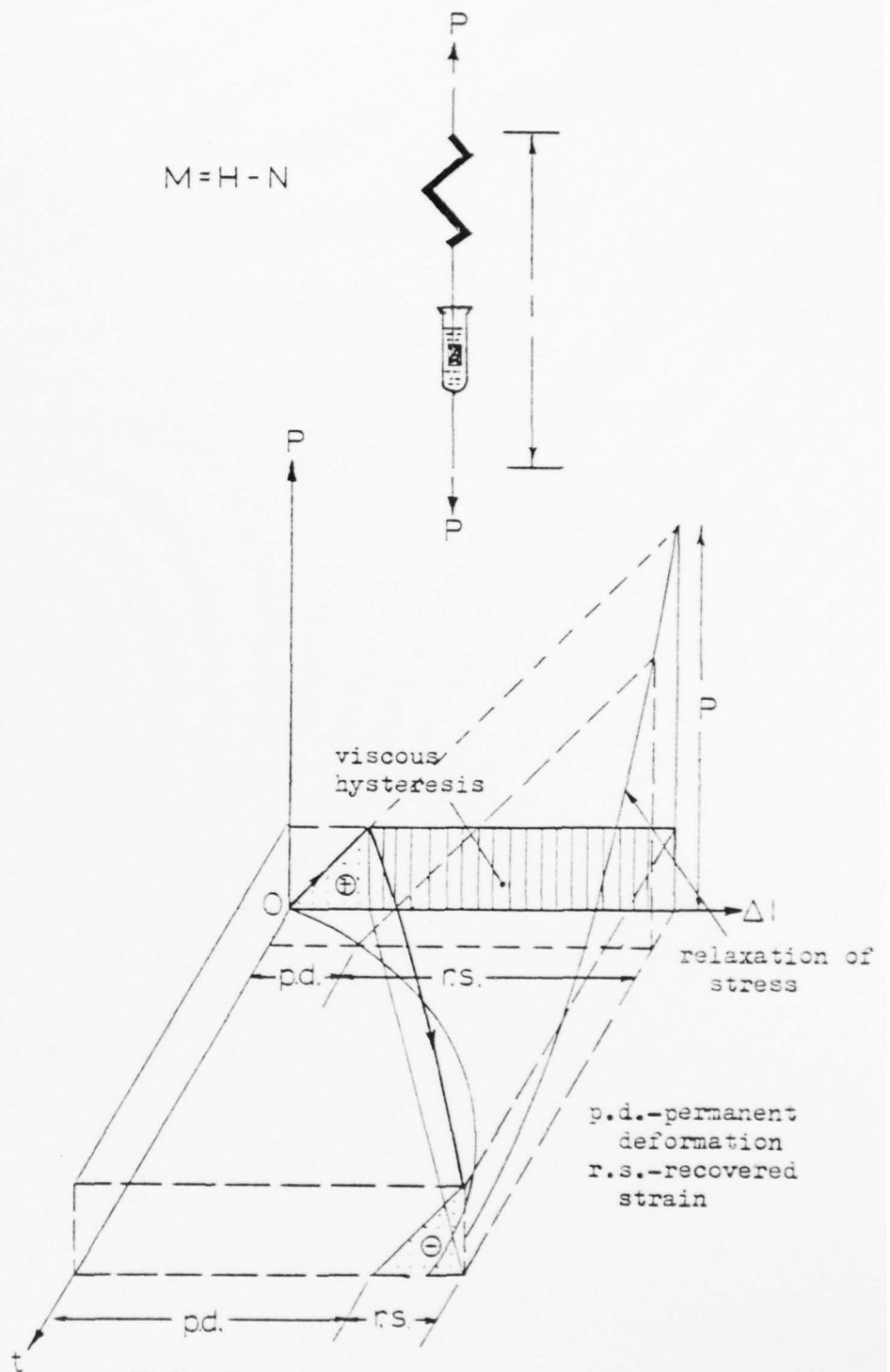


FIGURE 5-1

Model for Maxwell liquid (after [8])

$$\Delta l = \Delta l_p + \Delta l_r$$

These relations can be incorporated into a series of equations as in section 4.2 yielding:

$$\frac{d}{dt} \left\{ \frac{\partial}{\partial r} [I] \underline{Z}_m + [A] \underline{Z}_m \right\} = [E] \underline{Z}_m \quad (5.8)$$

Where:

$$0 \leq m \leq \infty$$

$[A]$ is the same matrix as expressed by (4.24)

And

$$[E] = \begin{bmatrix} 0 & 0 & -\frac{E^2 \alpha}{r^2} & -\frac{E^2 m \alpha}{r^2} \\ 0 & 0 & -\frac{E^2 m \alpha}{r^2} & -\frac{E^2 m^2 \alpha}{r^2} \\ 0 & 0 & \frac{E \alpha (1+\nu)}{r} & \frac{E m \alpha (1+\nu)}{r} \\ 0 & \frac{2 \alpha (1+\nu)}{E} & 0 & 0 \end{bmatrix} \quad (5.9)$$

5.3 Solution

Numerical solution of the series of differential equations (5.8) is carried as before, only the unknown variable, $\dot{\underline{Z}}_m$, represents rate at time t . The value \underline{Z}_m used on the right hand side of (5.8) is the elastic solution for \underline{Z}_m . Note that boundary conditions of load rate must be employed. The solution yields:

$$\frac{d}{dt} \left\{ \underline{Z}_m \right\} = \overset{\text{A CONSTANT}}{C_m} \quad (5.10)$$

This differential equation in time can be solved using the Euler or "one step" method to arrive at a solution for the next time step, where the process is repeated.

$$(\dot{\underline{Z}}_m)^t \Delta t + \underline{Z}_m^t = \underline{Z}_m^{t+\Delta t} \quad (5.11)$$

Non-dimensionalization with respect to another variable is required. The variable chosen was α , the viscosity coefficient, with units of LTM^{-1} .

If $\alpha_{\text{reference}}$ is chosen, and mass is preset by consideration of stress non-dimensionalization (Section 4.4), then derived time:

$$T_{\text{REF}} = \frac{1}{E_{\text{REF}} \alpha_{\text{REF}}} \quad (5.12)$$

Therefore any value of non-dimensional time is related:

$$\bar{T} = \frac{T_{\text{PHYSICAL}}}{T_{\text{REF}}} \quad (5.13)$$

As an example, using typical values for sea ice [],

$$E_{\text{REF}} = 2083 \text{ psf}$$

$$\alpha_{\text{REF}} = 1.2788 \times 10^{-9} (\text{psf} \cdot \text{sec})^{-1}$$

implies

$$\bar{E} = 1.$$

and

$$\bar{\alpha} = 1.$$

Thus

$$T_{\text{REF}} = 2607 \text{ sec}$$

or one unit of non-dimensional time

A flow chart of the numerical computer solution and time integration is presented as Figure 5-2.

5.4 Convergence in Time

The Euler method chosen for time integration assures convergence if the time step is small enough. Since it is not possible to analytically determine the solution, as was done for the elastic case, one approach is to run a general solution for increasingly small time steps until no numerical improvement is achieved. Unfortunately the solution time can be prohibitive. The results of two time convergence test series, for wave number zero and one, were found to converge at a time step of $.001 \overline{T}$, beyond which significant improvement was not achieved. The time increment to achieve this numerical stability comes out to be a constant independent of stress, for the upper bound prediction.

5.5 Range of Validity

The viscoelastic formulation presented in this chapter is not valid where the elastic theory is inappropriate or where the numerical limitations of subroutine elastic do not apply. The range of validity is further restricted on how well and on which range of parameters ice can be modeled as a linear viscoelastic material.

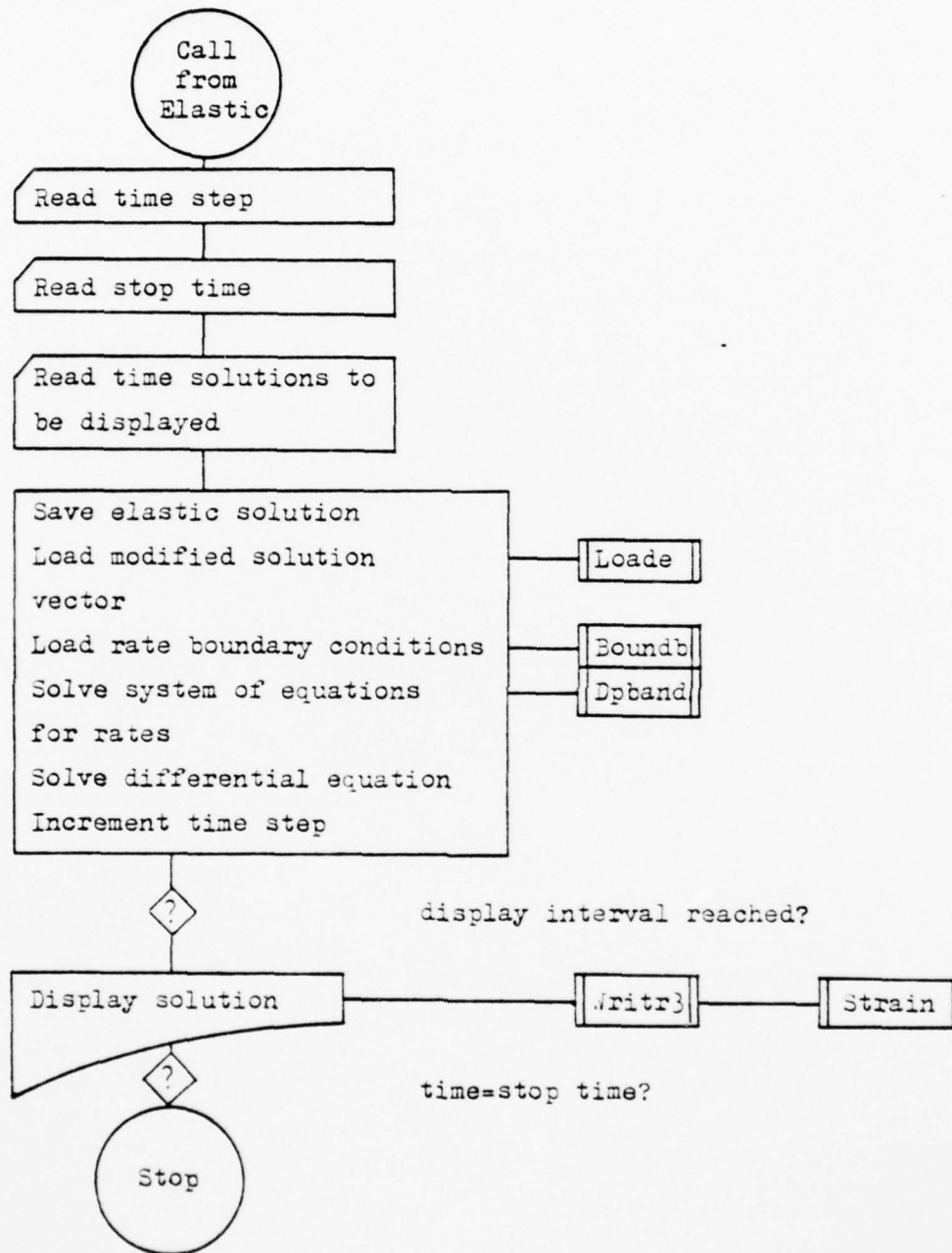
Subroutine Visco

FIGURE 5-2

Block diagram for subroutine Visco

CHAPTER 6

Analysis of Ice - Circular Pile Behavior with the Model

The previous chapters have dealt with the need for an analytical tool and the construction of a mathematical model. Without exhaustively analyzing the many combinations of loadings and important parameters that affect the circular pile problem, some interesting results will now be developed.

6.1 Material Behavior

Katona and Vaudrey [18] have presented a logical sequence of obtaining ice material behavior experimentally for a particular geometric configuration. The results of these data are then fitted into curves which can then yield a range of validity of ice material law as discussed in Section 2.3 and with Figure 2-2.

Of course, since this model formulated in this thesis responds only viscoelastically, the transition from viscoelastic to viscoplastic behavior cannot be obtained. The model can, however, define the elastic-viscoelastic transition.

As an example, consider the loading situation depicted in Figure 6-1. Physically, this could represent the rigid, frozen-in pile loaded by a large, thermally expanding ice sheet. Neglecting any temperature effects to viscosity and elastic modulus, the loading curves of Figure 6-2 are constructed. Stress-strain diagrams similar to Figure 6-3 show the viscoelastic creep behavior. The apparent relaxation of

Viscosity coefficient $\alpha = 1.$

Elastic Modulus $E = 1.$

[Non-dimensional quantities,
see text in Sections 4-4 and 5-3]

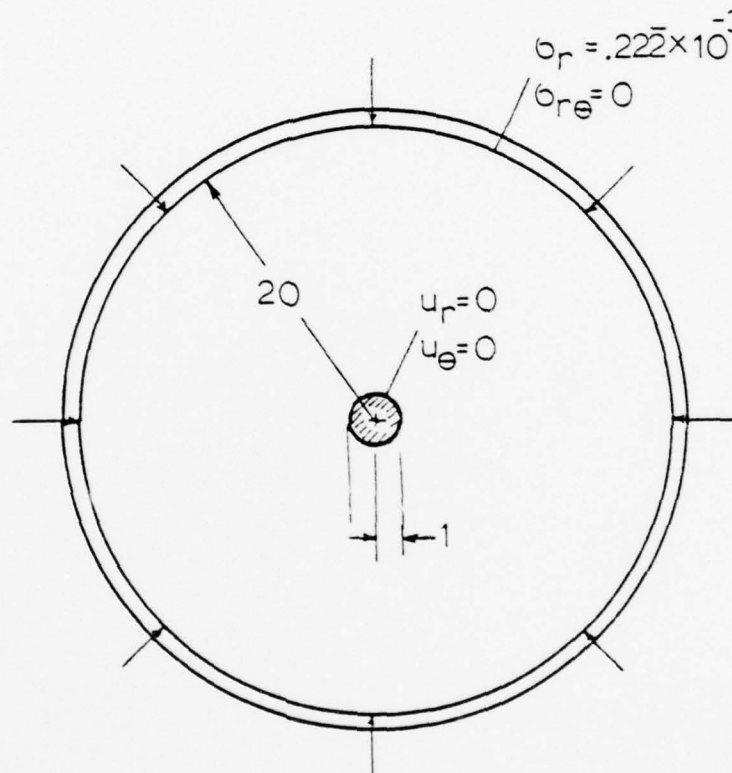


FIGURE 6-1

Circular ice sheet - rigid pile geometry and loading configuration used in viscoelastic behavior analysis of Section 6.1.

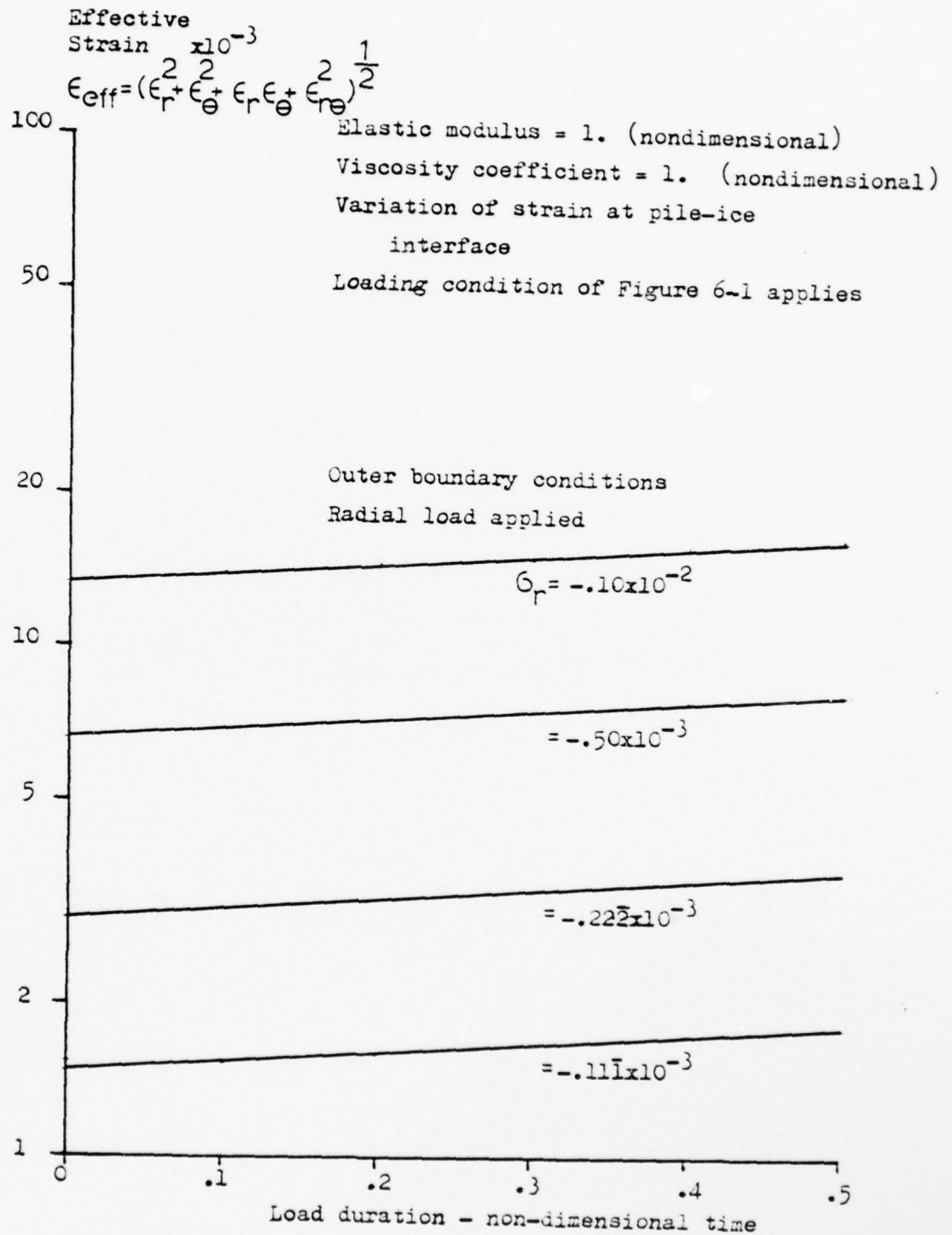


FIGURE 6-2

Viscoelastic behavior - Effective strain vs. load duration

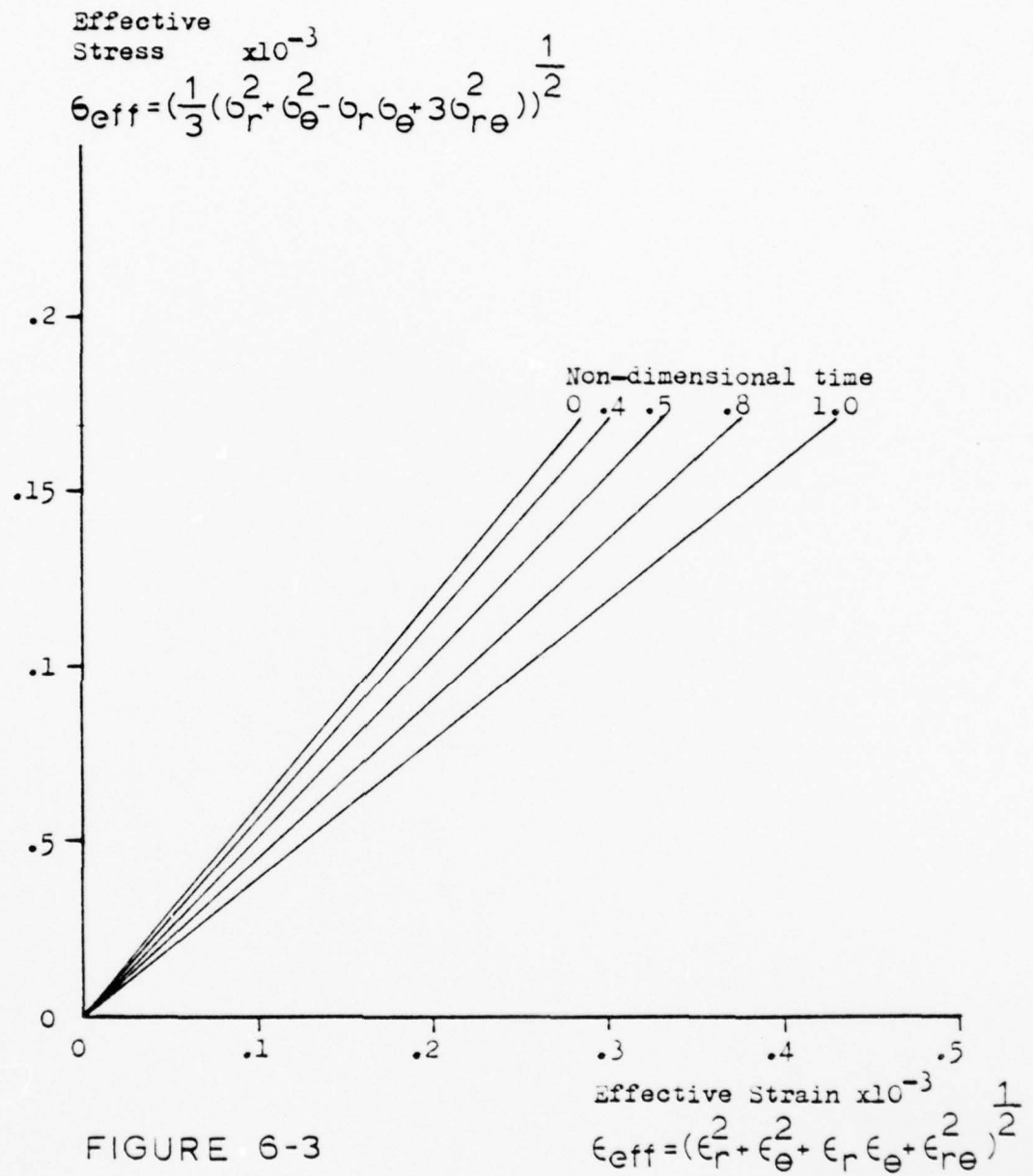


FIGURE 6-3

Viscoelastic behavior - stress-strain diagram showing creep for loading condition of Figure 6-1, at the pile-ice sheet interface.

elastic modulus is then limited to a value of 10% decrease. This then becomes the transition boundary between visco-elastic and elastic behavior of Figure 2-2.

In the example, loadings of those shown in Figure 6-2 are used to define a region of validity in Figure 6-4.

Using actual values such as those found in Section 2-4, it can be seen that a time of approximately 10 minutes defines the region at low stress levels (below yield).

The effective stress and strain plotted in Figure 6-3 are defined:

$$\sigma_{EFF}^2 = \frac{1}{3} (\sigma_r^2 + \sigma_\theta^2 - \sigma_r \sigma_\theta + 3 \sigma_{re}^2) \quad (6.1)$$

$$\epsilon_{EFF}^2 = (\epsilon_r^2 + \epsilon_\theta^2 + \epsilon_r \epsilon_\theta + \epsilon_{re}^2) \quad (6.2)$$

For this loading condition, it can be seen that a value for modulus of elasticity is about one half the uniaxial value. This will vary as well along each point in the radius of the ice sheet. Interestingly enough, the relaxation to 90% of its former value occurred at the same time, despite the variation. Under a more general loading, not confined to the zero wavenumber, it is likely that the material will behave not in the same region of Figure 2-2 over its entire geometry.

6.2 Under Rate Loading

The example in the previous Section was subjected to rate conditions on the loading. This was done to test the capacity for this parameter in the model. The load-time

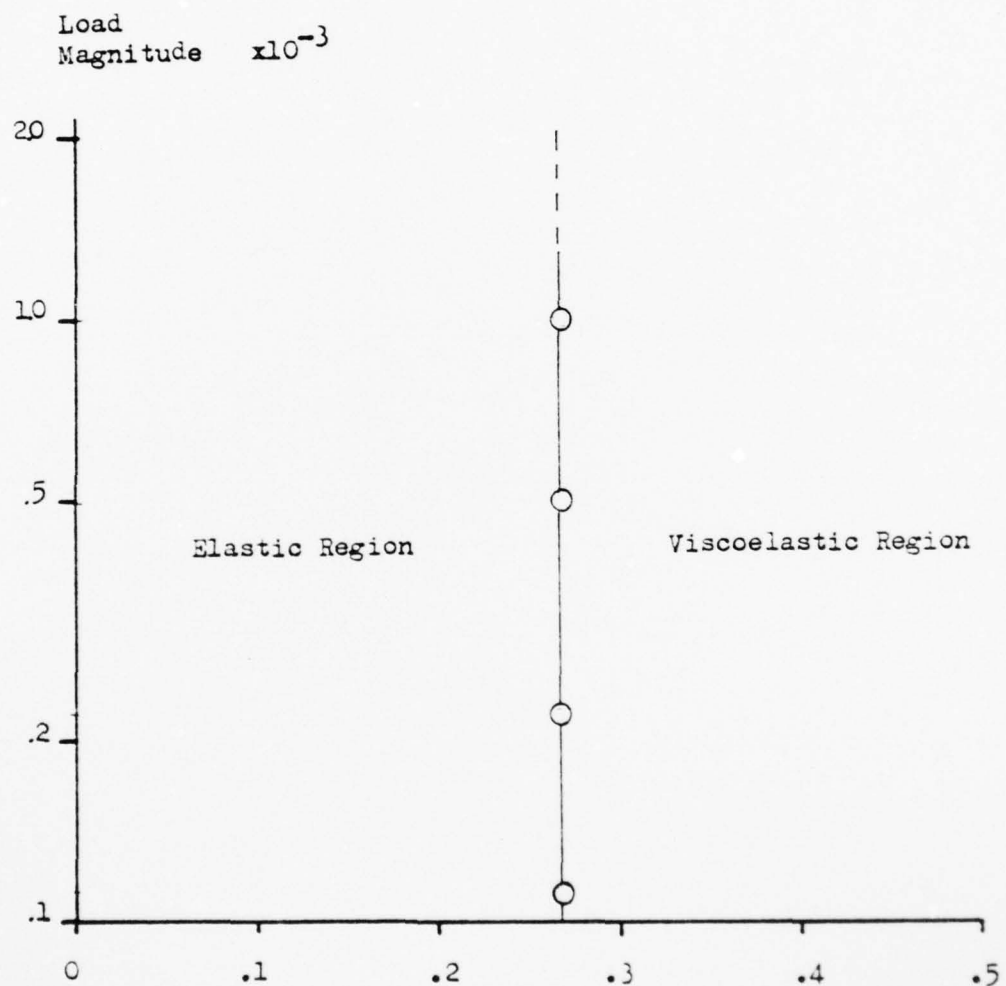


FIGURE 6-4 Load duration - non-dimensional time

Viscoelastic behavior - Elastic-Viscoelastic transition

from load curves of Figure 6-2. By definition, relaxation

of elastic modulus is limited to 10%.

curves for the loading of Figure 6-1 are presented in Figure 6-5 for three loading rates. The greatest rate is very close to the maximum of 5000 psi/min suggested by Katona and Vaudrey to avoid dynamic effects. No general conclusions are drawn here since the size of the initial load and the various rates have little significance without a specific physical problem to simulate.

6.3 Analysis of a Friction Coefficient

The loading situation in Figure 6-6 was applied to the model to determine the ratio of shear stress to (compressive) radial stress at the rigid pile interface. This could be construed to be an indication of a static type of frictional coefficient, but since the model also assumes capability of the interface to support a tension, in this region "friction coefficient" would be meaningless.

The analysis proceeded with those values that this edge loading produced. Defining the coefficient of static friction as:

$$\mu_s = \left| \frac{\sigma_{re}}{\sigma_r} \right| \quad (6.3)$$

it can be seen that this coefficient will vary about the interface at least to the point at $\theta = \frac{\pi}{2}$ where σ_r becomes tensile and a coefficient of friction becomes meaningless (Figure 6-7).

At a value of $\theta = .31$ radian (given this loading),

$$\mu_s = .3$$

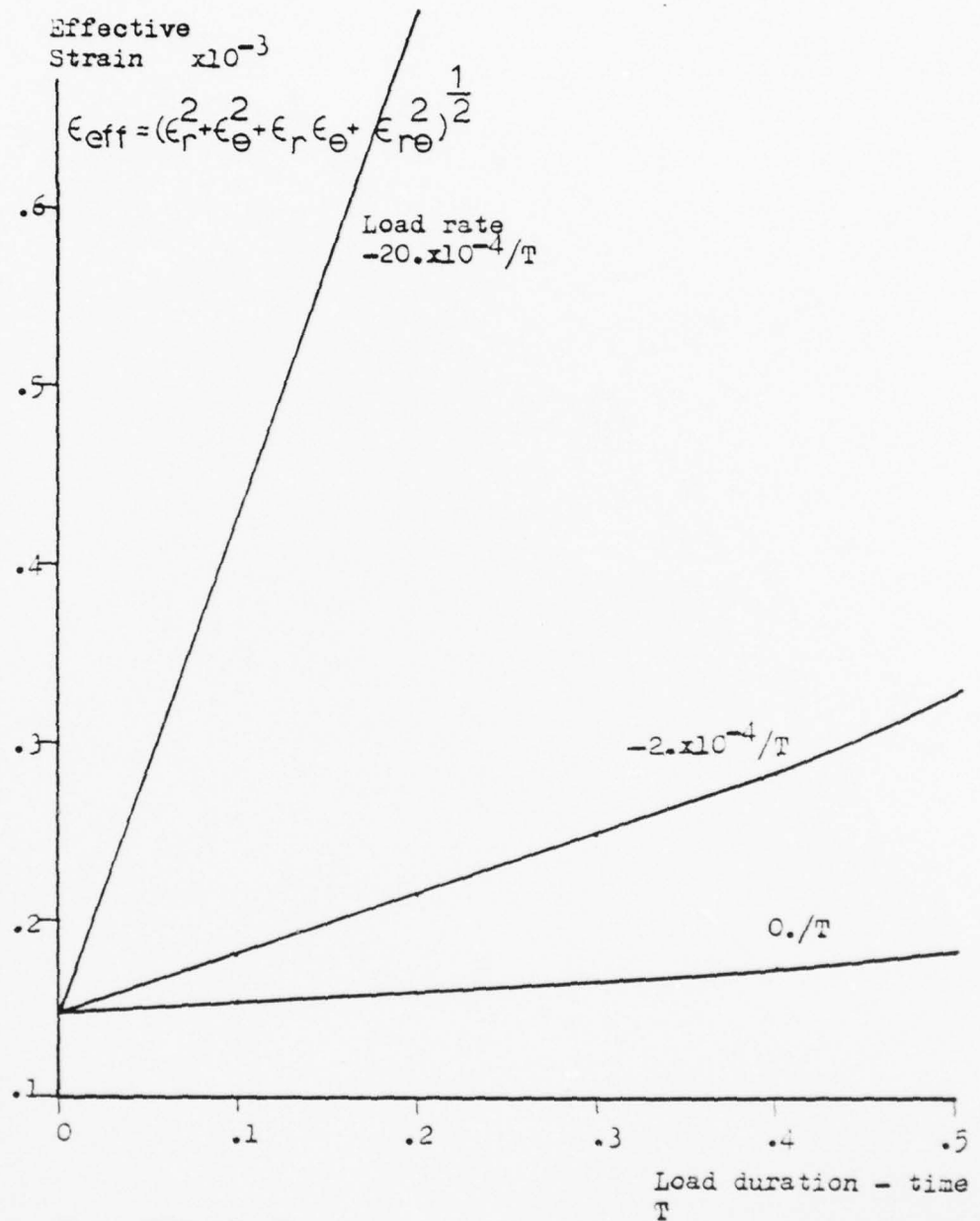


FIGURE 6-5

Visco-elastic behavior - ϵ_{eff} vs. time curve under three loading rates, at the pile - ice sheet interface. Loading condition of Figure 6-1 applies. with $\epsilon_r = .1111 \times 10^{-3}$

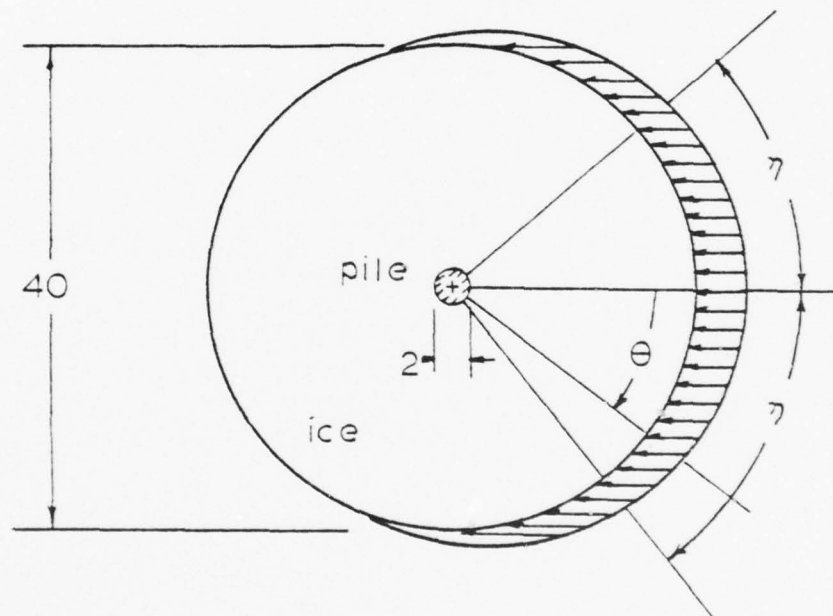
$R_{out} = 20.$

$\sigma_r = -.333 \cos^2 \theta$ outer boundary

$\sigma_{r\theta} = -.333 \sin \theta \cos \theta$ outer boundary

for $-\pi \leq \theta \leq \pi$

and 0. otherwise



at the inner boundary or pile-ice
sheet interface:

$R_{in} = 1.$

$u_r = u_\theta = 0.$ considering "friction"

and

$\sigma_{r\theta} = u_r = 0.$ "frictionless"

FIGURE 6-6

Loading condition circular pile - ice sheet interaction

for cases discussed in Sections 6-3 and 6-4.

AD-A072 676

NAVAL POSTGRADUATE SCHOOL MONTEREY CA

F/G 8/12

DEVELOPMENT OF A VISCOELASTIC FINITE DIFFERENCE FORMULATION FOR--ETC(U)

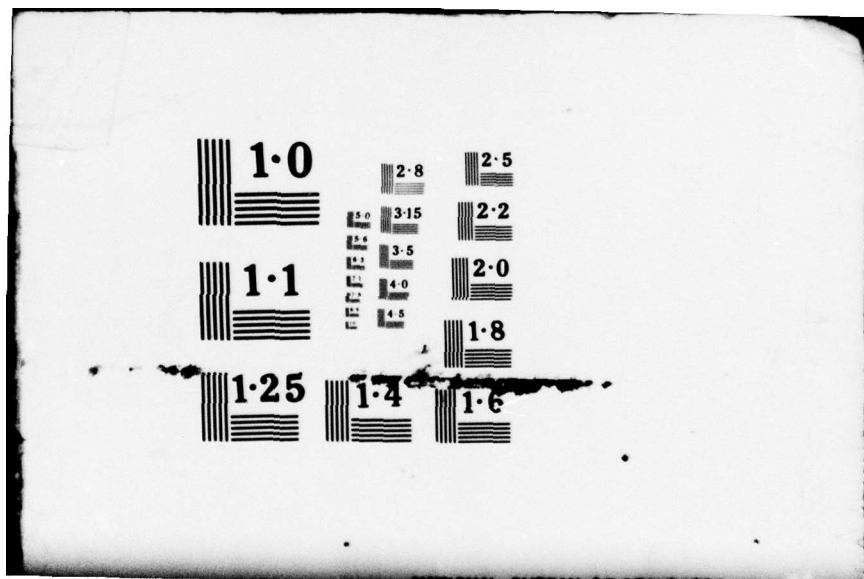
JAN 79 M W PRASKIEVICZ

UNCLASSIFIED

NL

2 OF 2
AD
A072676





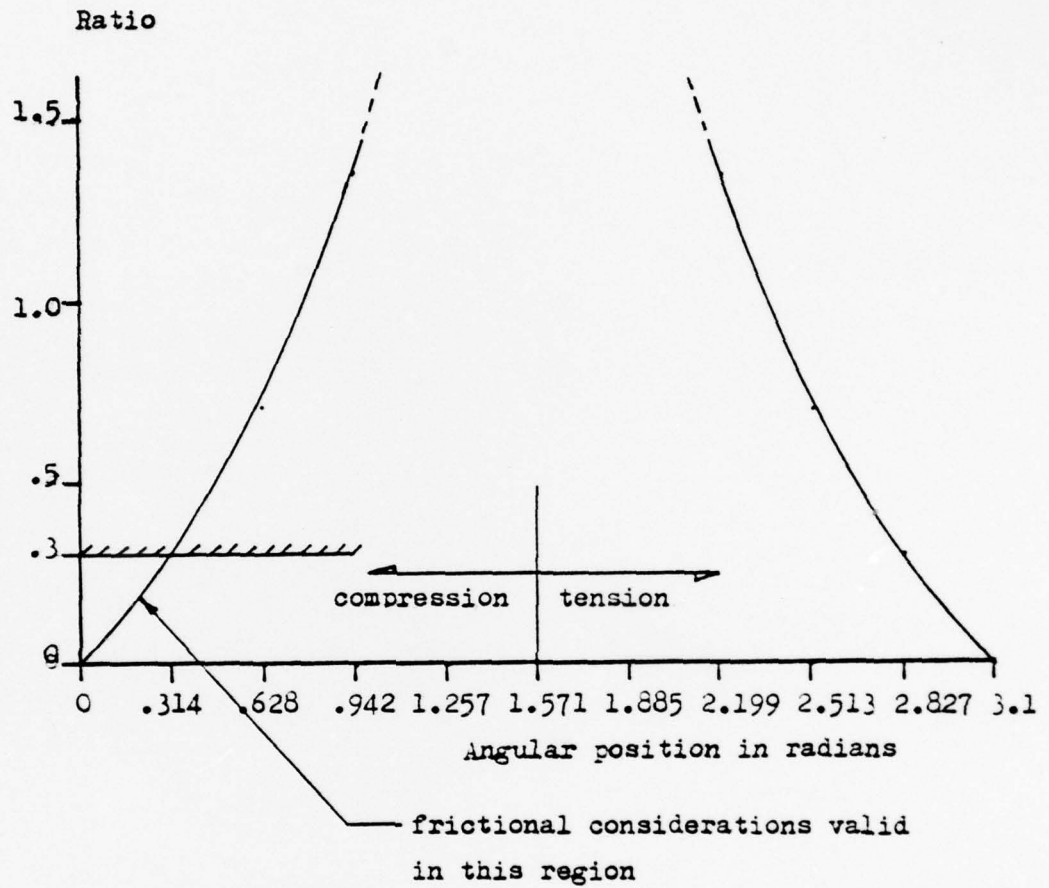


FIGURE 6-7

Ratio of shear stress to radial stress at the circular pile - ice sheet interface, loading of Figure 6-6 applies.

Now if there is no ice - pile adhesion present and if the frictional coefficient of smooth sea ice on a smooth steel circular pile is about .3 as some investigators indicate, then it is clear that for regions beyond .31 radian α_0 will be nonzero. A situation involving mixed boundaries and separation will then be evident.

By changing the loading to:

$$\sigma_r = -Q_r \cos \theta$$

$$\sigma_{re} = -Q_{re} \sin \theta$$

it was found that the coefficient of friction at the interface changed only slightly. Since for the wavenumber zero, only normal stresses are conveyed (being an odd function) and the higher wavenumbers lose their influence with increased radius, frictional forces are important only in the region $|\theta| \leq .31$ radian for non-axisymmetric loads.

A conclusion can be drawn that for the model of the circular pile - ice sheet interaction and unless ice adhesion is present, frictional behavior is confined to a small area preceding the pile and may be unimportant in analysis.

6.4 Analysis of the Behavior of Ice Floe - Pile Interaction Comparing Adhesive and Non-adhesive Behavior

Since the influence of friction at the circular pile is minimal, it is necessary now to compare the behavior at the interface using complete adhesion (frozen-in situation) and and using complete circumferential freedom.

The loading of Figure 6-6 again was applied to the model to consider the effect on the radial stresses of a "frictionless" boundary. Since the loading is the same for both, the net force felt by the pile is the same in both cases. Figure 6-8 presents the variation of radial stresses in both cases. The point where adhesion is required is precessed to 1.48 radians.

Noble and Hussein [24] obtain a value of 1.24 radians analytically in their formulation. Severe differences do exist in the problem as their model does not support tension. Therefore it would be expected that in the new model, the radial stress on the compression side would be supporting the lost force on the tension side, with basically the same shape in the loading curve.

At any rate, a conclusion can be drawn that the frictionless case is the worst as far as local normal pressures on the pile structure are concerned, and that the maximum force can be as high as three or four times the frozen-in case. Of course, the total lateral load remains the same.

6.5 Locations of Maximum Stress and Strain

As a final use of the model, information from the loading of Figure 6-6 will be presented. Physically, this edge loading might be produced by a wave driving force impinging on the circular floe. No failure mechanism is included, since some investigators feel that failure is ductile, caused by a

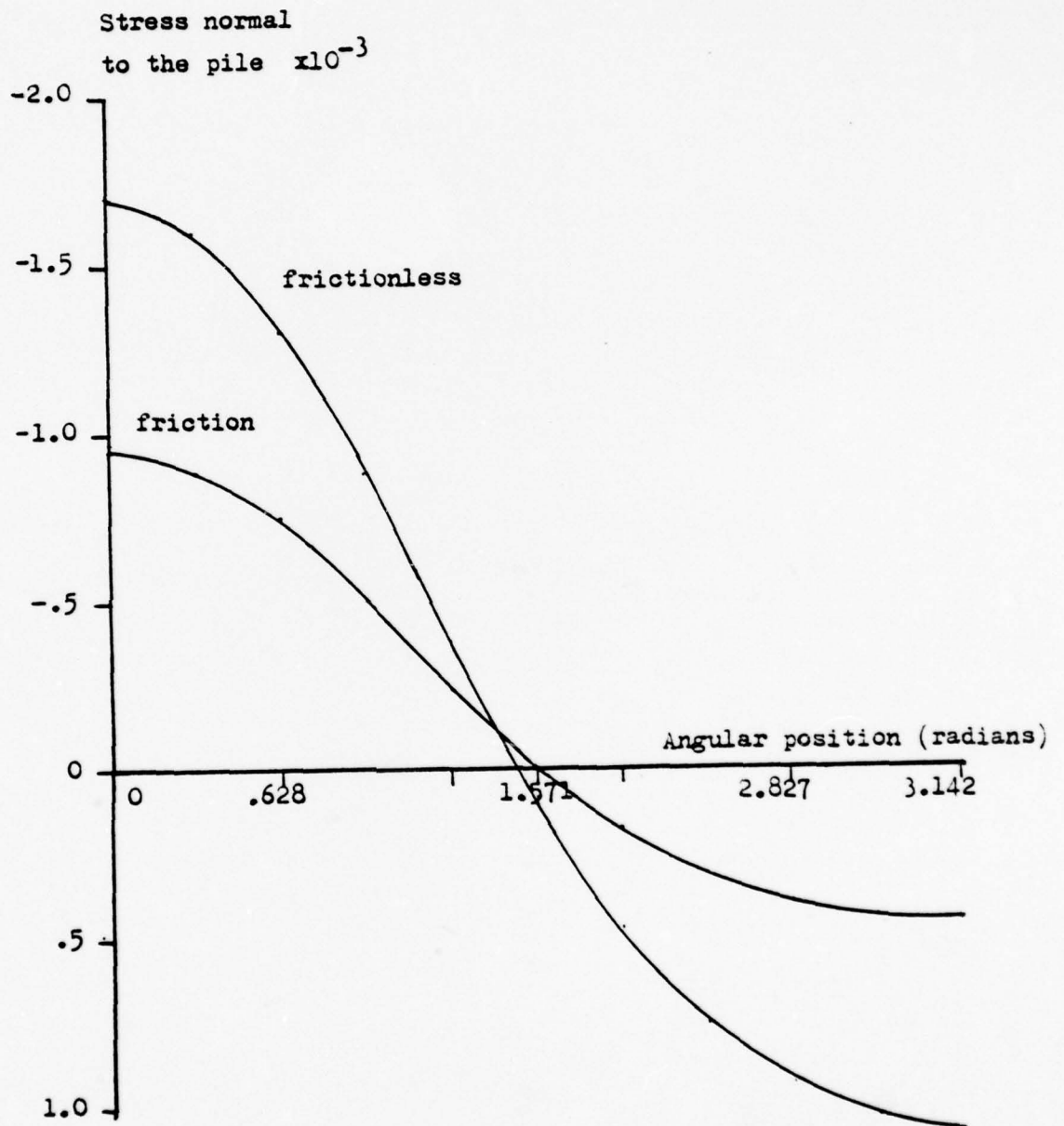


FIGURE 6-8

Comparison of normal (radial) stress at pile - ice sheet interface, with and without friction. Loading of Figure 6-6 applies.

limiting strain, and no reliable theory is available. Therefore no estimation of a maximum total force will be offered, but a good representation of stress and strain distribution can be presented.

Figure 6-9 depicts the variation of normal (radial) and shear stresses throughout the ice sheet and at selected angles Θ . The greatest radial stress is at $\Theta=0^\circ$ as would be expected. The crossover to tension occurs at $\Theta=90^\circ$. The maximum shear stress occurs at about 54° , again at the inner face.

Figures 6-10 and 6-11 show the variation in vertical and hoop strain around the pile. If tension strain failure is the failure mechanism, it can be seen that failure will occur in the sheet vertically (a horizontal crack) and horizontally (vertical crack) at angles of 0° and 54° respectively. Shear strain follows the shear stress and in this case is $2/3$ the σ_{re} value. Shear strain is shown in Figure 6-12. The values of these strains are plotted in Figures 6-10, 6-11, 6-12 only at the interface, since this is the location of their maxima. It should be pointed out that the basic shape is maintained some way into the ice sheet, so that a crack would be initiated at the ice - pile interface and propagate radially outward.

It would seem heuristically that the cracks at 54° would occur first due to the greater magnitude of the strain. It is then possible that the crack at 0° will then follow due to the redistribution of stress. Both types have been reported [15].

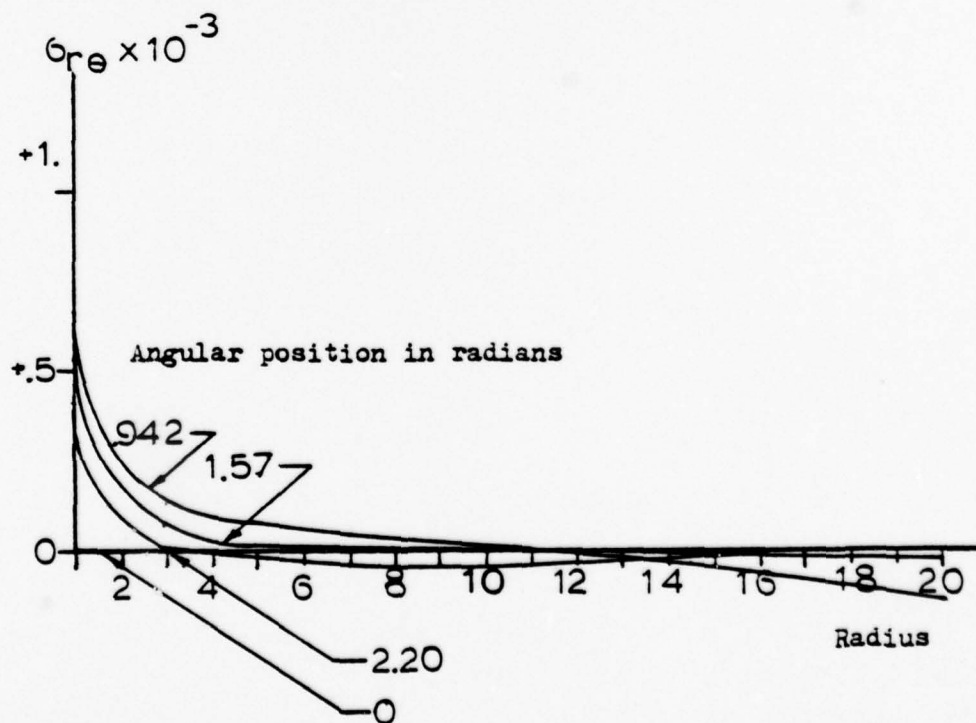
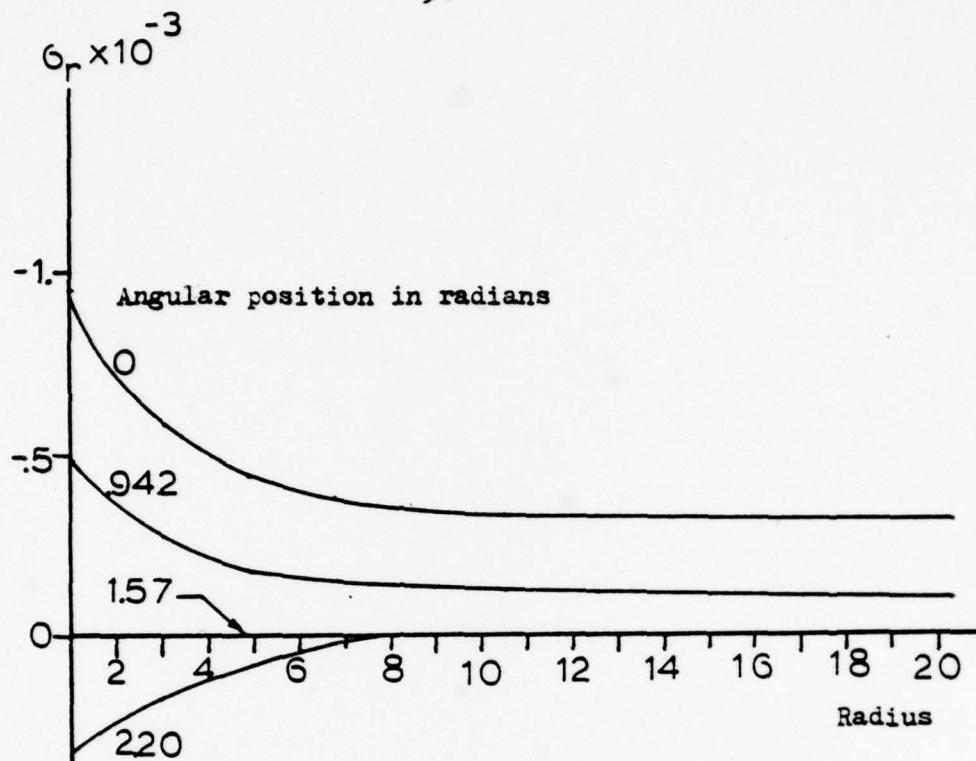


FIGURE 6-9

Elastic behavior - Loading of Figure 6-6 - Variation of normal (radial) and shear stresses throughout the ice plate

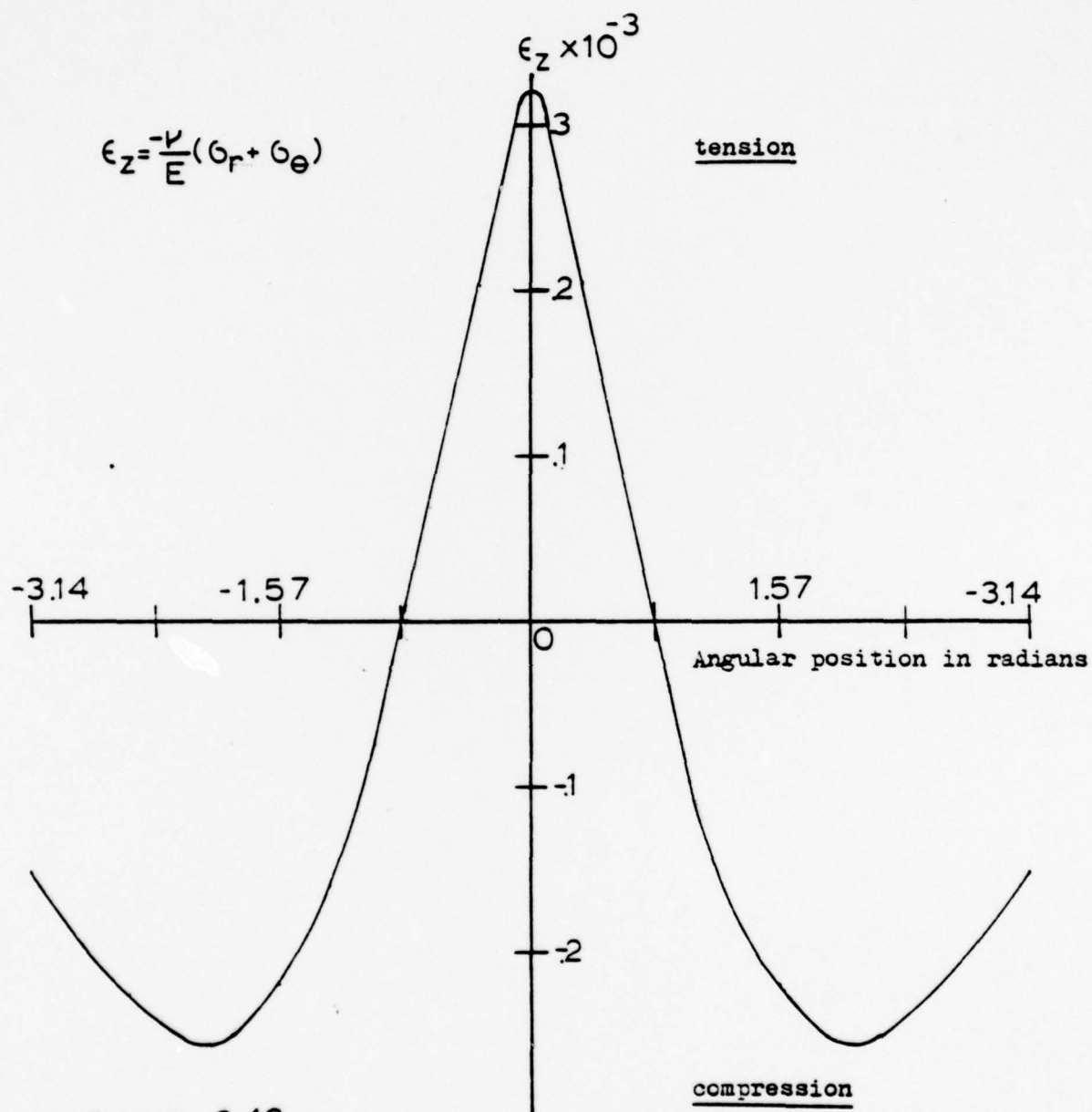


FIGURE 6-10

Elastic behavior - maximum vertical strain location on ice - pile interface. Plot of vertical strain vs. angular position at radius equal to 1. Loading of Figure 6-6 applies.

$$\epsilon_{\theta} = \frac{1}{E}(\sigma_{\theta} - \nu \sigma_r)$$

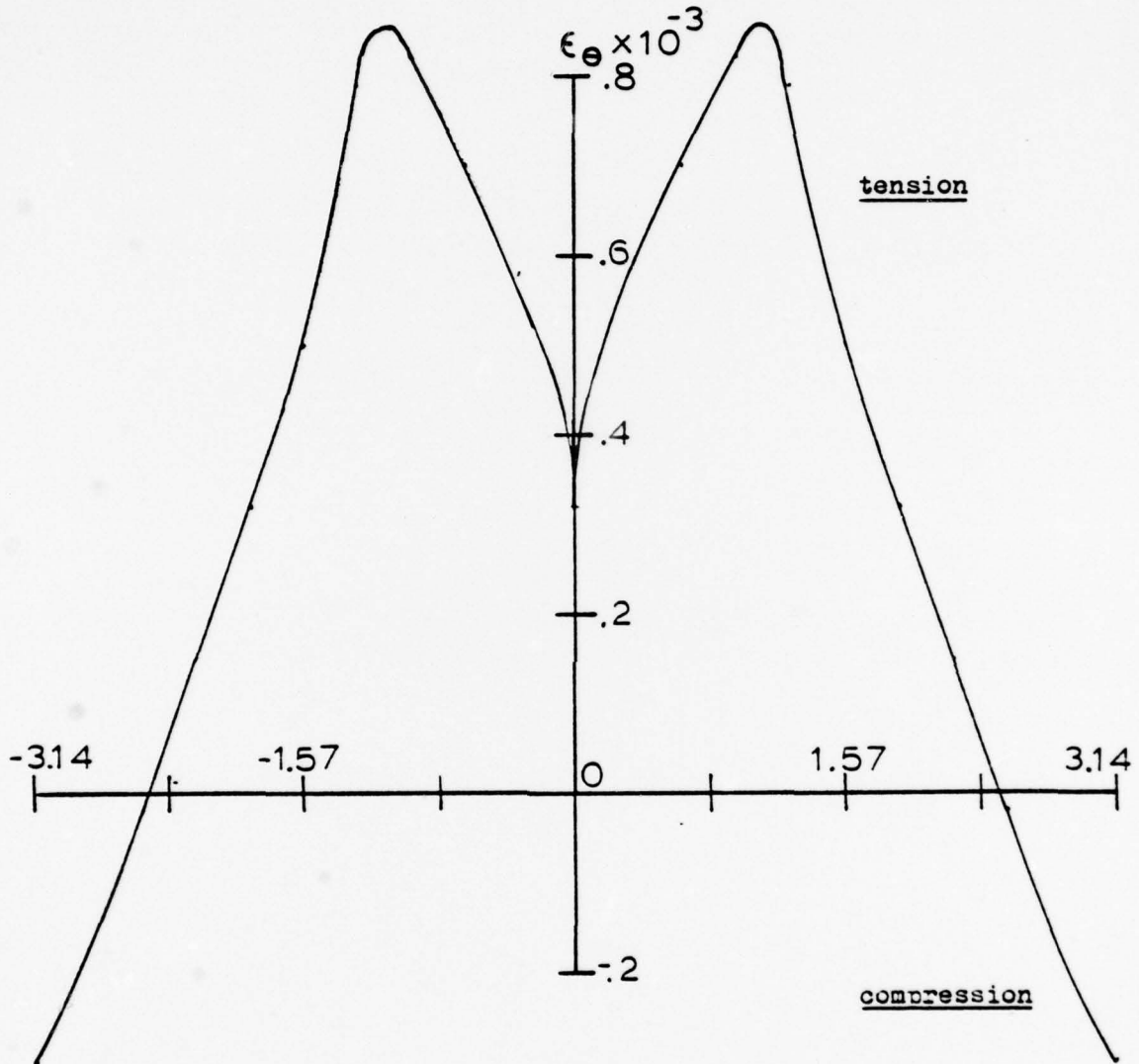


FIGURE 6-11

Elastic behavior - maximum hoop strain location on ice - pile interface. Plot of hoop strain vs. angular position at radius equal to 1. Loading of Figure 6-6 applies.

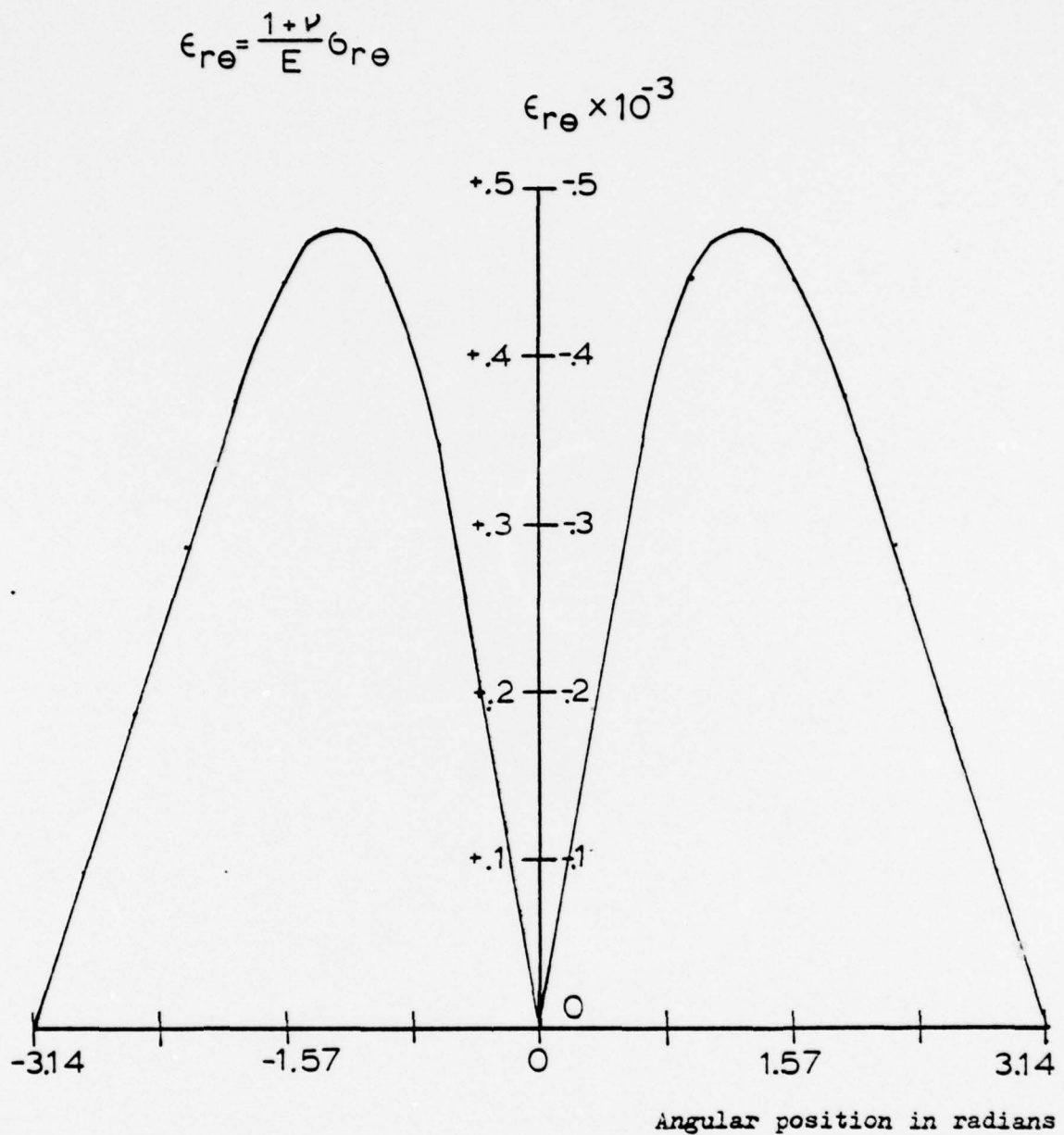


FIGURE 6-12

Elastic behavior - maximum shear strain location on ice - pile interface. Plot of shear strain vs. angular position at radius equal to 1. Loading of Figure 6-6 applies.

CHAPTER 7

Conclusions and Recommendations7.1 Conclusions

The model developed in the preceeding chapters is applicable to a circular elastic or viscoelastic sheet surrounding a rigid circular inclusion. The conditions of plane stress are assumed, although plane strain could be very easily implemented. Loading can be by displacement or stress at either boundary, although mixed conditions at a particular boundary are not allowed. The model is favorably disposed for inclusion of failure criteria, but none are included or proposed. Tension is required at the interface to support a valid operation and this corresponds to a frozen-in situation. This model can accept time dependent loadings below dynamic significance.

The model is very thrifty with computational resources and produces a very high degree of correlation with existing analytical solutions. The model is capable of considerable expansion.

Some results with a fictional loading predict frictional effects are present only at a small region immediately preceding the pile. If angular movement is allowed, the resultant loss of shear requires an increase in normal stresses. If a separation of boundary is to occur, and occurs where tension cannot be supported, then the contact angle will be $\leq 90^\circ$.

The range of time where ice can be considered elastic (below yield levels) with a uniaxial load is:

$$\text{time} \leq \frac{.28}{E \alpha}$$

Other loadings could be analyzed. Rate of loading is important insofar as time to failure and required force. Finally, viscoelastic behavior predicts ice failure (and maximum forces) for loading well below immediate fracture.

Lastly, it is possible to qualitatively see failure by limiting strain or shear at locations in the ice sheet that are physically relevant. Without knowing the values of biaxial strengths of the ice material, it is not possible to predict a maximum force before fracture, but it is likely that a limiting strain or shear strength precedes ultimate crush failure.

7.2 Recommendations for Future Work

The model developed in this thesis is extremely rudimentary and can be used for pile - ice sheet interaction under only the most generous conditions. Improvements can be made, however, to increase the usefulness into problems with more physical application. These improvements by order of importance are:

(1) Driving Forces

Ice sheets and ice floes are driven by the effects of wind and current shears. It would be desirable to develop an analytical or numerical procedure whereby these shears can

be approximated into edge loading conditions. The size of the ice sheet considered in this model would require negligible wind or current shear itself, so that the two-dimensional approximation could remain valid.

(2) Failure

The failure mechanism or mechanisms can be easily applied to the model if a good choice could be found. To date, investigators have proposed Tresca or Von Mises type criteria, failure by limiting strain, rate dependent crush strength, among others. The behavior of ice is poorly understood in biaxial loading and experimental work needs to be carried out to properly extend the model into realistic and workable significance.

(3) Two-dimensional Extension

The model should be given another co-ordinate in the plane such that more general geometries can be analyzed. Of course this could mean larger quantities of data to be handled and an attendant loss of simplicity. The problem of the mixed boundary conditions and different shapes of the ice floes or structures could be adjusted to fit physical requirements with a high degree of confidence.

(4) Multiple Structure

The model, once in a more general two-dimensional state, could be extended to study the effect of multiple structures such as support pilings on a pier or multilegged towers. Possible reductions in forces by interference could be shown.

(5) Other Material Behavior

Once in a two-dimensional form, the model could be extended into non-linear and non-elastic behavior in a straightforward manner. The one-dimensional form presented in this thesis is valid only where superposition is valid.

(6) Other Structural Behavior

Experimental work with the model could be extended into non-rigid analysis for study of structural responses and forced vibrations.

Data on the material properties of ice in a biaxial state of stress need to be acquired for realistic implementation in the model. Once this and the six stated improvements of the model are implemented, the behavior of the ice sheet-structure problem can be fully analyzed and more general design equations or curves offered. Additionally, the influence of other important parameters such as temperature profile or variation of ice thickness can then be included or discarded.

REFERENCES CITED

1. Assur, A., "Forces in Moving Ice Fields", International Conference on Port and Ocean Engineering under Arctic Conditions (P.O.A.C.), Trondheim, Norway, 1971.
2. Assur, A., "Structures in Ice Infested Waters", International Association for Hydraulic Research (I.A.H.R.) Symposium, Leningrad, U.S.S.R., 1972.
3. Assur, A., "Problems in Ice Engineering", Third I.A.H.R. Symposium, Hanover, New Hampshire, 1975.
4. Bercha, F.G., "Mathematical Simulation of Ice - Structure Interactions", Proceedings of the Fifth Canadian Congress of Applied Mechanics, Frederickton, Alberta, 1975.
5. Bercha, F.G. and J.V. Danys, "Prediction of Ice Forces on Conical Offshore Structures", Third I.A.H.R. Symposium, Hanover, New Hampshire, 1975.
6. Bercha, F.G., "On the Scale Effect in Ice Mechanics", Proceedings of the Sixth Canadian Congress of Applied Mechanics, Vancouver, British Columbia, 1977.
7. Carstens, T. and R.C. Byrd, "The Oscillating Icebreaking Platform", Third I.A.H.R. Symposium, Hanover, New Hampshire, 1975.
8. Condon, E.U. and H. Odishaw, Handbook of Physics, Second Edition, McGraw-Hill, New York, 1967.
9. Croasdale, K.R., "Ice Forces on Marine Structures", Third I.A.H.R. Symposium, Hanover, New Hampshire, 1975.
10. Det Norske Veritas, "Rules for the Design, Construction and Inspection of Fixed Offshore Structures", Oslo, 1974.
11. Frederking, R. and L.W. Gold, "Ice Forces on an Isolated Circular Pile", P.O.A.C. Trondheim, Norway, 1971.
12. Frederking, R., "Mechanical Properties of Ice and Their Application to Arctic Ice Platforms", Society of Naval Architects and Marine Engineers Symposium, ICE TECH 75, Montreal.
13. Glen, J.W., "The Mechanics of Ice", U.S. Army Cold Region Research and Engineering Laboratory (C.R.R.E.L.), Monograph ii-C2b, Hanover, New Hampshire, 1975.

14. Hirayama, K., J. Schwarz and H. Wu, "An Investigation of Ice Forces on Vertical Structures", Iowa Institute of Hydraulic Research, N.T.I.S. AD-A017879, 1974.
15. Hirayama, K., J. Schwarz and H. Wu, "Ice Forces on Vertical Piles, Indentation and Penetration", Third I.A.H.R. Symposium, Hanover, New Hampshire, 1975.
16. International Mathematical and Statistical Libraries Inc., Publication LIB02-0006V2, Houston, 1977.
17. Jazrawi, W. and J.F. Davies, "A Monopod Drilling System for the Canadian Beaufort Sea", S.N.A.M.E. ICE TECH 75, Montreal.
18. Katona, M.G. and K.D. Vaudrey, "Ice Engineering - Summary of Elastic Properties Research and Introduction to Viscoelastic and Nonlinear Analysis of Saline Ice", Naval Civil Engineering Laboratory Report R-797, Port Hueneme, California, 1973.
19. Korzhavin, K.N., "Action of Ice on Engineering Structures", U.S. Army C.R.R.E.L. translation, Hanover, New Hampshire, 1971.
20. Korzhavin, K.N., "Dynamic Ice Pressures and Deformation of Structures", I.A.H.R. Symposium, Reykavik, 1970.
21. Määtänen, M., "Ice Forces and Vibrational Behavior of Bottom Founded Steel Lighthouses", Third I.A.H.R. Symposium, Hanover, New Hampshire, 1975.
22. McKinney, W.M. and J.F. Lea, "Mobile Foundation for Off-shore Drilling Platform in an Arctic Environment", A.S.M.E. Paper n74-wa 1974.
23. Martin, R.S. and J.H. Wilkenson, "Solution of Symmetric and Unsymmetric Band Equations and the Calculation of", Numerische Mathematik 9(4) 1967.
24. Noble, B. and M.A. Hussein, "Exact Solution of Certain Dual Series for Indentation and Inclusion Problems", International Journal of Engineering, Volume 7, 1969.
25. Peyton, H.R., "Sea Ice Forces", Ice Pressures Against Structures, Conference Proceedings, Laval University, Montreal, 1966.
26. Peyton, H.R., "Ice and Marine Structures", Ocean Industry, (3 parts) Volume 3, numbers 3,9,12, 1968.

27. Ross, B., S. Hanugud and G.S. Sidhu, "Ice Floe-Offshore Platform Interaction", P.O.A.C., Trondheim, Norway, 1971.
28. Timoshenko, S. and J.M. Gere, Theory of Elastic Stability, McGraw-Hill, New York, 1961.
29. Timoshenko, S. and J.N. Goodier, Theory of Elasticity, Third Edition, McGraw-Hill, New York, 1970.
30. Tryde, P., "Intermittant Ice Forces Acting on Inclined Wedges", U.S. Army C.R.R.E.L. Report 77-10, Hanover, New Hampshire, 1977.
31. Wang, C., Applied Elasticity, McGraw-Hill, New York, 1953.
32. Watts, F.J., "Ice Loads on Bridge Piers", U.S. Department of Transportation, Federal Highway Administration, 1976.
33. Weeks, W.F. and A. Assur, "The Mechanical Properties of Sea Ice", Ice Pressures against Structures, Conference Proceedings, Laval University, Montreal, 1966.
34. Hanagud, S., B. Ross and G. Sidhu, "Elastic-Plastic Impact of Plates", Israel Journal of Technology, Volume 7, numbers 1, 2, 1968.

APPENDIX A-1
Program Variables

<u>Variables in Common</u>	<u>Purpose</u>
n	number of radial spaces
nn	number of circumferential spaces
nnpls	nn+1
ind	indicator of boundary conditions used (see listing under load- bdy)
m	wave number
ru	poisson ratio
el	Young's modulus
pi	3.1415...
alpha	viscous coefficient
mdes	number of wave numbers to be processed
rout	outer radius
rin	inner radius
ldsp	$4 \times N \div$ number of radial display intervals
ibar	termination variable
<u>Variables Consistently Used</u>	
irowmax	number of simultaneous equations to be solved

tstop	stop time limit (visco elastic solution)
tstep	time step interval
time	time since start (elastic: time = 0)
disint	time display interval of viscoelastic solutions
streslim	elastic limit of stress
strnlim	limiting strain
rad	radius
hoop	hoop stress

APPENDIX A-2

Description of Arrays

<u>Array</u>	<u>Subroutine</u>
/blok1/ <u>a</u> (1601,17) double precision	<u>elastic</u> , <u>zerabx</u> , <u>loada</u> , <u>strain</u> , <u>loadbdy</u> , <u>visco</u> , <u>dpband</u>
purpose: holds coefficient matrix in band compressed form - after call to <u>dpband</u> holds the factored matrix	
/blok2/ <u>b</u> (1601,1)	<u>elastic</u> , <u>zerabx</u> , <u>loadbdy</u> , <u>visco</u> , <u>loadb</u> , <u>boundb</u> , <u>strain</u> , <u>dpband</u>
purpose: solution vector of the system of linear equations represented by <u>a</u>	
/blok3/ <u>c</u> (204,21)	<u>elastic</u> , <u>zercdr</u> , <u>recomb</u> , <u>writr2</u>
purpose: stores total recombined solutions at every eighth node (rcw) and all circumferential positions	
/blok4/ <u>d</u> (11,8)	<u>elastic</u> , <u>zercdr</u> , <u>fourier</u> , <u>loadbdy</u> , <u>writr0</u>
purpose: stores fourier coefficients of boundary conditions for 0 through 10 wave numbers (row), inner conditions (first four columns), outer conditions (second four columns) as determined by variable <u>ind</u>	
<u>rl</u> (8,21)	<u>loader</u> , <u>fourier</u>
purpose: stores boundary information from <u>main</u> before fourier decomposition	

ws(21)fourier, simps .purpose: working vector to be integrated by simps/blok6/x1(14436)elastic, zerabx, dpband, visco

double precision

purpose: working storage used by dpband/blok8/r(204,11)elastic, zercdr, recomb

purpose: stores elastic wave number solutions for every eighth node

/blok9/t(51,11)elastic, zercdr, recomb

purpose: stores hoop stress wave number solutions for every eighth node (similar to /blok8/)

/blok10/tt(51,21)elastic, zercdr, recomb, writr2

purpose: stores total recombined elastic hoop stress solution (similar to /blok3/)

/blok11/rr(1604,1)visco, loade

double precision

purpose: working vector

APPENDIX A-3

Listing of programs

```

c main
common /blok5/n,nr,nr,nr,ind,m,ru,rel,ri,alpha,mdes
common /blok7/rout,rin
dimension put1(21),put2(21),put3(21),put4(21)
pi=3.1415193
ru=.290
cinc=pi/20.
do 10 i=1,21
  put1(i)=0.
  put2(i)=0.
  put3(i)=-1.*(cos(float(i-1)*cinc))
  put4(i)=-1.*(sin(float(i-1)*cinc))
10 continue
ind=1
rout=3.
rin=1.
call elastic (put1,put2,put3,put4)
stop
end

```

```

subroutine elastic (put1,put2,put3,put4)
common /blok1/a(1604,17)
common /blok2/b(1604,1)
common /blok3/c(204,21)
common /blok4/d(11,8)
common /blok5/n,nnn,nnpls,ind,m,ru,el,pi,alpha,mdes
common /blok6/xl(14436)
common /blok7/rout,rin
common /blok8/r(204,11)
common /blok9/t(51,11)
common /blok10/tt(51,21)
common /blok12/idsp,ibar
dimension put1(21),put2(21),put3(21),put4(21)

c this subroutine solves the elastic stress field
c
c
double Precision a,b,xl
write(6,100)
100 format(1x,'viscoelastic solution of stressed circular plate with',
& ' a rigid circular inclusion',//)
n=400
nn=20
nnpls=nn+1
alpha=1.
el=1.0
pi=3.141593
ibar=0
idsp=160
data nuc,nlc,ia,ib,ijob,irt/8,8,1604,1604,0,1/
irowmax=4*(nn+1)
call zerabx
call zercdr
call loader (put1,put2,put3,put4)
call writro
write(6,103)
read(5,101)mdes

```

```

103 format(1x,'up to how many wavenumbers desired?')
101 format(v)
    write(6,105)
    read(5,101)ivis
    write(6,106)
    read(5,101)ithe
105 format(1x,'viscoelastic solution? (1 or 0)')
106 format(1x,'display of theta information? (1 or 0)')
    do 20 i=1,mdes
        m=i-1
        call loada
        call loadbda
        call dfrband (a,irowmax,nlc,nuc,ia,b,irt,ib,0,xl,ier)
        irowsp=irowmax-3
        do 15 irow=1,irowsp,32
            i2=(irow-1)/8+1
            i3=i2/4+1
            r(i2,i)=sngl(b(irow,1))
            r(i2+1,i)=sngl(b(irow+1,1))
            r(i2+2,i)=sngl(b(irow+2,1))
            r(i2+3,i)=sngl(b(irow+3,1))
            rad=rin+float(i3-1)*(rout-rin)/float(n)
            t(i3,i)=el/rad*r(i2+2,i)+el/rad*r(i2+3,i)*float(m)+ru*r(i2,i)
15 continue
        call strain
        if(ivis.eq.1)call visco
        call recomb
        call zerabx
20 continue
    if(ithe.eq.1)call writr2
    return
end

```

c
c


```

subroutine zerabx
common /blok1/a(1604,17)
common /blok2/b(1604,1)
common /blok5/n,nn,nnpls,ind,m,ru,el,pi,alpha,mdes
common /blok6/xl(14436)

c this subroutine zeros common arrays a,b,d,xl
c
double precision a,b,xl
integer xlmax
irowmax=4*(n+1)
xlmax=9*irowmax
do 6 j=1,17
do 5 i=1,irowmax
a(i,j)=0.d0
b(i,1)=0.d0
5 continue
6 continue
do 9 i=1,xlmax
xl(i)=0.d0
9 continue
return
end

```

c
c

```

subroutine zerodr
common /blok3/c(204,21)
common /blok4/d(11,8)
common /blok5/n,nr,np,ls,ind,m,rur,el,pi,alpha,mides
common /blok8/r(204,11)
common /blok9/t(51,11)
common /blok10/tt(51,21)

```

```
c
c this subroutine zeros arrays c,d,r,t, and tt
```

```

irowmax=204
do 6 j=1,nnp1s
do 5 i=1,irowmax
ii=i/4+1
tt(ii,j)=0.
c(i,j)=0.
5 continue
6 continue
do 8 j=1,8
do 7 i=1,11
d(i,j)=0.
7 continue
8 continue
do 10 j=1,11
do 9 i=1,irowmax
ii=i/4+1
r(i,j)=0.
t(ii,j)=0.
9 continue
10 continue
return
end

```

U U

```

subroutine loader (put1,put2,put3,put4)
common /blok5/n,nnp1,ind,m,ru,el,pi,alpha,mdes
dimension put1(21),put2(21),put3(21),put4(21)
dimension rl(8,21)

c this subroutine passes boundary information into array rl
c which holds sigma(r)...u(theta) in row, circumferential in column.
c put1...put4 are sent from main.
c ind is the index used to specify which row in rl the data will
c occupy and corresponds to loading desired.
  do 4 j=1,nnp1s
    do 3 i=1,8
      rl(i,j)=0.
    3 continue
    4 continue
      if(ind.eq.1)go to 5
      if(ind.eq.2)go to 7
      if(ind.eq.3)go to 9
      if(ind.eq.4)go to 11
      go to 99
    5 do 6 j=1,nnp1s
      rl(3,j)=put1(j)
      rl(4,j)=put2(j)
      rl(7,j)=put3(j)
      rl(8,j)=put4(j)
    6 continue
      go to 12
    7 do 8 j=1,nnp1s
      rl(1,j)=put1(j)
      rl(2,j)=put2(j)
      rl(5,j)=put3(j)
      rl(6,j)=put4(j)
    8 continue
      go to 12
    9 do 10 j=1,nnp1s
      rl(3,j)=put1(j)
      rl(4,j)=put2(j)

```

```
      r1(5,j)=put3(j)
      r1(6,j)=put4(j)
10  continue
      go to 12
11  do 12 j=1,nnp1s
      r1(1,j)=put1(j)
      r1(2,j)=put2(j)
      r1(7,j)=put3(j)
      r1(8,j)=put4(j)
12  continue
      call fourier (r1)
99  return
      end
```

c
c

```

subroutine fourier (rl)
common /blk4/d(11,8)
common /blk5/n,nnp1s,ind,m,ru,el,pi,alpha,mde
dimension rl(8,21), ws(21)

c this subroutine calculates fourier coefficients and stores them in
c array d.
c wavenumber is row in d minus 1.
c ---column in d is z vector inner (1,...4), outer (5,...8).
c ---by construction columns 1,3,5,7 are fourier cosine coefficients
c ---by construction columns 2,4,6,8 are fourier sine coefficients.

c
c
      h=pi/float(nn)
      do 20 k=1,7,2
      do 15 i=1,11
      do 10 j=1,nnp1s
        ws(j)=rl(k,j)*cos(float(i-1)*h*float(j-1))
10      continue
        call simps (ws,h,nnp1s,x)
        d(i,k)=2.*x/pi
15      continue
20      continue
      do 35 k=2,8,2
      do 30 i=1,11
      do 25 j=1,nnp1s
        ws(j)=rl(k,j)*sin(float(i-1)*h*float(j-1))
25      continue
        call simps (ws,h,nnp1s,x)
        d(i,k)=2.*x/pi
30      continue
35      continue
      do 40 kk=1,8
        d(1,kk)=d(1,kk)/2.
40      continue
      return
      end
c
c

```



```

subroutine simps (a,h,nin,area)
dimension a(nin)

c  simpson's rule
c  arguments
c  ---a---integrand vector dimension nin
c  ---nin---number of points (must be odd)
c  ---h---interval or spacing
c  ---area---integral value
c

  nmin=nin-1
  nmin2=nin-2
  sum=a(1)+a(nin)
  do 10 j=2,nmin,2
    sum=sum+4.0*a(j)
  10 continue
  do 20 j=3,nmin2,2
    sum=sum+2.0*a(j)
  20 continue
  area=sum*h/3.0
  return
end

```

c c

```

subroutine loada
common /blok1/a(1604,17)
common /blok5/n,nn,nnpls,ind,m1,nu,el,pi,alpha,m,des
common /blok7/rout,rin

```

```

c
c variables specified in arguments
c ---n---number of radial subdivisions
c ---rout---outer radius
c ---m1---wave number
c ---nu---poisson ratio
c ---el---young's modulus
c --- (in common)---'a' or coefficient matrix
c with specified maximum row dimension of 1604 (n=400)
c
c

```

```

double precision a
real nu,m
a11(r)=(1.-nu)/r
a12(r)=m/r
a13(r)=-el/r**2
a14(r)=-el*m/r**2
a21(r)=-m*nu/r
a22(r)=2./r
a23(r)=-m*el/r**2
a24(r)=-el*m**2/r**2
a31(r)=-(1.-nu**2)/el+0.*r
a32(r)=0.*r
a33(r)=nu/r
a34(r)=nu*m/r
a41(r)=0.*r
a42(r)=-2.*(1.+nu)/el+0.*r
a43(r)=-m/r
a44(r)=-1./r
b11(r)=(1.-nu)/r-hd
b22(r)=2./r-hd
b33(r)=nu/r-hd
b44(r)=-1./r-hd

```

```

c11(r)=(1.-nu)/rthd
c22(r)=2./rthd
c33(r)=nu/rthd
c44(r)=-1./rthd
m=float(m1)
if(m1.eq.1.and.ind.eq.1)m=1.00001
h=(rout-rin)/float(n)
hb=1./(2.*h)
hc=2./h
hd=3.*hb
nmax=nt1
irowmax=4*nmax
irowsp=irowmax-4
irowst=irowmax-3
r=rin-h
do 5 irow=5,irowsp
a(irow,5)=-hb
a(irow,13)=hb
5 continue
do 6 irow=irowst,irowmax
a(irow,1)=hb
a(irow,5)=-hc
6 continue
do 7 irow=1,4
a(irow,13)=hc
a(irow,17)=-hb
7 continue
do 8 irow=4,irowmax,4
r=rth
a(irow, 6)=a41(r)
a(irow, 7)=a42(r)
a(irow, 8)=a43(r)
a(irow, 9)=a44(r)
a(irow-1,7)=a31(r)
a(irow-1,8)=a32(r)
a(irow-1,9)=a33(r)
a(irow-1,10)=a34(r)

```

```
a(irow-2, 8)=a21(r)
a(irow-2, 9)=a22(r)
a(irow-2,10)=a23(r)
a(irow-2,11)=a24(r)
a(irow-3, 9)=a11(r)
a(irow-3,10)=a12(r)
a(irow-3,11)=a13(r)
a(irow-3,12)=a14(r)
8 continue
r=rin
a(1,9)=b11(r)
a(2,9)=b22(r)
a(3,9)=b33(r)
a(4,9)=b44(r)
r=rout
a(irowmax-3,9)=c11(r)
a(irowmax-2,9)=c22(r)
a(irowmax-1,9)=c33(r)
a(irowmax ,9)=c44(r)
return
end
```

c c

```

subroutine recomb
common /blok8/r(204,11)
common /blok3/c(204,21)
common /blok5/n,nn,np1s,ind,m,r,uel,pi,alpha,m,des
common /blok9/t(51,11)
common /blok10/tt(51,21)

c this subroutine recombines a particular wave solution with the
c previous wavenumber and stores it in array c.
c
  mp1s=m+1
  irowmax=204
  if(m.st.0)go to 7
  do 6 j=1,np1s
  do 5 i=1,irowmax
    ii=i/4+1
    c(i,j)=r(i,mp1s)
    tt(ii,j)=t(ii,mp1s)
5 continue
6 continue
  go to 99
7 do 9 j=1,np1s
  cosmx=cos(float(m)*float(j-1)*pi/float(nn))
  do 8 i=1,irowmax,2
    ii=i/4+1
    c(i,j)=c(i,j)+r(i,mp1s)*cosmx
    tt(ii,j)=tt(ii,j)+t(ii,mp1s)*cosmx
8 continue
9 continue
  do 11 j=1,np1s
  sinmx=sin(float(m)*float(j-1)*pi/float(nn))
  do 10 i=2,irowmax,2
    c(i,j)=c(i,j)+r(i,mp1s)*sinmx
10 continue
11 continue
99 return
end

```

c
c


```

subroutine writr2
common /blok3/c(204,21)
common /blok5/n,nnn,nnp1s,ind,m,ru,rel,pi,alpha,m,des
common /blok7/rout,rin
common /blok10/tt(51,21)

c this subroutine displays output
c
irow=201
write(6,97)
write(6,98)
write(6,99)
write(6,100) el,ru,rout,rin,nnn
if(ind.ea.1)write(6,104)
if(ind.ea.2)write(6,105)
if(ind.ea.3)write(6,106)
if(ind.ea.4)write(6,107)
write(6,108)
write(6,109)
do 10 j=1,nnp1s,2
theta=pi*float(j-1)/float(nn)
write(6,111)theta
do 5 i=1,irow,20
l=2*i-1
ii=i/4+1
write(6,110) l,c(i,j),c(ii+1,j),c(ii+2,j),c(ii+3,j),tt(ii,j)
5 continue
10 continue
97 format(/,1x,'nondimens.',2x,'nondimens.',2x,'nondimens.',2x,
& 'nondimens.',2x,'radial ',2x,'circumf. ')
98 format(1x,'youngs ',2x,'poissons ',2x,'outer ',2x,
& 'inner ',2x,'interval',2x,'interval')
99 format(1x,'modulus ',2x,'ratio ',2x,'radius ',2x,
& 'radius ',2x,
& ',,')
100 format(1x,f10.3,2x,f10.5,2x,f10.3,2x,f10.3,2x,i8,2x,i8,/)
104 format(1x,'boundary conditions-inner and outer displacements',/)
105 format(1x,'boundary conditions-inner and outer stress',/)

```

```

106 format(1x,'boundary conditions-inner displacement, outer stress
    g',/)
107 format(1x,'boundary conditions-inner stress, outer displacement'
    g',/)
108 format(1x,'stresses and displacements, nondimens.')
```

```

109 format(1x,'node',2x,' radial stress', ' shear stress',
    g' radial displac', 'circ. displace', ' hoop stress',//)
```

```

110 format(1x,i4,2x,5e14.5)
```

```

111 format(1x,7htheta= ,f6.3,8h radians)
```

```

    return
```

```

end
```

```

c
```

```

c
```

```

subroutine loadbds
common /blok1/a(1604,17)
common /blok2/b(1604,1)
common /blok4/d(11,8)
common /blok5/n,nr,nrpls,ind,m,rj,rel,pi,alpha,mdes

c
c this subroutine loads boundary conditions into a and b.
c ---ind---boundary conditions specified where:
c ---1=u(inner), u(outer)
c ---2=sigma(inner), sigma(outer)
c ---3=u(inner), sigma(outer)
c ---4=sigma(inner), u(outer)
c
c
c double precision a,b
irowmax=4*(nr1)
if(ind.eq.1)go to 5
if(ind.eq.2)go to 6
if(ind.eq.3)go to 7
if(ind.eq.4)go to 8
5 continue
do 20 k=1,17
a(3,k)=0.d0
a(4,k)=0.d0
a(irowmax-1,k)=0.d0
a(irowmax ,k)=0.d0
20 continue
a(3,9)=1.d0
a(4,9)=1.d0
a(irowmax-1,9)=1.d0
a(irowmax ,9)=1.d0
b(3,1)=dble(d(m+1,3))
b(4,1)=dble(d(m+1,4))
b(irowmax-1,1)=dble(d(m+1,7))
b(irowmax ,1)=dble(d(m+1,8))
so to 99
6 continue
do 21 k=1,17

```

```

a(1,k)=0.d0
a(2,k)=0.d0
a(irowmax-3,k)=0.d0
a(irowmax-2,k)=0.d0
21 continue
a(1,9)=1.d0
a(2,9)=1.d0
a(irowmax-3,9)=1.d0
a(irowmax-2,9)=1.d0
b(1,1)=dble(d(m+1,1))
b(2,1)=dble(d(m+1,2))
b(irowmax-3,1)=dble(d(m+1,5))
b(irowmax-2,1)=dble(d(m+1,6))
so to 99
7 continue
do 22 k=1,17
a(3,k)=0.d0
a(4,k)=0.d0
a(irowmax-3,k)=0.d0
a(irowmax-2,k)=0.d0
22 continue
a(3,9)=1.d0
a(4,9)=1.d0
a(irowmax-3,9)=1.d0
a(irowmax-2,9)=1.d0
b(3,1)=dble(d(m+1,3))
b(4,1)=dble(d(m+1,4))
b(irowmax-3,1)=dble(d(m+1,5))
b(irowmax-2,1)=dble(d(m+1,6))
so to 99
8 continue
do 23 k=1,17
a(1,k)=0.d0
a(2,k)=0.d0
a(irowmax-1,k)=0.d0
a(irowmax ,k)=0.d0
23 continue

```

```
a(1,9)=1.d0
a(2,9)=1.d0
a(irowmax-1,9)=1.d0
a(irowmax,9)=1.d0
b(1,1)=dble(d(m+1,1))
b(2,1)=dble(d(m+1,2))
b(irowmax-1,1)=dble(d(m+1,7))
b(irowmax,1)=dble(d(m+1,8))
99 return
end
```

c
c


```

subroutine writr0
common /blok4/d(11,8)

: this subroutine displays fourier coefficients

write(6,100)
write(6,101)
write(6,102)
do 5 i=1,11
  m=i-1
  write(6,103)m,d(i,1),d(i,2),d(i,3),d(i,4)
5 continue
write(6,104)
do 10 i=1,11
  m=i-1
  write(6,103)m,d(i,5),d(i,6),d(i,7),d(i,8)
10 continue
100 format(1x,'fourier coefficients of boundary conditions')
101 format(1x,14h wavenumber,2x,14h sigma-r,2x,
      14h sigma-r-th,2x,14hdisplacement-r,2x,14hdisplacement-t)
102 format(1x,'inner boundary conditions')
103 format(1x,12x,i2,4(2x,e14.5))
104 format(1x,'outer boundary conditions')
return
end

```

```

subroutine visco
common /blok1/a(1604,17)
common /blok2/b(1604,1)
common /blok5/n,nnn,nnpls,ind,m,ru,el,pi,alpha,mdes
common /blok6/xl(14436)
common /blok7/rout,rin
common /blok11/r(1604,1)
common /blok12/idsf,ibar

```

```

c viscoelastic solution
c

```

```

double precision a,b,xl,r
time=0.
ibar=0

```

```

kount=0
irowmax=4*(nt1)
write(6,100)
read(5,101)tstep
write(6,102)

```

```

102 read(5,101)tstop
format(1x,15henter stop time)
write(6,103)

```

```

103 read(5,101)disint
format(1x,'enter time display interval')
100 format(1x,15henter time step)
101 format(v)

```

```

ister=int(tstop/tstep)
isint=int(disint/tstep)

```

```

do 7 kk=1,ister
do 5 i=1,irowmax
r(i,1)=b(i,1)

```

```

5 continue

```

```

call loadc

```

```

call boundb

```

```

call dband(a,irowmax,8,8,irowmax,b,1,irowmax,2,xl,ier)
do 6 i=1,irowmax

```

```
      b(i,1)=tstep*b(i,1)+r(i,1)
6 continue
   time=time+tstep
   kount=kount+1
   if(kount.eq.isint)call writr3(time,kount)
   if(ibar.eq.55)return
7 continue
   return
end
```

c
c

```

subroutine loadc
common /blok2/b(1604,1)
common /blok5/n,nr,nrpls,ind,m,ru,rel,pi,alpha,mde
common /blok7/rout,rin
common /blok11/rr(1604,1)

```

```

c
c this subroutine loads correct rate information into array b
c and performs numerical time integration by Euler's method
c

```

```

double precision b,rr
real mf
e13(r)=-alpha/r**2*el**2
e33(r)=alpha*el*(1.tru)/r
mf=float(m)
irowmax=4*(nt1)
irowsp=irowmax-3
e42=2.*(1.tru)/el*alpha
h=(rout-rin)/float(n)
r=rin-h
do 5 i=1,irowsp,4
r=r+h
b(i,1)=e13(r)*rr(i+2,1)+mf*e13(r)*rr(i+3,1)
b(i+1,1)=e13(r)*mf*rr(i+2,1)+e13(r)*mf**2*rr(i+3,1)
b(i+2,1)=e33(r)*rr(i+2,1)+e33(r)*mf*rr(i+3,1)
b(i+3,1)=e42*rr(i+1,1)
5 continue
return
end

```

```

c
c

```

```

subroutine boundb
common /blok2/b(1604,1)
common /blok5/n,nnn,nnpls,ind,m,ru,el,pi,alpha,mdes

c this subroutine places loading rate boundary information into
c the appropriate row in array b
c
double precision b,zero
zero=0.d0
irowmax=4*(n+1)
if(ind.eq.1)go to 5
if(ind.eq.2)go to 6
if(ind.eq.3)go to 7
if(ind.eq.4)go to 8
5 continue
b(3,1)=zero
b(4,1)=zero
b(irowmax-1,1)=zero
b(irowmax ,1)=zero
go to 99
6 continue
b(1,1)=zero
b(2,1)=zero
b(irowmax-3,1)=zero
b(irowmax-2,1)=zero
go to 99
7 continue
b(3,1)=zero
b(4,1)=zero
b(irowmax-3,1)=zero
b(irowmax-2,1)=zero
go to 99
8 continue
b(1,1)=zero
b(2,1)=zero
b(irowmax-1,1)=zero
b(irowmax ,1)=zero

```



```
99 return  
end
```

```
c c
```

```
subroutine writr3(time,kount)  
c this subroutine displays desired timewise stress and displace  
c ment  
c  
c kount=0  
write(6,101)time  
101 format(1x,'time is ',f6.4)  
call strain  
return  
end
```

```
c c  
c c
```

```

subroutine dband (a,n,nlc,nuc,ia,b,m,ib,ijob,xl,ier)
dimension a(ia,17),xl(n,9),b(ib,1)
double precision a,xl,b,p,q,zero,one,rn

c ---n---number of equations to be solved
c ---nlc---number of lower codiagonals
c ---nuc---number of upper codiagonals
c ---m---number of right hand sides to be solved
c ---ijob---equals zero-decompose and solve
c ---equals one-factor a matrix only
c ---equals two-solve only, a matrix is already factored
c ---ier---error message--equals 129-singular 'a' matrix
      data zero/0.0d0/,one/1.0d0/
      ier=0
      jbes=nlc+1
      nlcl=jbes
      if(ijob.eq.2)go to 80
      rn=n
c restructure the matrix--find reciprocal of the largest
c absolute value in row i
      i=1
      nc=jbestnuc
      nn=nc
      jend=nc
      if(n.eq.1.or.nlc.eq.0)go to 25
5    k=1
      p=zero
      do 10 j=jbes,jend
        a(i,k)=a(i,j)
        q=dabs(a(i,k))
        if(q.gt.p)p=q
        k=k+1
10   continue
      if(p.eq.zero)go to 135
      xl(i,nlcl)=one/p
      if(k.st.nc)go to 20

```

```

do 15 j=k,nc
a(i,j)=zero
15 continue
20 i=i+1
jbeg=jbeg-1
if(jend-jbeg,eq,n)jend=jend-1
if(i.le.nlc)go to 5
jbeg=i
nn=jend
25 jend=n-nuc
do 40 i=jbeg,n
p=zero
do 30 j=1,nn
a=dabs(a(i,j))
if(a.gt.p)p=a
30 continue
if (p.eq.zero)go to 135
xl(i,nlc1)=one/p
if(i.eq.jend)go to 37
if(i.lt.jend)go to 40
k=nn+1
do 35 j=k,nc
a(i,j)=zero
35 continue
37 nn=nn-1
40 continue
l=nlc
c 1-u decomposition
do 75 k=1,n
p=dabs(a(k,1))*xl(k,nlc1)
i=k
if(1.lt.n)l=l+1
kl=k+1
if(k1.gt.l)go to 50
do 45 j=k1,l
a=dabs(a(j,1))*xl(j,nlc1)
if(a.le.p)go to 45

```

```

p=a
i=j
45 continue
50 xl(i,nlc1)=xl(k,nlc1)
  xl(k,nlc1)=i
c singularity found
  q=rn+p
  if(a.eq.rn)go to 135
c interchange rows i and k
  if(k.eq.i)go to 60
  do 55 j=1,nc
    p=a(k,j)
    a(k,j)=a(i,j)
    a(i,j)=p
55 continue
60 if(k1.st.1)go to 75
  do 70 i=k1,1
    p=a(i,1)/a(k,1)
    ik=i-k
    xl(k1,ik)=p
  do 65 j=2,nc
    a(i,j-1)=a(i,j)-p*a(k,j)
65 continue
  a(i,nc)=zero
70 continue
75 continue
c forward substitution
80 l=nlc
  do 105 k=1,n
    i=xl(k,nlc1)
    if(i.eq.k)go to 90
    do 85 j=1,m
      p=b(k,j)
      b(k,j)=b(i,j)
      b(i,j)=p
85 continue

```

```

90 if(l.lt.n)l=l+1
   k1=k+1
   if(k1.st.l)go to 105
   do 100 i=k1,l
     ik=i-k
     p=x1(k1,ik)
     do 95 j=1,m
       b(i,j)=b(i,j)-p*b(k,j)
     95 continue
   100 continue
   105 continue
c  back substitution
   jbes=nuctnlc
   do 125 j=1,m
     l=1
     k1=n+1
     do 120 i=1,n
       k=k1-i
       p=b(k,j)
       if(l.eq.1)go to 115
       do 110 kk=2,l
         ik=kk+k
         p=p-a(k,k)*b(ik-1,j)
       110 continue
       115 b(k,j)=p/a(k,l)
       if(l.le.jbes)l=l+1
     120 continue
   125 continue
   go to 9005
   135 ier=129
9000 continue
   write(6,555)ier
   555 format(1x,i3)
9005 return
     end

```



```

subroutine strain
common /blok2/b(1601,1)
common /blok5/n,nnn,nnpls,ind,m,ru,rel,fi,alpha,mdes
common /blok7/rout,rin
common /blok12/ids,ibar

c this subroutine calculates effective stresses and strns,
c displays them, and signals if a preset limit is exceeded
c

double precision b
write(6,90)m
90 format(/,1x,'wavenumber solution for m=',i2)
irowmax=4*(nt1)
irowsp=irowmax-3
strolim=100.
streslim=100.
ru1=1.-ru*ru**2
ru2=1.-4.*ru*ru**2
ru3=4.+8.*ru*ru**2
write(6,93)
do 2 i=1,irowsp,ids
i2=i/4+1
rad=rintfloat(i2-1)*(rout-rin)/float(n)
write(6,94)i2,rad,b(i,1),b(i+1,1),b(i+2,1),b(i+3,1)
2 continue
93 format(1x,4hnode,2x,6hradius,9x,7hsigma-r,7x,8hsigma-th,6x,
89hdisplac-r,5x,10hdisplac-th,/)
94 format(2x,i3,f8.3,2x,4(e14.7,1x))
write(6,100)
do 10 i=1,irowsp,ids
i2=i/4+1
rad=rintfloat(i2-1)*(rout-rin)/float(n)
hoop=el/rad*snsl(b(i+2,1))tel/rad*snsl(b(i+3,1))*float(m)+
8 ru*snsl(b(i,1))
strn=1./el*sert(ru1*snsl(b(i,1))*2+ru1*hoop**2+ru2*snsl
8 (b(i,1))*hoop+ru3*snsl(b(i+1,1))*2)

```

```

      & (b(i,1))*hoop*ru3*snsl(b(i+1,1))**2)
      stress=.57735*sqrt( snsl(b(i,1))**2thoop**2-hoop*snsl(b(i,1))+
      &3*snsl(b(i+1,1))**2)
      write(6,101)i2,hoop,stress,snrn
      if(abs(stress).st.streslim)go to 30
      if(abs(stress).st.streslim)go to 50
10 continue
   go to 99
30 continue
   write(6,102)i2,snrnlim
102 format(1x,'snrn at node ',i3,' has exceeded preset failure'
      &,'limit of ', e14.7)
      iber=555
      go to 10
50 continue
   write(6,103)i2,streslim
103 format(1x,'stress at node ',i3,'has exceeded preset elastic'
      &,'limit of ',e14.7)
      iber=555
      go to 10
100 format(/,1x,4hnode,2x,14h   hoop stress,2x,8x,6hstress,
      &2x,8x,6hstrain,/)
101 format(1x,1x,i3,2x,3(e14.7,2x))
99 return
end

```

APPENDIX A-4

User NotesProgram Operation

The program flow is described in Figures 4-10 and 5-2. The material constants E , ν , α are set in either the main calling program or subroutine elastic prior to compilation. In the listing presented in A-3, E and α are non-dimensional with a value of 1.0. The program is not restricted to non-dimensional solution, however, and any consistent values could be used.

User inputs are via keyboard and consist of 3 inputs.

For elastic:

- 1) mdes - after reviewing fourier coefficients of boundary conditions, the user is asked for the number of fourier coefficients to be used in the solution. This feature is incorporated to save calculation of meaningless higher wave number solutions.
- 2) The user is queried on whether a viscoelastic solution is required. This feature is used to permit an elastic solution only.
- 3) Display of theta information - This feature automatically combines elastic wave solutions and calculates circumferential variation for intervals of $.05 \pi$ and radial variation of 50 intervals.

Display here is set for $.01\pi$ and radial variation of ten intervals.

If a viscoelastic solution is desired, additional keyboard inputs are:

- 1) tstop - desired stop time, entered in units of non-dimensional time.
- 2) tstep - interval calculation time - This is important as a small step must be chosen to ensure convergence.
- 3) disint - time display interval of wave number solutions - It is anticipated that not all small discrete time intervals will require display.

disint should be an integral multiple of tstep.

Loading Input - rout must be set in the main program. The vectors put1 and put4 contain boundary condition loading information as determined by ind, also sent from main. put1 - put4 contain discrete data for loading circumferentially through $\Theta = \pi$. (The other half is identical by symmetry).

<u>ind</u>	<u>Inner Boundary Conditions</u>		<u>Outer Boundary Conditions</u>	
	<u>put1</u>	<u>put2</u>	<u>put3</u>	<u>put4</u>
1	u_r	u_θ	u_r	u_θ
2	σ_r	σ_θ	σ_r	σ_θ
3	u_r	u_θ	σ_r	σ_θ
4	σ_r	σ_θ	u_r	u_θ

Caution must be exercised with $\text{ind} = 2$, since a rigid body

translation may be produced.

Output of Program - Three distinct listings are produced:

- 1) Fourier coefficients of boundary conditions - all wave numbers
- 2) Wave number solutions of $\sigma_r, \sigma_{re}, u_r, u_e, \sigma_e, \sigma_{eff}$
 ϵ_{eff} , node, radius for upto 400 nodes. In the listing of Appendix A-3, only ten radial intervals are displayed. idsp will vary display points. Wave number solutions are displayed for the elastic case and at each time display intervals determined by disint. The headings "stress" and "strain" contain an effective stress and strain as defined

by:

$$\sigma = \frac{1}{\sqrt{3}} (\sigma_r^2 + \sigma_e^2 - \sigma_r \sigma_e + 3\sigma_{re}^2)^{\frac{1}{2}}$$

$$\epsilon = (\epsilon_r^2 + \epsilon_e^2 + \epsilon_r \epsilon_e + \epsilon_{re}^2)^{\frac{1}{2}}$$

- 3) Stresses by angular position - contains up to fifty radial intervals with the total recombined fourier series representation of the elastic solution displayed at intervals of $.01\pi$.

Other Notes

Viscoelastic boundary conditions (rates) are preset to zero in this program, but are not necessarily restricted to this value or even a constant value. Rate information must be in size with integration of time step and convergence must be ensured overall.

streslim and strainlim are preset constants corresponding to an elastic limit and a strain failure limit. The solution is deemed inappropriate beyond these levels and a solution is terminated for that particular wave number.

The accuracy of the fourier subroutine is dependent on the circumferential interval. For complex loading it is conceivable that this interval can be decreased by increasing nn and of course pertinent array sizes.

Storage of solutions in the B, C, and R arrays for a particular variable are in every fourth row, e.g.;

solution

$$\underline{Z}_i = b(i,1), b(i+1,1), b(i+2,1), b(i+3,1)$$

APPENDIX A-5

Sample output

```

print main.fortran
main.fortran      09/02/78  1628.3 edt Sat

c main
common /blok5/n,nn,nnfsl,ind,m,ru,el,pi,alpha,mdes
common /blok7/rout,rin
dimension put1(21),put2(21),put3(21),put4(21)
pi=3.1415193
ru=.33333333
cinc=pi/20.
do 10 i=1,21
  put1(i)=0.
  put2(i)=0.
  put3(i)=-1.*cos(float(i-1)*cinc)
  put4(i)=-1.*sin(float(i-1)*cinc)
10 continue
ind=1
rout=20.
rin=1.
call elastic (put1,put2,put3,put4)
stop
end

r 1628 0.363 16.892 148

```

main
viscoelastic solution of stressed circular plate with a rigid circular inclusion
con

fourier coefficients of boundary conditions			
wavenumber	sigma-r	sigma-r-th	displacement-r
inner boundary conditions			
0	0.00000e+00	0.00000e+00	0.00000e+00
1	0.00000e+00	0.00000e+00	0.00000e+00
2	0.00000e+00	0.00000e+00	0.00000e+00
3	0.00000e+00	0.00000e+00	0.00000e+00
4	0.00000e+00	0.00000e+00	0.00000e+00
5	0.00000e+00	0.00000e+00	0.00000e+00
6	0.00000e+00	0.00000e+00	0.00000e+00
7	0.00000e+00	0.00000e+00	0.00000e+00
8	0.00000e+00	0.00000e+00	0.00000e+00
9	0.00000e+00	0.00000e+00	0.00000e+00
10	0.00000e+00	0.00000e+00	0.00000e+00
outer boundary conditions			
0	0.00000e+00	0.00000e+00	0.00000e+00
1	0.00000e+00	0.00000e+00	-0.23349e-04
2	0.00000e+00	0.00000e+00	-0.99999e+00
3	0.00000e+00	0.00000e+00	0.15853e-04
4	0.00000e+00	0.00000e+00	-0.60896e-05
5	0.00000e+00	0.00000e+00	0.33401e-05
6	0.00000e+00	0.00000e+00	-0.21693e-05
7	0.00000e+00	0.00000e+00	0.15525e-05
8	0.00000e+00	0.00000e+00	-0.11683e-05
9	0.00000e+00	0.00000e+00	0.92834e-06
10	0.00000e+00	0.00000e+00	-0.75847e-06
up to how many wavenumbers desired?			
2			0.62734e-06
viscoelastic solution? (1 or 0)			
1			
display of theta information? (1 or 0)			
1			

wavenumber solution for m= 0

node	radius	sigma-r	sigma-th	displac-r	displac-th
1	1.000	-0.2632434d-05	0.0000000d+00	0.0000000d+00	0.0000000d+00
41	2.900	-0.1860157d-05	0.0000000d+00	-0.2990102d-05	0.0000000d+00
81	4.800	-0.1793748d-05	0.0000000d+00	-0.5373770d-05	0.0000000d+00
121	6.700	-0.1775155d-05	0.0000000d+00	-0.7666712d-05	0.0000000d+00
161	8.600	-0.1767446d-05	0.0000000d+00	-0.9929052d-05	0.0000000d+00
201	10.500	-0.1763527d-05	0.0000000d+00	-0.1217740d-04	0.0000000d+00
241	12.400	-0.1761266d-05	0.0000000d+00	-0.1441820d-04	0.0000000d+00
281	14.300	-0.1759843d-05	0.0000000d+00	-0.1665444d-04	0.0000000d+00
321	16.200	-0.1758891d-05	0.0000000d+00	-0.1888775d-04	0.0000000d+00
361	18.100	-0.1758222d-05	0.0000000d+00	-0.2111903d-04	0.0000000d+00
401	20.000	-0.1757735d-05	0.0000000d+00	-0.2334888d-04	0.0000000d+00

hoop stress stress strain

1	-0.8774781e-06	0.1796592e-11	0.2339942e-05
41	-0.1651122e-05	0.1038348e-11	0.2032022e-05
81	-0.1717451e-05	0.1028832e-11	0.2027830e-05
121	-0.1736004e-05	0.1027736e-11	0.2027337e-05
161	-0.1743690e-05	0.1027481e-11	0.2027217e-05
201	-0.1747595e-05	0.1027395e-11	0.2027175e-05
241	-0.1749846e-05	0.1027358e-11	0.2027156e-05
281	-0.1751261e-05	0.1027340e-11	0.2027145e-05
321	-0.1752207e-05	0.1027329e-11	0.2027139e-05
361	-0.1752872e-05	0.1027322e-11	0.2027134e-05
401	-0.1753355e-05	0.1027318e-11	0.2027131e-05
enter	time step		
.001			
enter	stop time		
.001			
enter	time display interval		
.001			

time is 0.0010

wavenumber solution for m= 0

node	radius	sigma-r	sigma-th	displac-r	displac-th
1	1.000	-0.2630706d-05	0.0000000d+00	0.0000000d+00	0.0000000d+00
41	2.900	-0.1858569d-05	0.0000000d+00	-0.2989559d-05	0.0000000d+00
81	4.800	-0.1792090d-05	0.0000000d+00	-0.5373314d-05	0.0000000d+00
121	6.700	-0.1773467d-05	0.0000000d+00	-0.7666345d-05	0.0000000d+00
161	8.600	-0.1765743d-05	0.0000000d+00	-0.9928760d-05	0.0000000d+00
201	10.500	-0.1761814d-05	0.0000000d+00	-0.1217171d-04	0.0000000d+00
241	12.400	-0.1759547d-05	0.0000000d+00	-0.1441802d-04	0.0000000d+00
281	14.300	-0.1758121d-05	0.0000000d+00	-0.1665432d-04	0.0000000d+00
321	16.200	-0.1757166d-05	0.0000000d+00	-0.1888767d-04	0.0000000d+00
361	18.100	-0.1756495d-05	0.0000000d+00	-0.2111899d-04	0.0000000d+00
401	20.000	-0.1756006d-05	0.0000000d+00	-0.2334888d-04	0.0000000d+00

node	hoop stress	stress	strain
1	-0.8769020e-06	0.1794233e-11	0.2338405e-05
41	-0.1650405e-05	0.1036908e-11	0.2030655e-05
81	-0.1716804e-05	0.1027445e-11	0.2026482e-05
121	-0.1735386e-05	0.1026367e-11	0.2025996e-05
161	-0.1743088e-05	0.1026119e-11	0.2025881e-05
201	-0.1747002e-05	0.1026037e-11	0.2025840e-05
241	-0.1749259e-05	0.1026003e-11	0.2025822e-05
281	-0.1750678e-05	0.1025986e-11	0.2025812e-05
321	-0.1751627e-05	0.1025977e-11	0.2025806e-05
361	-0.1752294e-05	0.1025971e-11	0.2025802e-05
401	-0.1752779e-05	0.1025967e-11	0.2025799e-05

wavenumber solution for m=1

node	radius	sigma-r	sigma-th	dislac-r	dislac-th
1	1.000	-0.8883102d+00	-0.9241438d+00	0.0000000d+00	0.0000000d+00
41	2.900	-0.7063498d-01	-0.8300261d-01	-0.6202069d+00	0.8863436d+00
81	4.800	-0.3580747d-01	-0.4328023d-01	-0.7643741d+00	0.1004949d+01
121	6.700	-0.3120746d-01	-0.3656135d-01	-0.8451073d+00	0.9703687d+00
161	8.600	-0.3266565d-01	-0.3683690d-01	-0.9003050d+00	0.8513372d+00
201	10.500	-0.3634296d-01	-0.3975962d-01	-0.9405457d+00	0.6679486d+00
241	12.400	-0.4119540d-01	-0.4408873d-01	-0.9699297d+00	0.4290377d+00
281	14.300	-0.4685058d-01	-0.4935968d-01	-0.9901955d+00	0.1396447d+00
321	16.200	-0.5315502d-01	-0.5537005d-01	-0.1001987d+01	-0.1967593d+00
361	18.100	-0.6004187d-01	-0.6202457d-01	-0.1005356d+01	-0.5774360d+00
401	20.000	-0.6748344d-01	-0.6927799d-01	-0.9999884d+00	-0.1000012d+01

node	hoop stress	stress	strain
1	-0.2961034e+00	0.1058622e+01	0.2532190e+01
41	0.6822628e-01	0.1171053e-01	0.2350893e+00
81	0.3818401e-01	0.3242334e-02	0.1230085e+00
121	0.8293244e-02	0.1770564e-02	0.9964219e-01
161	-0.1658248e-01	0.1623739e-02	0.1006011e+00
201	-0.3807595e-01	0.2043092e-02	0.1120798e+00
241	-0.5735212e-01	0.2818377e-02	0.1285612e+00
281	-0.7509593e-01	0.3875074e-02	0.1477322e+00
321	-0.9171505e-01	0.5186506e-02	0.1686304e+00
361	-0.1074610e+00	0.6747292e-02	0.1908565e+00
401	-0.1224945e+00	0.8563627e-02	0.2142547e+00
enter	time step		
.001			
enter	stop time		
.005			
enter	time display interval		
.005			

time is 0.0050

wavenumber solution for m=1

node	radius	sigma-r	sigma-th	dislac-r	dislac-th
1	1.000	-0.8946531d+00	-0.9309246d+00	0.0000000d+00	0.0000000d+00
41	2.900	-0.7106877d-01	-0.8358751d-01	-0.6172738d+00	0.8870667d+00
81	4.800	-0.3590916d-01	-0.4347322d-01	-0.7607368d+00	0.1005261d+01
121	6.700	-0.3120679d-01	-0.3662609d-01	-0.8412523d+00	0.9705631d+00
161	8.600	-0.3261230d-01	-0.3683451d-01	-0.8965017d+00	0.8515559d+00
201	10.500	-0.3625663d-01	-0.3971502d-01	-0.9369931d+00	0.6682403d+00
241	12.400	-0.4108683d-01	-0.4401550d-01	-0.9667960d+00	0.4293959d+00
281	14.300	-0.4672684d-01	-0.4926659d-01	-0.9876331d+00	0.1400275d+00
321	16.200	-0.5302130d-01	-0.5526338d-01	-0.1000140d+01	-0.1964177d+00
361	18.100	-0.5990227d-01	-0.6190918d-01	-0.1004363d+01	-0.5772181d+00
401	20.000	-0.6734134d-01	-0.6915780d-01	-0.9999884d+00	-0.1000012d+01

node	hoop stress	stress	strain
1	-0.2982177e+00	0.1074133e+01	0.2550721e+01
41	0.6934244e-01	0.1191595e-01	0.2368941e+00
81	0.3897290e-01	0.3292534e-02	0.1237123e+00
121	0.8897859e-02	0.1785040e-02	0.9986452e-01
161	-0.1609702e-01	0.1622686e-02	0.1005388e+00
201	-0.3768105e-01	0.2033355e-02	0.1118644e+00
241	-0.5703432e-01	0.2803258e-02	0.1282705e+00
281	-0.7484873e-01	0.3856625e-02	0.1474088e+00
321	-0.9153537e-01	0.5166260e-02	0.1682986e+00
361	-0.1073476e+00	0.6726556e-02	0.1905312e+00
401	-0.1224471e+00	0.8543601e-02	0.2139461e+00

nondimens. youngs modulus	nondimens. poissons ratio	nondimens. outer radius	nondimens. inner radius	radial interval	circumf. interval	
1.000	0.33333	20.000	1.000	400	20	
boundary conditions--inner and outer displacements						
stresses and displacements, nondimens.						
node	radial stress	shear stress	radial displac	circ. displace	hoop stress	
theta= 0.000 radians						
1	-0.88831e+00	0.00000e+00	0.00000e+00	0.00000e+00	-0.59221e+00	
41	-0.70637e-01	0.00000e+00	-0.62021e+00	0.00000e+00	0.38303e+00	
81	-0.35809e-01	0.00000e+00	-0.76438e+00	0.00000e+00	0.30233e+00	
121	-0.31209e-01	0.00000e+00	-0.84511e+00	0.00000e+00	0.12548e+00	
161	-0.32667e-01	0.00000e+00	-0.90031e+00	0.00000e+00	-0.72006e-01	
201	-0.36345e-01	0.00000e+00	-0.94056e+00	0.00000e+00	-0.27347e+00	
241	-0.41197e-01	0.00000e+00	-0.96994e+00	0.00000e+00	-0.47357e+00	
281	-0.46852e-01	0.00000e+00	-0.99021e+00	0.00000e+00	-0.67015e+00	
321	-0.53157e-01	0.00000e+00	-0.10020e+01	0.00000e+00	-0.86217e+00	
361	-0.60044e-01	0.00000e+00	-0.10054e+01	0.00000e+00	-0.10490e+01	
401	-0.67485e-01	0.00000e+00	-0.10000e+01	0.00000e+00	-0.12302e+01	
theta= 0.314 radians						
1	-0.84484e+00	-0.28558e+00	0.00000e+00	0.00000e+00	-0.56322e+00	
41	-0.67180e-01	-0.25649e-01	-0.58985e+00	0.27390e+00	0.36428e+00	
81	-0.34057e-01	-0.13374e-01	-0.72697e+00	0.31055e+00	0.28753e+00	
121	-0.29682e-01	-0.11298e-01	-0.80375e+00	0.29986e+00	0.11934e+00	
161	-0.31069e-01	-0.11383e-01	-0.85625e+00	0.26308e+00	-0.68482e-01	
201	-0.34566e-01	-0.12286e-01	-0.89452e+00	0.20641e+00	-0.26008e+00	
241	-0.39181e-01	-0.13624e-01	-0.92247e+00	0.13258e+00	-0.45039e+00	
281	-0.44559e-01	-0.15253e-01	-0.94175e+00	0.43153e-01	-0.63735e+00	
321	-0.50555e-01	-0.17110e-01	-0.95297e+00	-0.60802e-01	-0.81997e+00	
361	-0.57105e-01	-0.19167e-01	-0.95617e+00	-0.17844e+00	-0.99765e+00	
401	-0.64182e-01	-0.21408e-01	-0.95107e+00	-0.30902e+00	-0.11700e+01	
theta= 0.628 radians						
1	-0.71866e+00	-0.54320e+00	0.00000e+00	0.00000e+00	-0.47911e+00	
41	-0.57147e-01	-0.48788e-01	-0.50176e+00	0.52098e+00	0.30987e+00	
81	-0.28971e-01	-0.25439e-01	-0.61840e+00	0.59069e+00	0.24459e+00	
121	-0.25249e-01	-0.21490e-01	-0.68371e+00	0.57037e+00	0.10151e+00	
161	-0.26429e-01	-0.21652e-01	-0.72837e+00	0.50040e+00	-0.58255e-01	

APPENDIX B

Analytic Elastic Solution for the Case of a Circular RingWavenumber $m=0$

The stress function is known to satisfy the biharmonic relation

$$\nabla^4 \psi = 0 \quad (\text{B.1})$$

In a two-dimensional elastic material. For the case of no circumferential variation (as in wavenumber 0), (B.1) reduces

to

$$\left(\frac{\partial^2}{\partial r^2} + \frac{1}{r} \frac{\partial}{\partial r} \right) \left(\frac{\partial^2 \psi}{\partial r^2} + \frac{1}{r} \frac{\partial \psi}{\partial r} \right) = 0$$

or

$$\frac{d^4 \psi}{dr^4} + \frac{2}{r} \frac{d^3 \psi}{dr^3} - \frac{1}{r^2} \frac{d^2 \psi}{dr^2} + \frac{1}{r^3} \frac{d \psi}{dr} = 0 \quad (\text{B.2})$$

Let

$$\xi = \log r$$

Then

$$\frac{d \psi}{dr} = \frac{d \psi}{d \xi} \frac{d \xi}{dr} = \frac{1}{r} \frac{d \psi}{d \xi}$$

$$\frac{d^2 \psi}{dr^2} = \frac{d}{dr} \left(\frac{d \psi}{d \xi} \right) = \frac{1}{r^2} \left(\frac{d^2 \psi}{d \xi^2} - \frac{d \psi}{d \xi} \right)$$

$$\frac{d^3 \psi}{dr^3} = \frac{1}{r^3} \left(\frac{d^3 \psi}{d \xi^3} - 3 \frac{d^2 \psi}{d \xi^2} + 2 \frac{d \psi}{d \xi} \right)$$

$$\frac{d^4 \psi}{dr^4} = \frac{1}{r^4} \left(\frac{d^4 \psi}{d \xi^4} - 6 \frac{d^3 \psi}{d \xi^3} + 11 \frac{d^2 \psi}{d \xi^2} - 6 \frac{d \psi}{d \xi} \right)$$

(B.2) becomes

$$\frac{d^4 \psi}{d \xi^4} - 4 \frac{d^3 \psi}{d \xi^3} + 4 \frac{d^2 \psi}{d \xi^2} = 0$$

The general solution of which is

$$\psi = C_1 \xi e^{2\xi} + C_2 e^{2\xi} + \xi C_3 + C_4$$

or

$$\psi = C_1 (\log r) e^{2 \log r} + C_2 e^{2 \log r} + (\log r) C_3 + C_4$$

Finally $\phi = C_1 r^2 \log r + C_2 \log r + C_2 r^2 + C_3 \log r + C_4$

Now $\sigma_r = \frac{1}{r} \frac{d\phi}{dr} = C_1 (1 + 2 \log r) + 2C_2 + \frac{C_3}{r^2} \quad (\text{B.3})$

$$\sigma_\theta = \frac{d^2\phi}{dr^2} = C_1 (3 + 2 \log r) + 2C_2 - \frac{C_3}{r^2} \quad (\text{B.4})$$

$$\sigma_{r\theta} = 0$$

Strain relations

$$\epsilon_r = \frac{du}{dr} \quad \epsilon_\theta = \frac{u}{r} \quad \epsilon_{r\theta} = \frac{dv}{dr} - \frac{v}{r}$$

In plane stress

$$\sigma_z = 0$$

$$\frac{du}{dr} = \frac{1}{E} (\sigma_r - \nu \sigma_\theta) \quad (\text{B.5})$$

$$\frac{u}{r} = \frac{1}{E} (\sigma_\theta - \nu \sigma_r) \quad (\text{B.6})$$

Integrating (B.5)

$$Eu = \int (B.3) dr - \nu \int (B.4) dr$$

Into
$$Eu = C_1 \left[r(1-3\nu) + 2(1-\nu)(r \log r - r) \right] + 2C_2(1-\nu)r - C_3(1+\nu)\frac{1}{r} + C_5 \quad (\text{B.7})$$

(B.6) becomes

$$Eu = C_1 \left[r(3-\nu) + 2r(1-\nu) \log r \right] + 2C_2(1-\nu)r - C_3(1+\nu)\frac{1}{r} \quad (\text{B.8})$$

For (B.7) to have the same representation as (B.8)

$$C_1 = C_5 = 0$$

Therefore, for wavenumber 0

$$Eu = 2C_2(1-\nu)r - C_3(1+\nu)\frac{1}{r} \quad (\text{B.9})$$

$$\begin{aligned} \sigma_r &= 2C_2 + \frac{C_3}{r^2} \\ \sigma_\theta &= 2C_2 - \frac{C_3}{r^2} \end{aligned} \quad (\text{B.10})$$

From the general solution for the stress function in circular coordinates presented by Timoshenko [29], that portion corresponding to the first wavenumber is:

$$\psi = \frac{a_1}{2} r \theta \sin \theta + (b_1 r^3 + a_1' r^{-1} + b_1' r \log r) \cos \theta$$

Since

$$G_r = \frac{1}{r} \frac{\partial \psi}{\partial r} + \frac{1}{r^2} \frac{\partial^2 \psi}{\partial \theta^2}$$

$$G_\theta = \frac{\partial^2 \psi}{\partial r^2}$$

$$G_{r\theta} = -\frac{\partial}{\partial r} \left(\frac{1}{r} \frac{\partial \psi}{\partial \theta} \right)$$

Then

$$G_r = [(a_1 + b_1') r^{-1} + 2b_1 r - 2a_1' r^{-3}] \cos \theta$$

$$G_\theta = (6b_1 r + 2a_1' r^{-3} + b_1' r^{-1}) \cos \theta$$

$$G_{r\theta} = (2b_1 r - 2a_1' r^{-3} + b_1' r^{-1}) \sin \theta$$

Employing stress-strain (4.11) and integrating with respect to r

$$Eu_r = \left\{ [(a_1 + b_1') \log r + b_1 r^2 + a_1' r^{-2}] - \nu [3b_1 r^2 - a_1' r^{-2}] + [b_1' \log r] \right\} \cos \theta + f(\theta) \quad (B.11)$$

Employing (4.12) and integrating with respect to θ

$$Eu_\theta = [-(a_1 + b_1') \log r + 5b_1 r^2 + a_1' r^{-2} + b_1'] \sin \theta + \\ -\nu [-b_1' \log r + (a_1 + b_1') - b_1 r^2 - a_1' r^{-2}] \sin \theta \\ - \int f(\theta) d\theta + F(r) \quad (B.12)$$

$$\text{From (B.11)} \quad \frac{E}{r} \frac{\partial u_r}{\partial \theta} = -[(a_1 + b_1') \frac{\log r}{r} + b_1 r + a_1' r^{-3}] \sin \theta + \\ + \nu [3b_1 r - a_1' r^{-3} + b_1' \frac{\log r}{r}] \sin \theta + \frac{f'(\theta)}{r} \quad (B.13)$$

$$\text{From (B.12)} \quad E \frac{\partial u_\theta}{\partial r} = \left[-\frac{(a_1 + b_1')}{r} + 10b_1 r - 2a_1' r^{-3} \right] \sin \theta + \\ + \nu [b_1' r^{-1} + 2b_1 r - 2a_1' r^{-3}] \sin \theta + F' \quad (B.14)$$

And also from (B.12)

$$\begin{aligned}
 -E \frac{u_\theta}{r} = & - \left[- (a_1 + b_1') \frac{\log r}{r} + 5b_1 r + a_1' r^{-3} + b_1 r^{-1} \right] \sin \theta \\
 & + \nu \left[- b_1' \frac{\log r}{r} + (a_1 + b_1') r^{-1} - b_1 r - a_1' r^{-3} \right] \sin \theta \\
 & + \int \frac{f(\theta) d\theta}{r} - \frac{F}{r} \quad (B.15)
 \end{aligned}$$

Equating (4.8) and (4.5) and using (B.13), (B.14), and (B.15)

$$\frac{f'(\theta)}{r} + F' + \frac{\int f(\theta) d\theta}{r} - \frac{F}{r} = [4b_1' + (1-\nu)a_1] \sin \theta / r$$

or

$$f'(\theta) + \int f(\theta) d\theta + (rF' - F) = [4b_1' + (1-\nu)a_1] \sin \theta \quad (B.16)$$

$(rF' - F)$ must necessarily be zero

$$rF' - F = 0 \Rightarrow F = Cr$$

Differentiating with respect to θ

$$f'' + f = [4b_1' + (1-\nu)a_1] \cos \theta \quad (B.17)$$

The solution to the differential equation (B.17)

$$f(\theta) = A \sin \theta + B \cos \theta + \left[2b_1' + \frac{(1-\nu)}{2} a_1 \right] \theta \sin \theta$$

From [29]

$$\phi = (a_n r^n + b_n r^{n+2} + a'_n r^{-n} + b'_n r^{-n+2}) \cos n\theta$$

$$\phi_r = -[n(n-1)a_n r^{n-2} + (n^2 - n - 2)b_n r^n + n(n+1)a'_n r^{-n-2} + (n^2 + n - 2)b'_n r^{-n}] \cos n\theta$$

$$\phi_\theta = [n(n-1)a_n r^{n-2} + (n+1)(n+2)b_n r^n + n(n+1)a'_n r^{-n-2} + (n-1)(n-2)b'_n r^{-n}] \sin n\theta$$

$$\phi_{r\theta} = [n(n-1)a_n r^{n-2} + n(n+1)b_n r^n - n(n+1)a'_n r^{-n-2} - n(n-1)b'_n r^{-n}] \sin n\theta$$

Again employing (4.11) and integrating

$$E u_r = -[n a_n r^{n-1} + (n-2)b_n r^{n+1} - n a'_n r^{-n-1} - (n+2)b'_n r^{-n+1}] \cdot \cos n\theta - \mu [n a_n r^{n-1} + (n+2)b_n r^{n+1} - n a'_n r^{-n-1} - (n-2)b'_n r^{-n+1}] \cos n\theta + f(\theta) \quad (\text{B.18})$$

Employing (4.12) and integrating

$$E u_\theta = [n a_n r^{n-1} + (n+4)b_n r^{n+1} + n a'_n r^{-n-1} + (n-4)b'_n r^{-n+1}] \cdot \sin n\theta + \mu [n a_n r^{n-1} + n b_n r^{n+1} + n a'_n r^{-n-1} + n b'_n r^{-n+1}] \sin n\theta - \int f(\theta) d\theta + F(r) \quad (\text{B.19})$$

$$\text{From (B.18)} \quad \frac{E}{r} \frac{\partial u_r}{\partial \theta} = \left\{ [n^2 a_n r^{n-2} + n(n-2)b_n r^n - n^2 a'_n r^{-n-2} - n(n+2)b'_n r^{-n}] + \mu [n^2 a_n r^{n-2} + n(n+2)b_n r^n - n^2 a'_n r^{-n-2} - n(n-2)b'_n r^{-n}] \right\} \sin n\theta + \frac{f'}{r} \quad (\text{B.20})$$

$$\text{From (B.19)} \quad E \frac{\partial u_\theta}{\partial r} = \left\{ [n(n-1)a_n r^{n-2} + (n+1)(n+4)b_n r^n - n(n+1)a'_n r^{-n-2} - (n-1)(n-4)b'_n r^{-n}] + \mu [n(n-1)a_n r^{n-2} + n(n+1)b_n r^n - n(n+1)a'_n r^{-n-2} - n(n-1)b'_n r^{-n}] \right\} \sin n\theta + F' \quad (\text{B.21})$$

Also from (B.19)

$$-E \frac{u_\theta}{r} = - \left[n a_n r^{n-2} + (n+4) b_n r^n + n a'_n r^{-n-2} + (n-4) b'_n r^{-n} \right] \cdot \sin n\theta + n \left[n a_n r^{n-2} + n b_n r^n + n a'_n r^{-n-2} + n b'_n r^{-n} \right] \sin n\theta + \frac{1}{r} \int f(\theta) d\theta - \frac{F}{r} \quad (\text{B.22})$$

Equating (4.8) and (4.9) and using (B.20), (B.21), & (B.22)

$$\frac{f'}{r} + F' + \frac{1}{r} \int f(\theta) d\theta - \frac{F}{r} = 0$$

$$f' + \int f(\theta) d\theta = F - r F' = \text{CONSTANT}$$

$$F = C + Dr$$

$$f = A \sin \theta + B \cos \theta$$

These general solutions must be employed with the correct boundary conditions to find the unique constants associated with each wavenumber.

APPENDIX C

Buckling of a Circular Ring Subject to Stresses Uniformly
Distributed Around the Edge

The loading applied to the condition depicted in Figure C-1 is analyzed for the first buckling mode. Assuming the deflection surface is a surface of revolution, Timoshenko [28] gives the required differential equation:

$$r^2 \frac{d^2 \phi}{dr^2} + r \frac{d\phi}{dr} - \phi = \frac{Qr^2}{D} \quad (C.1)$$

where Q is the shearing force/length
and D is the flexural rigidity

$$Q = N_R \sin \phi \doteq N_R \phi \quad (C.2)$$

Let $\frac{N_R}{D} = \alpha^2 \quad (C.3)$

(C.3) becomes

$$r^2 \frac{d^2 \phi}{dr^2} + r \frac{d\phi}{dr} + (\alpha^2 r^2 - 1) \phi = 0 \quad (C.4)$$

If $u = \alpha r$ (variable change)

Then $u^2 \frac{d^2 \phi}{du^2} + u \frac{d\phi}{du} + (u^2 - 1) \phi = 0 \quad (C.5)$

The general solution of which is

$$\phi = A_1 J_1(u) + A_2 Y_1(u) \quad (C.6)$$

Applying boundary conditions

$$\phi(r=a) = 0 \quad \text{clamped inner edge} \quad (C.7)$$

$$\left(\frac{d\phi}{dr} + \nu \frac{\phi}{r} \right) = 0 \quad r=b \text{ free outer edge} \quad (C.8)$$

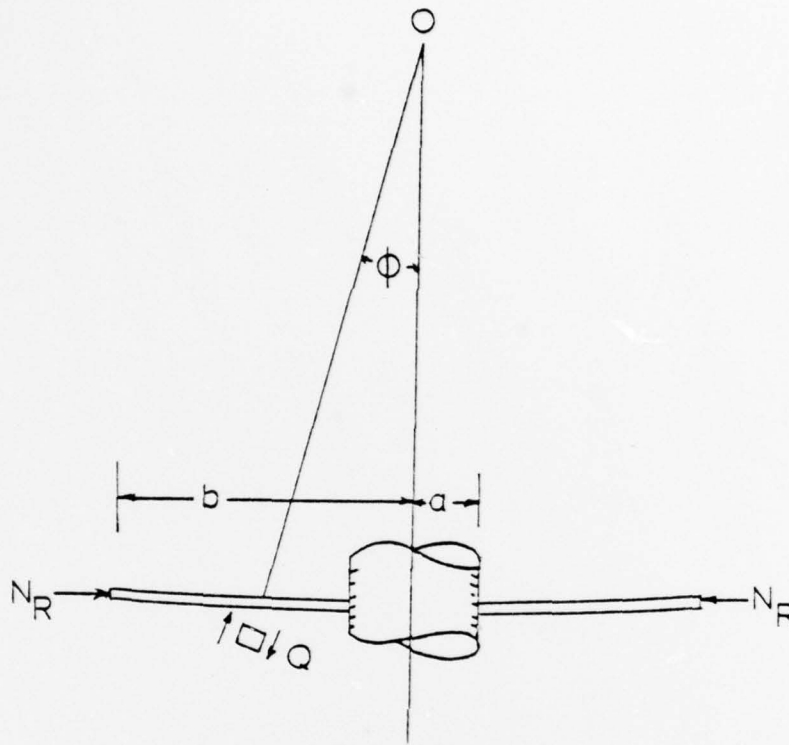


Figure C-1

Buckling of a thin circular plate around a rigid inclusion

Since
$$\frac{d\phi}{dr} = A_1 \alpha J_1'(u) + A_2 \alpha Y_1'(u) \quad (C.9)$$

The boundary conditions (C.7), (C.8) become

$$A_1 J_1(\alpha a) + A_2 Y_1(\alpha a) = 0 \quad (C.10)$$

$$\begin{aligned} & \alpha (A_1 J_1'(\alpha b) + A_2 Y_1'(\alpha b)) + \\ & + \frac{\nu}{b} (A_1 J_1(\alpha b) + A_2 Y_1(\alpha b)) = 0 \end{aligned} \quad (C.11)$$

(C.10) is
$$A_2 = -A_1 \frac{J_1(\alpha a)}{Y_1(\alpha a)} \quad (C.12)$$

And (C.11)
$$\begin{aligned} & \alpha \left(J_1'(\alpha b) - \frac{J_1(\alpha a)}{Y_1(\alpha a)} Y_1'(\alpha b) \right) + \frac{\nu}{b} \left(J_1(\alpha b) - \right. \\ & \left. - \frac{J_1(\alpha a)}{Y_1(\alpha a)} Y_1(\alpha b) \right) = 0 \end{aligned} \quad (C.13)$$

$$\frac{d}{du} J_1 = J_0 - \frac{1}{u} J_1 \quad (C.14)$$

(C.12), (C.13), (C.14) are combined into a single equation.

The first zero appears at about a value of .42

To apply
$$\alpha = 1, \quad \frac{a}{b} = \frac{1}{20}, \quad \nu = \frac{1}{3}$$

Where
$$\alpha \approx .42/a \quad \text{then} \quad N_{cr} \approx .176 D$$

$$D = \frac{Eh^3}{12(1-\nu)} \quad , \quad \text{the flexural rigidity}$$

Yields
$$\sigma_{cr} = \frac{N_{cr}}{h} \approx .0165 E h^2 / a^2$$

